UNIVERSITY OF CALIFORNIA
RIVERSIDE

Soil Genesis, Hydrology, and Biogeochemistry of the White Mountains, Eastern California, USA

A Dissertation submitted in partial satisfaction
of the requirements for the degree of

Doctor of Philosophy

in

Environmental Sciences

by

Simmi Tomar

September 2024

Dissertation Committee:

Dr. Hoori Ajami, Co-Chairperson
Dr. Andrew Gray, Co-Chairperson
Dr. Daniel Hirmas
Dr. Jirka Šimůnek

The Dissertation of Simmi Tomar is approved:

Committee Co-Chairperson

Committee Co-Chairperson

University of California, Riverside

Acknowledgments

I am deeply grateful to my advisor, Daniel Hirmas, whose support and guidance were instrumental in completing this dissertation. His encouragement and wisdom shaped every aspect of this project, and I am thankful for the knowledge I gained under his mentorship. I extend my sincere appreciation to my co-advisors, Hoori Ajami and Andrew Gray, for their invaluable support and contributions that ensured the smooth progress of this work. I would like to thank Bob Graham for his insightful contributions, which provided a crucial foundation for this research. Special thanks to the dedicated team who assisted in extensive fieldwork in remote locations: Matt Cole, Andrew Brown, Karla Jarecke, Marc Dumont, Julio Pachon, Alyssa Duro, Jessica Specht, and Manoj Tomar. I am grateful to the Bureau of Land Management for granting permission to access and sample remote sites in the White Mountains, and to the Natural Resources Conservation Services for providing the essential data. The completion of laboratory analyses would not have been possible without the support of Ruiming Ye, Angie Villalobos, Diane Johnson, Clarissa Caretta, and Swagata Mukhopadhyay. I owe a debt of gratitude to my parents, Mohan Lal and Anju Rajput, and to my husband, Manoj Tomar, whose constant support and encouragement sustained me throughout the challenges and triumphs of completing this dissertation. I would also like to thank my parents, as well as my in-laws, for their incredible support in caring for my newborn. Their willingness to travel overseas to help during this time allowed me to focus on the final phase of my dissertation, and I am deeply grateful for their love. Lastly, I want to express my gratitude to my newborn daughter, Elina, for bringing endless joy and providing the motivation I needed to complete this dissertation.

To my parents, whose support and courage allowed me to pursue my dreams in a foreign land.

ABSTRACT OF THE DISSERTATION

Soil Genesis, Hydrology, and Biogeochemistry of the White Mountains, Eastern California, USA

by

Simmi Tomar

Doctor of Philosophy, Graduate Program in Environmental Sciences
University of California, Riverside, September 2024
Dr. Hoori Ajami, Co-Chairperson
Dr. Andrew Gray, Co-Chairperson

The arid White Mountains in eastern California are characterized by a steep temperature and precipitation gradient making them an ideal site to study the integrated effects of vegetation and climate on soil properties. Soil physical and hydrologic properties are particularly important in this dry environment because they control infiltration, runoff, and the distribution of plant available water. In addition, these mountains are constantly receiving enormous amount of dust from the Owens Lake playa in the adjacent Owens valley. Deposition of dust and incorporation below surface clasts leads to the development of vesicular horizons which decreases percolation of water in the profile because of the non-interconnected nature of these separated pores and, often, the presence of platy structure. Therefore, pedogenic processes like eluviation and illuviation are restricted in the profiles that form these surface horizons. To study the soil morphology and soil development in arid mountains, a transect ranging from 2,200 to 4,300 m was established in 2009 in the WMs on two primary lithologies present in the range—granodiorite and quartzite. Eleven sites

in total were established and at least 4 soil pits were hand dug to 50 cm at each site and morphological information recorded. After examining the 4 pedons, a representative pedon was chosen, excavated further to 1 m, and described and sampled for standard soil physical and chemical analysis. Pedons were described under shrubs or trees when present to fully characterize each site. Soil physical and chemical properties including 1:1 pH, NaF pH, EC, soil organic and inorganic carbon, and particle-size distribution were measured in the lab. Bulk density was measured in horizons where the compliant cavity method could be used and was extrapolated to other horizons through the development of a pedotransfer function for the site. Qualitative soil morphological data collected in the field were integrated and quantified using a profile development index and a vesicular horizon index. Soil moisture and temperature sensors were installed at the site between 2013 and 2022 to monitor the dynamics of soil hydrology along this transect. In addition, geochemical weathering indices were calculated such as the chemical index of alteration, eluvial-illuvial coeffcients, and strain to compare weathering processes in granodiorite and quartzite soils. This study sheds light on the response of soil properties and hydrology to predicted climatic changes in the area and serves as a baseline to measure future regional and global climate change .

Contents

List of Figures

List of Tables

Chapter 1

INTRODUCTION

Drylands occur on all continents and cover about 40% of Earth's terrestrial surface (Ramond et al., 2022). They are defined as the regions where annual potential evapotranspiration (PET) is greater than annual precipitation (P) (i.e., P/PET ratio—also called the aridity index—is less than 0.65) (Hulme, 1996). These arid regions, which currently support about 20% of the world's population, are increasingly prone to desertification due to a rising population (Wickens, 1998; McNeely, 2003). Water is the main limiting factor in drylands, and understanding how rainfall amount and frequency affect ecological processes in these ecosystems is even more important since these regions are more prone to desertification with changing precipitation patterns (Collins et al., 2014).

Due to the extremely dry climate and patchy vegetation cover, these ecosystems are a source of dust and the amount of dust produced from these areas is continually increasing in the western US (Brahney et al., 2013; Hand et al., 2017). Dust carried from low lying areas gets deposited on the windward side of mountains and acts as a parent material for soil

development (Munroe et al., 2024). Several studies have shown the importance of dust in the soil development of these ecosystems (Litaor, 1987; Muhs & Benedict, 2006; Lawrence et al., 2013). The long-term deposition of dust on soil surfaces that traps this eolian sediment forms vesicular (V) horizons which are unique to arid and semi-arid environments (Turk & Graham, 2011; Lebedeva et al., 2009). Vesicular horizons control the soil hydrology of these landscapes by greatly restricting the infiltration of water and promoting surface runoff because of non-interconnected vesicular pores (Anderson et al., 2002). Vesicular horizons occupy over 156,000 km^2 of the western United States and have important hydrological implications as they can create a positive feedback for desertification in these arid regions (Turk & Graham, 2011).

Arid and semi-arid ecosystems hold a significant repository of soil inorganic carbon, contributing approximately 78% and 14% of the global soil inorganic carbon (SIC) pool, respectively (Lal et al., 2021). With the increase in atmospheric CO_2, it is predicted that the carbon sequestration capacity of these arid and semi-arid ecosystems will increase by at least 200 Tg due to CO_2 fertilization (Guo et al., 2022; Grünzweig et al., 2003; Koch et al., 2000). Arid ecosystems are fragile and are vulnerable to climate change (Tu et al., 2023). Yet, the mechanisms and interactions involving soil, dust, climate, hydrology, and geomorphology that contribute to this substantial C reservoir are not well understood.

The White Mountains (WMs) in eastern California are an ideal site to study arid mountain ecosystems. This study was established on an elevational transect ranging from 2,200 to 4,300 m. This elevation gradient provides a range of precipitation and temperatures to compare soil development under different climatic conditions. Additionally, these

mountains are sinks for dust from Owens lake playa (Reheis & Kihl, 1995; Marchand, 1970); the WMs receive about 30 g m^{-2} yr^{-1} of dust, annually (Reheis, 1997). In addition, at the first four elevations (i.e., 2,200–3,100 m), the study sites were situated on contrasting lithologies—granodiorite and quartzite—that exhibit distinct differences in their physical weathering characteristics (Ross, 1965). Granodiorite weathers into grus, while quartzite physically breaks down into coarse, angular rock fragments. Consequently, the interaction of dust with each of these residuum parent materials varies significantly.

Dust influx into weathered granodiorite pedons forms V horizons. In contrast, the clast-supported matrix under quartzite forms large interstitial macropores that translocate dust inputs deeper into the profile, discouraging the formation of V horizons. Vesicular horizons control the hydrology in these water-limited ecosystems by encouraging surface runoff (Valentin, 1994; Meadows et al., 2008; Graham et al., 2008). This effect on soil hydrology is especially important since these mountains are home to the oldest living plant species on Earth—the bristlecone pines (*Pinus longaeva*) (Bentz et al., 2017). Growing in the scarce water conditions near the treeline makes this species vulnerable to changing climate and upward shifts in the mountain range (LaMarche, 1973; Forzieri et al., 2022). The younger seedlings of these trees are susceptible to a high mortality rate due to a warmer climate, as soil moisture availability is predicted to decrease with climate change (Smithers et al., 2021).

The exploratory study, conducted in the WMs, aimed to understand how climate, dust, vegetation, and parent material interact and control the distribution of soils and soil properties in arid mountains. The WMs provide an unique opportunity to tackle this goal.

Chapter 2 is focused on understanding the genesis and distribution of soils in the WMs by quantifying soil development using soil profile development indices. This chapter also explores the development and quantification of V horizons under contrasting lithologies of the WMs in addition to studying the distribution of soil physical and chemical properties. Soil inorganic C, organic C, and dust stocks are calculated and compared under granodiorite and quartzite. Chapter 3 compares soil water movement under granodiorite and quartzite and examines the influence of vegetation and V horizon formation on soil hydrology. This chapter sheds light on the impact of granodiorite and quartzite on the hydrology of these fragile arid ecosystems. Chapter 4 studies the geochemistry of soils developed under quartzite and granodiorite by utilizing chemical weathering indices to quantify soil weathering and eluviation/illuviation in soil profiles. Ultimately, understanding the geochemistry of soils of the WMs will help us understand landscape evolution and hydrological functioning of arid mountains, explore the effects of past climatic conditions, and predict the response to future global change.

References

Anderson, K., Wells, S., & Graham, R. (2002). Pedogenesis of vesicular horizons, Cima Volcanic Field, Mojave Desert, California. *Soil Science Society of America Journal*, *66*(3), 878–887.

Bentz, B. J., Hood, S. M., Hansen, E. M., Vandygriff, J. C., & Mock, K. E. (2017). Defense traits in the long-lived great basin bristlecone pine and resistance to the native herbivore mountain pine beetle. *New Phytologist*, *213*(2), 611-624. doi: https://doi.org/10.1111/nph.14191

Brahney, J., Ballantyne, A., Sievers, C., & Neff, J. (2013). Increasing ca2+ deposition in the western us: The role of mineral aerosols. *Aeolian Research*, *10*, 77-87. doi: https://doi.org/10.1016/j.aeolia.2013.04.003

Collins, S. L., Belnap, J., Grimm, N., Rudgers, J., Dahm, C. N., D'odorico, P., ... others (2014). A multiscale, hierarchical model of pulse dynamics in arid-land ecosystems. *Annual Review of Ecology, Evolution, and Systematics*, *45*, 397–419.

Forzieri, G., Dakos, V., McDowell, N., Alkama, R., & Cescatti, A. (2022, 08). Emerging signals of declining forest resilience under climate change. *Nature*, *608*, 1-6. doi: 10.1038/s41586-022-04959-9

Graham, R. C., Hirmas, D. R., Wood, Y. A., & Amrhein, C. (2008). Large near-surface nitrate pools in soils capped by desert pavement in the Mojave Desert, California. *Geology*, *36*(3), 259–262.

Grünzweig, J., TL, L., Rotenberg, E., Schwartz, A., & Yakir, D. (2003, 05). Carbon sequestration in arid-land forest. *Global Change Biology*, *9*, 791 - 799. doi: 10.1046/j.1365-2486.2003.00612.x

Guo, W., Safeeq, M., Liu, H., Wu, X., Cui, G., Ma, Q., ... Bales, R. C. (2022). Mechanisms controlling carbon sinks in semi-arid mountain ecosystems. *Global Biogeochemical Cycles*, *36*(3), e2021GB007186. doi: https://doi.org/10.1029/2021GB007186

Hand, J., Gill, T., & Schichtel, B. (2017). Spatial and seasonal variability in fine mineral dust and coarse aerosol mass at remote sites across the united states: Fine mineral dust and coarse mass. *Journal of Geophysical Research: Atmospheres*, *122*. doi: 10.1002/2016JD026290

Hulme, M. (1996). Recent climatic change in the world's drylands. *Geophysical Research Letters*, *23*(1), 61–64.

Koch, J., Dayan, U., & Mey-Marom, A. (2000). Inventory of emissions of greenhouse gases in israel. *Water, air, and soil pollution*, *123*, 259–271.

Lal, R., Monger, C., Nave, L., & Smith, P. (2021). The role of soil in regulation of climate. *Philosophical Transactions of the Royal Society B*, *376*.

LaMarche, V. C. (1973). Holocene climatic variations inferred from treeline fluctuations in the White Mountains, California. *Quaternary Research*, *3*(4), 632–660.

Lawrence, C. R., Reynolds, R. L., Ketterer, M. E., & Neff, J. C. (2013). Aeolian controls of soil geochemistry and weathering fluxes in high-elevation ecosystems of

the rocky mountains, colorado. *Geochimica et Cosmochimica Acta*, *107*, 27-46. doi: https://doi.org/10.1016/j.gca.2012.12.023

Lebedeva, M., Golovanov, D., & Inozemtsev, S. (2009, 11). Microfabrics of desert soils of mongolia. *Eurasian Soil Science*, *42*, 1204-1217. doi: 10.1134/S1064229309110027

Litaor, M. (1987, 01). The influence of eolian dust on the genesis of alpine soils in the front range, colorado1. *Soil Science Society of America Journal - SSSAJ*, *51*. doi: 10.2136/sssaj1987.03615995005100010031x

Marchand, D. E. (1970). Soil contamination in the White Mountains, Eastern California. *Geological Society Of America Bulletin*, *81*(8), 2497–2506. doi: 10.1130/0016-7606(1970)81

McNeely, J. (2003). Biodiversity in arid regions: values and perceptions. *Journal of Arid Environments*, *54*(1), 61-70. doi: https://doi.org/10.1006/jare.2001.0890

Meadows, D. G., Young, M. H., & McDonald, E. V. (2008). Influence of relative surface age on hydraulic properties and infiltration on soils associated with desert pavements. *Catena*, *72*(1), 169–178.

Muhs, D. R., & Benedict, J. B. (2006). Eolian additions to late quaternary alpine soils, indian peaks wilderness area, colorado front range. *Arctic, Antarctic, and Alpine Research*, *38*(1), 120–130. doi: 10.1657/1523-0430(2006)038[0120:EATLQA]2.0.CO;2

Munroe, J. S., Santis, A. A., Soderstrom, E. J., Tappa, M. J., & Bauer, A. M. (2024). Mineral dust and pedogenesis in the alpine critical zone. *SOIL*, *10*(1), 167–187. doi: 10.5194/soil-10-167-2024

Ramond, J.-B., Jordaan, K., Díez, B., Heinzelmann, S. M., & Cowan, D. A. (2022). Microbial biogeochemical cycling of nitrogen in arid ecosystems. *Microbiology and Molecular Biology Reviews*, *86*(2), e00109-21. doi: 10.1128/mmbr.00109-21

Reheis, M. C. (1997). Dust deposition downwind of Owens (dry) Lake, 1991-1994: Preliminary findings. *Journal of Geophysical Research Atmospheres*, *102*(22). doi: 10.1029/97jd01967

Reheis, M. C., & Kihl, R. (1995). Dust deposition in southern Nevada and California,1984-1989: Relations to climate, source area, and source lithology. *Journal of Geophysical Research Atmospheres*, *100*, 8893–8918.

Ross, D. C. (1965). *Geology of the independence quadrangle, inyo county, california* (Tech. Rep.). U.S. Geological Survey Bulletin. doi: 10.3133/b1181O

Smithers, B. V., Alongi, F., & North, M. P. (2021). Live fast, die young: Climate shifts may favor great basin bristlecone pine or limber pine in sub-alpine forest establishment. *Forest Ecology and Management*, *494*, 119339. doi: https://doi.org/10.1016/j.foreco.2021.119339

Tu, H., Jiapaer, G., Yu, T., Zhang, L., Chen, B., Lin, K., & Li, X. (2023). Effects of land cover change on vegetation carbon source/sink in arid terrestrial ecosystems of northwest china, 2001–2018. *Remote Sensing*, *15*(9). doi: 10.3390/rs15092471

Turk, J. K., & Graham, R. C. (2011). Distribution and properties of vesicular Horizons in the western United States. *Soil Science Society of America Journal*, *75*(4), 1449–1461.

Valentin, C. (1994). Surface sealing as affected by various rock fragment covers in West Africa. *Catena*, *23*(1-2), 87–97.

Wickens, G. E. (1998). Arid and semi-arid environments of the world. In *Ecophysiology of economic plants in arid and semi-arid lands* (pp. 5–15). Berlin, Heidelberg: Springer Berlin Heidelberg. doi: 10.1007/978-3-662-03700-3_2

Chapter 2

SOIL DISTRIBUTION AND DEVELOPMENT IN THE ARID WHITE MOUNTAINS, CA

Abstract

Arid mountain ecosystems are unique environments characterized by low precipitation, extreme diurnal temperature fluctuations, sparse vegetation, abundant coarse fragments, and eolian dust. These interactions give rise to distinct properties of arid mountain soils. To understand the complex processes driving soil genesis in these regions, an elevational transect, ranging from 2,200 m to 4,300 m in the White Mountains of eastern California was examined focusing on two primary lithologies: granodiorite and quartzite. Soil physical and chemical properties including 1:1 pH, NaF pH, EC, soil organic and in-

organic carbon, and particle-size distribution were measured in the lab. Bulk density was measured in horizons where the compliant cavity method could be used and was extrapolated to other horizons through the development of a pedotransfer function for the site. Qualitative soil morphological data collected in the field were integrated and quantified using a profile development index (PDI) and a vesicular horizon index (VHI). Results indicate that at lower elevations, increased rainfall facilitates rapid water percolation through soil macropores, leading to relatively deep translocation of fines. Conversely, higher elevations receive more precipitation in the form of snowfall, which directs infiltration towards matrix pores resulting in shallower soil development but a matrix that is more influenced by leaching and chemical weathering. Lithology also influences soil formation due to distinct weathering pattern differences between granodiorite and quartzite. Granodiorite weathers to produce grus which ultimately contributes to the development of relatively shallow soils as dust is retained near the surface, while the more resistant quartzite accumulates rock fragments with larger institial macropores that promote deeper soil development. The deposition and subsequent translocation of eolian dust is important in these processes and significantly modifies soil properties. In granodiorite-dominated sites, eolian deposition of dust tends to form V horizons which restricts meteoric water infiltration and limits translocation leading to a greater concentration of dust near the surface. In contrast, quartzite pedons exhibited deeper soil development due to their capacity for translocation of dust via preferential flow through interstitial macropores. These findings enhance our understanding of soil genesis in arid mountain environments and highlight the combined impact of climatic and lithologic factors on soil formation. The use of morphological indices of soil develop-

ment in combination with standard chemical indicators of weathering allowed differences in long-term hydrological processes (i.e., preferential flow vs matrix flow) to be distinguished at this site and may serve as a model for similar studies in the future.

2.1 Introduction

Arid and semi-arid ecosystems cover about a third of the Earth's surface, with arid and semi-arid lands covering approximately 12.1 and 17.7% of the world area (Huenneke, 2001; Parsons & Abrahams, 2009). A significant proportion of these areas are occupied by desert mountains; in the southwestern United States, desert mountains cover around 38% of desert lands (Clements et al., 1957). Although, in general, arid and semi-arid regions are a significant repository of soil inorganic carbon (SIC) contributing approximately 78% and 14% of the global SIC stocks (Lal et al., 2021), arid mountains have the potential to contribute up to an additional 1,485 Pg significantly increasing the estimate of total SIC (Hirmas et al., 2011; Harrison & Dorn, 2014). However, the mechanisms and interactions of soil, dust, climate, hydrology, and geomorphology that are responsible for this massive pool remain poorly understood.

Dust is frequently transported from basin floors (e.g., playas) and alluvial fans to arid and semi-arid mountain ranges (Marchand, 1970; J. A. Young & Evans, 1986; Reheis & Kihl, 1995; Ziyaee et al., 2018). The southern Fry Mountains in the Mojave Desert of California, for instance, has been reported to have trapped an average of 41 kg m^{-2} silicate dust reaching a maximum of 156 kg m^{-2} on the windward side of the range (Hirmas et al., 2011). Eolian dust plays a central role in the formation of desert pavements and vesicular

horizons, both of which are prevalent features in arid regions; approximately 50% of arid lands in North America are covered with desert pavement (Evenari et al., 1985). Desert pavement—a layer of gravels and stones tightly packed and embedded in the land surfaces—forms when dust accumulates beneath and rafts upward a surface layer of rock fragments (McFadden et al., 1987). The layer of dust accumulating beneath surface rock fragments often contain vesicular pores formed as air bubbles get trapped by infiltrating water and deform the plastic silty material around semi-spherical, non-interconnected voids. Soil layers with these properties are known as vesicular (V) horizons and their genesis is linked to the formation of desert pavements (McFadden et al., 1998). The presence of desert pavement promotes the formation of V horizons; these horizons are distinctive morphological features of arid soils, associated with rough, rocky surfaces that trap eolian dust (Valentin, 1994; Meadows et al., 2008; Turk & Graham, 2011).

Because the parent material for V horizons is deposited from eolian processes, these layers are concentrated with silt compared to underlying soil horizons (Cooke, 1970; Dixon, 1994). The embedding of the surface clasts is an important part of the formation of V horizons as it seals the surface and prevents the escape of air bubbles formed from subsequent wetting and drying cycles. The wetting of the surface leads to the entrapment of air below the wetting front and forms isolated air bubbles that, with subsequent drying, forms vesicular pores in the matrix. Overtime, this process repeats leading to an elongation of the vesicular pores and eventual collapse to form platy structure (Turk & Graham, 2011). Development of vesicular horizons affects the soil hydrology by reducing soil infiltration rates

due to the presence of unconnected vesicles in the horizon (Valentin, 1994; Turk & Graham, 2011) and promoting surface runoff (Reheis & Kihl, 1995).

In arid mountains, clasts are formed by the physical weathering and/or transport of bedrock. Eolian dust gets deposited between the clasts and transported deeper into the profile by infiltrating water (Marchand, 1973; Blair, 1999). In arid mountains of the Mojave Desert, dust has been reported to translocate to a depth of >1 m between coarse clasts and into weathered and fractured bedrock (Hirmas et al., 2011). Because eolian dust is often laden with salts, carbonate, and clay particles (Reheis & Kihl, 1995), the trapping of dust by arid mountain surfaces facilitates the formation of calcic, petrocalcic, and argillic horizons in these environments (McFadden & Tinsley, 1985). Precipitation flushes these salts, carbonates and clay minerals through the interclast macropores and concentrates them deep in rock fractures. The presence of these horizons in arid mountain landforms indicates geomorphic stability because these horizons need a long period to form especially in such water-limited environments (Hirmas et al., 2011). The stability of these landforms have allowed significant quantities of dust to be incorporated into arid mountain soils with profound implications on geochemical cycling. For example, in the Catalina Critical Zone Observatory in Southern Arizona, the dust fraction is estimated to contribute 2% to 21% by mass in desert soils, with the interaction of dust, climate, and topography significantly influencing the nutrient cycling and geochemical evolution of the soils (Lybrand & Rasmussen, 2018).

Arid ecosystems of the southwestern US are sensitive to climate change because most of the plant species live near the edge of their physiological water needs (Munson

et al., 2011). Therefore, only slight changes in precipitation and temperature may change species cover, composition, and geographic distribution (Archer & Predick, 2008). Climate change will affect the plant zones asscociated with arid lands, with treelines moving up in elevation in response to warmer and drier conditions (LaMarche, 1973; Gaire et al., 2014). As a response to future climate change, species distributions are expected to shift, such as big sagebrush (*Artemisia tridentata*) moving northward and the spread of creosote bush (*Larrea tridentata*) in areas currently occupied by big sagebrush (S. L. Shafer et al., 2001). Due to climate-induced increases in temperature, plant mortality rates are higher than regeneration rates, which has significant negative ecological impacts such as reduced carbon sequestration, changes in species composition and diversity, nutrient cycling, and altered ecohydrological patterns of runoff and erosion (Dale et al., 2001; Allen, 2007).

A large elevational range provides the opportunity for studying future climate change in arid mountains because it provides an environmental gradient, to observe how vegetation, soil, and hydrology respond to varying temperatures and precipitation. This range can serve as a natural laboratory, providing insights into how different ecosystems may adapt to or be impacted by climate change, making it a valuable tool for understanding and predicting the effects of global warming on mountainous regions. One mountain range where the effects of future climate change are likely to be important is the White Mountains (WMs) of eastern California which span a considerable range in elevation (2,134 to 3,048 m) and are home to the ancient bristlecone pines (*Pinus longaeva*) (Schulman, 1958; Wright & Mooney, 1965). A large amount of dust containing soluble salt, gypsum, and fine soil particles has been deposited on the WMs with an average rate of approximately 5-10 g m^{-2} yr^{-1}

from Owens lake playa (Reheis, 1997). Approximately 30% of the very fine sand and 50% of the silt content in soils of the WMs are derived from eolian processes (Marchand, 1970). The dominant lithologies in the WMs are granodiorite (coarse-grained intrusive plutonic rock), quartzite, and dolomite (Marchand, 1973); the average surface rock cover is estimated to be 27% on granodiorite, 54% on quartzite, and 77% on dolomite (Wright & Mooney, 1965). Eolian dust is an important component in the soils formed in these regions; however, its presence adds to the complexity in understanding soil genesis in these environments since clay, soluble salts, and carbonate are added to the surface throughout soil development (McFadden et al., 1987). For instance, in northern Arizona, south-facing slopes of cinndercones in the San Francisco volcanic field area have vegetation cover linked with higher dust trapping potential leading to the formation of argillic horizons; dust accumulation on the southern slopes increases the water holding capacity and enhances soil physical and chemical weathering resulting in more developed soils on the south-facing slopes compared to north facing slopes (Rasmussen et al., 2017). Dust-influenced soils of the WMs, varying lithology, different vegetation zones across the transect and both snowmelt and rainfall driven hydrologic cycles offer unique opportunities to study soil development and processes in arid mountain ecosystems. The overall goal of this project is to understand how the interactions of climate, dust, vegetation, and parent material control the distribution of soils and soil properties in the arid WMs and how future climate change might influence these interactions, altering the water cycle, soil-landscape evolution, and carbon dynamics in these ecosystems.

2.2 Methods

2.2.1 Study site

The arid WMs in eastern California lie immediately to the east of the Sierra Nevada range and extend approximately 60 km in the north-south direction with a width of about 20-25 km; they are separated from the Sierras by the upper Owens valley (Rundel, 2008) (Fig. 2.1a). The range rises rapidly from the valley floor at 1,220 m to more than 4,300 m at WM peak—the third highest summit in California (Hall, 1991). The WMs are in the rain shadow of the Sierras and receive only approximately one-third of the precipitation received by the west side of the Sierras at the same elevation (Wright & Mooney, 1965). As moist air from the Pacific is forced upwards on the westward side of the Sierras, it cools adiabatically resulting in significant precipitation. After summiting the Sierras, the air is compressed and warmed adiabatically at a steeper rate on the lee side than it cooled on the windward side resulting in warmer and less humid air on the western side of the WMs. This strong orographic rain shadow effect is responsible for the arid conditions in the WMs (North et al., 2009). Mean annual precipitation (MAP) at the lower elevations ranges from 125–150 mm to 508 mm or higher at the upper elevations (Hall, 1991). Mean annual precipitation determined for each site from 1981–2010 normals in the PRISM dataset (PRISM Climate Group, 2014) is shown in Table 2.1. In addition to MAP, the snow water equivalent (SWE)—a measure of the amount of water contained in the peak snowpack—was determined using Landsat 5 data between 2000–2016 (Margulis et al., 2016). The mean peak SWE value was found for each year and averaged for the years 2000-2016 (Table 2.1).

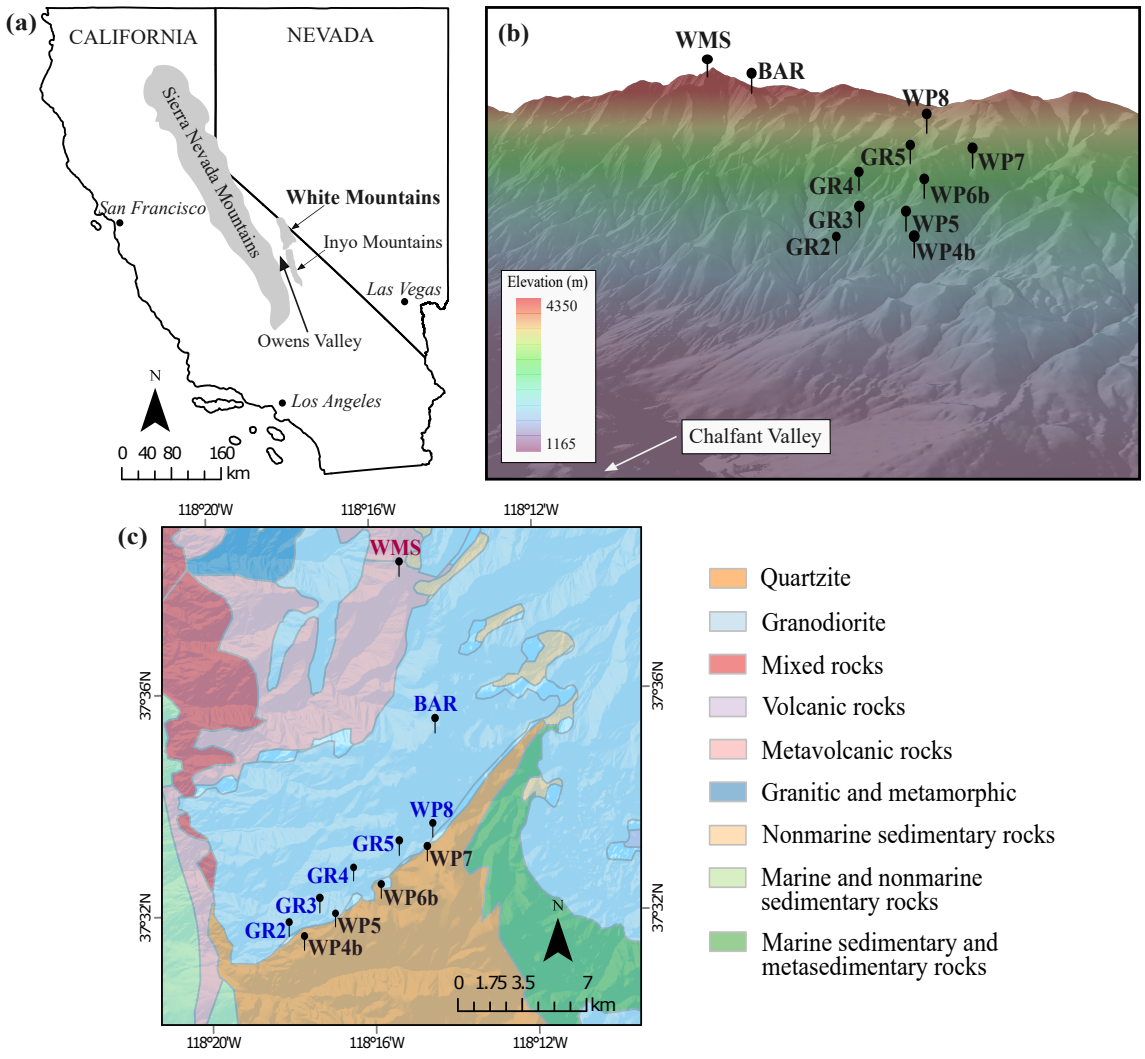

Figure 2.1: a) Location of the WMs relative to the Sierra Nevada Mountains. b) Locations of the study sites across the elevational transect. Chalfant Valley shown in panel b is part of the Owens Valley adjacent to the study area. c) The geologic map of the study area shows that the sites are primarily located on two lithologies: granodiorite and quartzite. Additionally, the highest elevation site (WMS) is located on metavolcanic rock. Geologic units were obtained from (USGS, 2021)

.

Vegetation in the WMs is broadly divided into the following four major plant zones based on elevation beginning with desert scrub, pinyon wood-land, subalpine forest, and alpine tundra (Mooney, 1973). Above 3,500 meters, the alpine zone is characterized by non forested areas, dominated by broad-leaved herbaceous perennials (53%), graminoid perennials (22%) and mats and cushions (11%). Woody shrubs and annuals are less common in this area, as they are more typically found in communities at lower elevations (Rundel, 2008).

2.2.2 Fieldwork and sampling layout

The WMs are characterized by a steep temperature and precipitation gradient. As such, this range is an ideal site to study the integrated effects of biota, lithology, and climate on the distribution of arid mountain soils. A transect ranging from 2,200 to 4,300 m was established in 2009 on three different parent materials present in the range (Fig. 2.1c). Eleven sites in total were established: six were located on granodiorite (GR2, GR3, GR4, GR5, WP8, and BAR), four on quartzite (WP4b, WP5, WP6b, and WP7), and one on metavolcanic parent materials (WMS) (Fig. 2.1 and Table 2.1). These sites fall within three of the four vegetation zones defined by Mooney (1973) across the WMs (Table 2.1). The soil sampling design at each of the sites is shown in Fig. 2.2a. At each site, soil morphological information was recorded from a minimum of 4 hand-dug pits (approximately 30 cm wide $\times$ 40 cm long $\times$ 50 cm deep). One of the 4 pits was chosen as a representative soil profile, excavated further to 1 m, described following Schoeneberger et al. (2012), classified using US Soil Taxonomy (Soil Survey Staff, 2022), and sampled for standard soil physical and chemical analysis. In addition, pedons were described under shrubs and trees when present

Table 2.1: Elevation, lithology, vegetation, mean annual precipitation (MAP), and mean peak snow water equivalent (SWE) of the sites used in this study. Mean annual precipitation was determined for each site from 1981–2010 normals in the PRISM dataset (PRISM Climate Group, 2014). Mean peak SWE was determined using Landsat 5 data between 2000–2016 (Margulis et al., 2016)

.

Site	Elevation (m)	Lithology	Vegetation	MAP (mm)	SWE (mm)
GR2	2,200	Granodiorite	Pinyon-woodland	232	34
WP4b	2,200	Quartzite	Pinyon-woodland	232	34
GR3	2,500	Granodiorite	Pinyon-woodland	282	58
WP5	2,500	Quartzite	Pinyon-woodland	282	58
GR4	2,800	Granodiorite	Pinyon-woodland	367	103
WP6b	2,800	Quartzite	Pinyon-woodland	367	103
GR5	3,100	Granodiorite	Sub-alpine	397	100
WP7	3,100	Quartzite	Sub-alpine	397	100
WP8	3,700	Granodiorite	Alpine	557	254
BAR	4,000	Granodiorite	Alpine	557	–
WMS	4,300	Metavolcanic	Alpine	584	357

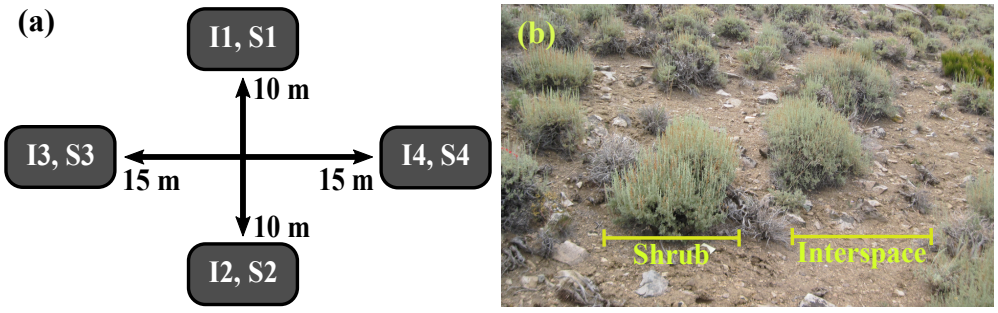

Figure 2.2: a) Soil sampling design at each site. A reference center point was chosen and used to locate four endpoints: Interspace and shrub sites upslope (I1, S1) and downslope (I2, S2) were 10 m from the center; interspace and shrub sites along the contour were 15 m to the left (I3, S3) and right (I4, S4) of the center point. Soils were sampled under shrub, interspace, and tree (if present) at each site. b) Photo showing the shrub and interspace distribution at the GR5 site.

to fully characterize each site (Fig. 2.2b). Due to time and logistical constraints, bulk density (BD) was sampled with the plaster cast method (Frisbie et al., 2014) in triplicate on 47 horizons across the study site. This method is a good alternative for measuring soil bulk density in situations where conventional methods like clod or core sampling are not feasible, such as in loose or rocky soil. Horizontal shelves were carved into the soil profile at each horizon, cardboard rings were inserted from the top down on these shelves, soil material was excavated within and below the rings, and dental plaster was used to fill the resulting cavity.

2.2.3 Laboratory analyses of soil properties

Soil material sampled for bulk density was dried in the laboratory at 105°C and weighed. Volumes of the plaster casts were determined via water displacement and used to calculate dry bulk density of the sample following Frisbie et al. (2014). The bulk density sample was sieved to separate the fine-earth (<2 mm) from the coarse (>2 mm) fraction and the resulting values used to calculate the fine-earth bulk density (ρ_{fe}) following Grossman & Reinsch (2002).

Bulk soil samples collected from the field were sieved to separate fine-earth from coarse particles. The mass of each of these two fractions were recorded and combined with the volume fraction of coarse gravel, cobbles, and stones estimated using percentage charts in the field to calculate a total coarse volume fraction (f_{cf}) in the soil as:

$$f_{\mathrm{cf}} = \frac{m_c \rho_s}{m_s \rho_p}(1 - f_{\mathrm{gcs}}) + f_{\mathrm{gcs}} \tag{2.1}$$

where m_c is the mass of coarse particles in the bulk sample, m_s is the combined masses of the fine-earth and coarse fractions in the sample, ρ_s is the dry bulk density of the sample determined from the plaster cast compliant cavity method, ρ_p is the particle density (assumed to be 2.65 g cm^{-3}), and f_{gcs} is the combined field-estimated volume fraction of coarse gravel, cobbles, and stones.

Bulk samples were analyzed for particle-size distribution (PSD) using the integral suspension pressure (ISP) method following Durner et al. (2017). The ISP method quasi-continuously records the pressure of a settling, dispersed soil suspension with a pressure transducer (PARIO, METER Group, Pullman, WA) at a fixed depth below the height of the suspension. Samples were pretreated to remove soil organic matter with 30% H_2O_2 following Gee & Or (2002). Samples that effervesced when tested with 1 N HCl were pretreated to remove soil carbonates using 1 M NaOAc buffered at pH 5 (Gee & Or, 2002). Pretreated samples were rinsed with deionized water using a filtration aparatus to remove residual pretreatment reagents and dispersed in 5 g L^{-1} $(NaPO_3)_6$ prior to analysis.

In order to account for slight variations in temperature during the procedure, the particle diameter (d_p) associated with the ith measurement time (t_i) recorded by the PARIO was calculated using the Stoke's law:

$$dp(t_i) = \left\{ \frac{18\eta_i L}{(\rho_p - \rho_{\mathrm{sol}_i})g} \left[\frac{18\eta_{i-1} L}{(\rho_p - \rho_{\mathrm{sol}_{i-1}}) g d_{p_{i-1}}^2} + t_i - t_{i-1} \right]^{-1} \right\}^{\frac{1}{2}} \tag{2.2}$$

where L is the depth of the pressure transducer below the height of the suspension, g is the acceleration due to gravity, and η and ρ_{sol} are the dynamic viscosity and density of the solution, respectively, calculated using the temperature at the ith and ith-1 time measurement

and concentration of the dispersant following Durner et al. (2017). The mass fraction of the particles corresponding to the diameters of each time interval (f_i) was calculated following Durner et al. (2017) as:

$$f_i = \frac{C_{p_i} V}{m_p} \tag{2.3}$$

where C_{p_i} is the concentration of particles with effective particle diameters between $d_p(t_{i-1})$ and $d_p(t_i)$, V is the total suspension volume, and m_p is the total dry mass of particles in the suspension. In Eq. 2.3, C_p is determined as:

$$C_p = \frac{\Delta P}{\left(1 - \frac{\rho_{\text{sol}}}{\rho_p}\right) g L} \tag{2.4}$$

where ΔP is the difference in consecutive pressure measurements. After recording settling suspension pressures for 24 h following mixing, samples were sieved for sand. The sand fraction of each sample was dried, separated by sieving into very fine (50-100 μm), fine (100-250 μm), medium (250-500 μm), coarse (500-1000 μm), and very coarse (1000-2000 μm) sand, and the masses recorded. The mass fraction of particles with d_{p_i} diameters determined with the PARIO were replaced with the sieved mass fractions of sand. To preserve mass balance, the total sand concentration ($C_{p_{\text{sand}}}$) was used to define a scale factor (f_s) as:

$$f_s = \frac{C_{p_0} - C_{p_{\text{sand}}}}{C_{p_{\text{silt+clay}}}} \tag{2.5}$$

where C_{p_0} is the total concentration of particles per volume in the sedimentation cylinder and $C_{p_{\text{silt+clay}}}$ is the sum of the C_{p_i} values for particles smaller than sand to adjust their total concentration such that $\sum C_{p_i} = C_{p_0}$.

Soil pH and electrical conductivity (EC) were determined on 1:1 extracts of each sample following Soil Survey Laboratory Staff (2022). To qualitatively assess the amount of amorphous soil material in each sample, pH was also determined 2 min after mixing 1 g of soil with 50 mL of 1 N NaF initially adjusted to a pH of 7.5-7.8 (Soil Survey Laboratory Staff, 2022). Total carbon (TC) was measured on an elemental analyzer (Flash EA1112, CE Elantech, Inc., Lakewood, NJ). Samples that reacted with 1 N HCl were analyzed for soil inorganic carbon (SIC) by coulometric titration (CM5017, UIC Inc., Joliet, IL) following Engleman et al. (1985). Soil organic carbon (SOC) was determined as the difference between TC and SIC.

2.2.4 Data analyses

Calculation of morphological indices

Profile development (PDI) and vesicular horizon indices (VHI) were used to quantify soil and vesicular horizon development from profile descriptions. Profile development indices have been used to quantify pedogenic development in soils based on field measured soil properties since their introduction by Bilzi & Ciolkosz (1977) and Harden (1982). Six properties were used in the PDI calculations including particle-size, calcium carbonate equivalent (CCE), soil color (i.e., in the CIELAB color space), clay films, pedogenic carbonate morphology, and silica development stages as these soil properties are relevant to pedogenic processes in arid mountains. For each horizon, PDI scores were assigned following the approach proposed by Koop et al. (2020). Properties were compared to the same properties in layers directly above or below the horizon being scored. Property scores were

converted to a standardized point system, ranging from 0 to 1 to ensure equal weighting when combined with scores for different properties. To calculate the PDI for a soil profile, scores for each soil horizon were weighted by horizon thickness and divided by the total pedon depth. Although based on the same logic, the PDI in this work differed slightly from Koop et al. (2020) as follows.

First, V horizons and transitional or mixed horizons such as AV or A/V were defined as eluvial horizons since clay accumulation was only observed in the subsurface horizons. In addition, Koop et al. (2020) compared soil color of darkened surface horizons due to organic matter accumulation with lighter and redder subsurface horizons. Since the V, AV or A/V horizons occur at or near the surface but were generally lighter than B horizons, they were assigned 'NA' for the respective horizon development index (HDI) to avoid penalizing the V horizons for not developing darker color. Second, two additional soil properties were added (i.e., pedogenic carbonate morphology and silica development stage). For the pedogenic carbonate morphology, we followed the criteria outlined by Schoeneberger et al. (2012) to assign carbonate stages for coarse fragment matrices. These stages were then normalized by dividing them by 6 (representing the maximum possible stage of pedogenic carbonate development) resulting in values scaled between 0 and 1 for each horizon. Silica development stages were assigned based on criteria indicating the presence of cementation due to opaline silica or the recording of a subordinate 'q' designation within the horizon. Horizons meeting these criteria were assigned a value of 1, while those that did not were given a value of 0.

Morphological descriptions of vesicular pore size and quantity were given numeric values following the scoring system proposed by Turk & Graham (2011). However, unlike Turk & Graham (2011), the VHI in this work was calculated using the normalized score without multiplying by the thickness of the V horizons. This was done to isolate and assess the developmental character of the V horizons without reference to the thickness. In cases where multiple V horizons were recorded (e.g., V1 and V2), we calculated the VHI separately and took the average of the relevant horizons to get a single VHI for the pedon.

Extrapolating bulk density measurements

We developed a pedotransfer funcion (PTF) to extrapolate bulk density to horizons not sampled with the compliant cavity plaster cast method. A backward selection, Akaike information criterion (AIC)-based stepwise linear model (Venables & Ripley, 2002) was fit to the measured fine-earth bulk density data using the volume fractions of coarse gravel and cobbles estimated in the field, percent sand, horizon midpoint depth and their interation terms. Gravel and cobble volume fraction data were square root- and log-transformed, respectively, after histograms were visually inspected for normality. Model fit was assessed using the coefficient of determination (R^2) and root mean square error (RMSE) from a leave-one-out cross validation (LOOCV) (Hastie et al., 2009). The resulting PTF was applied across the study sites to obtain fine-earth bulk density for each horizon not measured with the plaster cast method.

Particle-size distribution

To assess the origin of different soil particle sizes (e.g., residuum vs eolian), high-resolution PSD data from the ISP method were fit with a double Weibull cumulative distribution function of the form:

$$F(d_p) = 1 - w \exp\left[-\left(\frac{d_p}{\lambda_1}\right)^{k_1}\right] + (w-1)\exp\left[-\left(\frac{d_p}{\lambda_2}\right)^{k_2}\right] \tag{2.6}$$

where $F(d_p)$ is the cumulative particle-size mass fraction, the subscripts 1 and 2 refer to the fine and coarse domains, respectively, of the bimodal distribution, λ and k are the scale and shape parameters of the distribution, respectively, for each domain (treated as fitting parameters), and w is the weighting coefficient with values between 0 and 1 that represents the contribution of the first domain to the cumulative PSD. To assess the appropriateness of fitting Eq. 2.6 to the PSD data, we additionally fit a unimodal Weibull distribution to the $F(d_p)$ data from each sample and compared the difference in the AIC of the two models following Burnham & Anderson (2004). Values of this difference criterion greater than 4 supported the use of Eq. 2.6 (Burnham & Anderson, 2004) and confirmed bimodality of the PSD.

The quantity of eolian material in each sample was assessed as the weighted cumulative distribution function of the fine particle-size domain:

$$f_{\text{em}} = w\left\{1 - \exp\left[-\left(\frac{d_p}{\lambda_1}\right)^{k_1}\right]\right\} \tag{2.7}$$

where f_{em} is the mass fraction of the sample likely attributable to eolian (i.e., dust) deposition and vertical translocation. A similar PSD-based approach was used by Hirmas & Graham (2011) to characterize dust contributions in the fine-earth fraction of arid mountain soils in the Mojave Desert. Dust stocks (C_{em}) of each pedon were calculated using the mass fraction of dust in the fine-earth sample, the fine-earth bulk density, and the volume fraction of coarse fragments in the soil as:

$$C_{\mathrm{em}} = \sum_{i=1}^{h} f_{\mathrm{em}_i} \rho_{\mathrm{fe}_i} (1 - f_{\mathrm{cf}_i}) T_i \tag{2.8}$$

where T_i is the thickness of the ith horizon in the profile. To compare pedons with different lower depths across the WMs, Eq. 2.8 was calculated for h number of horizons in the profile above 50 cm; if a horizon extended above and below 50 cm, it was truncated at 50 cm in the calculation. The resulting values represent dust stocks in the upper 50 cm of each pedon in units of kg m^{-2}. In addition, the geometric mean particle diameter (GMD) of each PSD was calculated to assess lithologic differences in residuum contribution to the fine-earth fraction of each soil.

Soil carbon stocks

Total inorganic (f_{sic}) and organic carbon (f_{soc}) mass fractions were converted into carbon concentrations on a volume basis by multiplying the respective carbon fraction with fine-earth bulk density, volume fraction of fine earth ($1 - f_{\mathrm{cf}}$), and horizon thickness. As with dust (Eq. 2.8), volume fractions of soil carbon were summed to 50 cm to calculate stocks of SIC or SOC in the upper 50 cm of each pedon in units of kg m^{-2}.

Statistical analyses

Linear models were fit to soil pedon data aggregated by elevation, lithology, and/or vegetation. Coefficients of determination were used to evaluate the fraction of the variability in the response variables explained by the predictor variables. Full model and slope comparisons were conducted for fits to different subsets of the data following the methods described by Neter & Wasserman (1974) and Edwards (1976), respectively. All graphical plotting of the data and statistical analyses were conducted using R version 4.4.0 (R Core Team, 2024).

2.3 Results

2.3.1 Soil classification

Six soil taxonomic subgroups were identified in this study and exhibited distinct patterns across different elevations, lithologies, and vegetation (Table 2.2). The most commonly occurring subgroups at lower elevations are Typic Haplocambids and Typic Haplargids, with Typic Haplocryids and Typic Haplorthels being the only subgroups at 4,000 and 4,300 m, respectively. Most of the soil types identified were more common at granodiorite sites with the exception of Typic Haplocambids, which were more commonly found under quartzite (47.2%) than granodiorite (11.5%). Although Bt horizons under quartzite were thicker and more abundant than granodiorite, they did not meet the criteria for argillic horizons. A higher frequency of calcic and argillic horizons were observed under granodiorite compared to quartzite. Soils were classified as Typic Haplargids at 63.5% of granodiorite

Table 2.2: Frequency distribution (%) of soil types across elevation, lithology and vegetation classified to the subgroup level of US Soil Taxonomy. Soil types included Typic Haplocambids (THD), Typic Haplocalcids (THC), Typic Haplargids (THA), Typic Calciargids (TCA), Typic Haplocryids (THY), and Typic Haplorthels (THL).

Environment	**THD**	**THC**	**THA**	**TCA**	**THY**	**THL**
Elevation (m)						
2,200	6.3	31.3	37.5	25.0	0	0
2,500	10.0	0	75.0	15.0	0	0
2,800	54.2	0	45.8	0	0	0
3,100	31.3	0	68.8	0	0	0
3,700	25	0	75.0	0	0	0
4,000	0	0	0	0	100.0	0
4,300	0	0	0	0	0	100.0
Lithology						
Granodiorite	11.5	7.7	63.5	9.6	7.7	0
Quartzite	47.2	2.8	44.4	5.6	0	0
Metavolcanic	0	0	0	0	0	100
Vegetation						
Interspace	20.5	2.3	50.0	9.1	9.1	9.1
Shrub	25.0	11.1	55.6	8.3	0	0
Tree	41.7	0	58.3	0	0	0

site compared to 44.4% under quartzite. Additionally, Typic Halplargids were the most common subgroup in all three vegetation types. Typic Haplocryids and Typic Haplorthels only occurred under interspaces. Soils under trees in the study were classified exclusively into Typic Haplocambids and Typic Haplargids subgroups.

2.3.2 Soil morphological indices

Profile development indices significantly declined ($H_0 : \beta_1 = 0$; $P < 0.01$) from the low to high elevation explaining approximately 63% of the variation in PDI aggregated across lithology-vegetation combinations (Fig. 2.3a). Both granodiorite ($R^2 = 0.43$; $H_0 : \beta_{1,\mathrm{g}} = 0$; $P < 0.05$) and quartzite pedons ($R^2 = 0.77$; $H_0 : \beta_{1,\mathrm{q}} = 0$; $P < 0.01$) showed significant declines in morphological development with increasing elevation (Fig. 2.3b) with

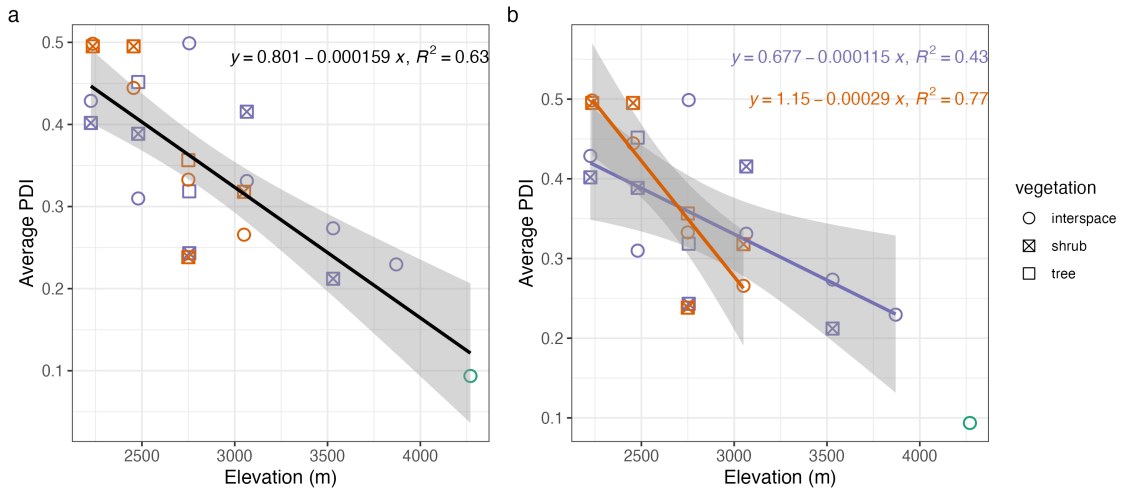

Figure 2.3: Profile development index (PDI) averaged across the 4 replicates of each lithology-vegetation combination showing (a) the overall negative linear trend and (b) the linear trends for granodiorite (purple) and quartzite (orange) separately. The green circle in the plot represents the interspace metavolcanic site (WMS).

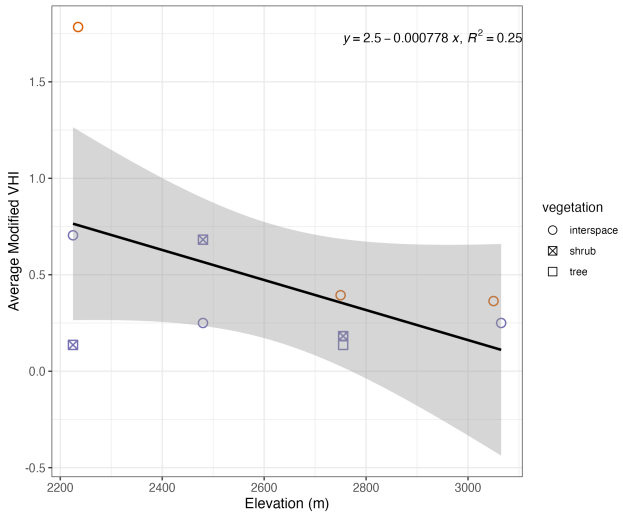

Figure 2.4: Elevational trends in vesicular horizon index (VHI) averaged across the 4 replicates of each lithology-vegetation cover combination. V horizons were not observed in the sites above 3,100 m. Points in purple represent granodiorite and points in orange represent quartzite.

the slope steeper for quartzite than granodiorite although not significantly so ($H_0 : \beta_{1,\mathrm{g}} = \beta_{1,\mathrm{q}}$; $P = 0.14$). Indeed, no significant differences were found when comparing the overall negative trend in PDI (i.e., Fig. 2.3a) to the trends with elevation observed when aggregating the data by lithology or vegetation cover suggesting that elevation-induced changes in precipitation and temperature are likely controlling the morphological development of soils across the range although vegetation and, especially, lithology may be modifying these trends more locally.

Vesicular horizon indices showed a moderately significant decline with increasing elevation ($R^2 = 0.25$; $H_0 : \beta_1 = 0$; $P = 0.07$) although this trend was partly driven by an anomalously high value observed for quartzite at 2,200 m (Fig. 2.4). V horizons were observed in 17 pedons under granodiorite and in 8 pedons under quartzite, out of a total of 40 and 36 pedons, respectively. At elevations where V horizons occurred on quartzite

Table 2.3: Coefficients, standard error (SE), and P-values for the stepwise linear model (PTF) fit (with R^2=0.42 and P=0.02) to the measured fine-earth bulk density data. Gravel and cobble volume fraction data were square root and log transformed, respectively. The sand fraction is the weight percentage of the fine-earth fraction. Depth is the midpoint of a given horizon.

Variable	**Coefficient**	**SE**	P**-value**
Intercept	1.67	0.510	<0.01
Gravel	-0.101	0.0651	0.13
Cobbles	0.278	0.493	0.58
Sand	-0.00858	0.00624	0.18
Depth	-0.0183	0.0138	0.19
Gravel × sand	0.00163	0.000820	0.06
Cobbles × sand	-0.00437	0.00697	0.53
Gravel × depth	-0.00157	0.00101	0.13
Cobbles × depth	0.0242	0.0150	0.12
Sand × depth	0.000384	0.000182	<0.01
Cobbles × sand × depth	-0.000299	0.000196	0.14

(i.e., 2,200, 2,800, and 3,100 m), average VHIs were consistently larger than for V horizons that occurred on granodiorite (Fig. 2.4). Above 3,100 m, V horizons were not observed at the study site. Compared to shrub vegetation, pedons in interspace areas were consistently more likely to have V horizons and, except for the 2,500 m elevation, had more strongly expressed vesicular morphology (Fig. 2.4).

2.3.3 Soil physical and chemical properties

The coefficients of the linear model for the fine-earth bulk density are shown in Table 2.3. Ignoring the intercept, the most significant terms in the final stepwise model were the interactions between sand and depth and between gravel and sand followed by cobbles and depth, gravel and depth, and cobbles, sand, and depth. While the relationship between sand and bulk density is well established (Hillel, 1998), the gravel and cobble results indicate that the coarse fraction is also an important determinant of fine-earth bulk

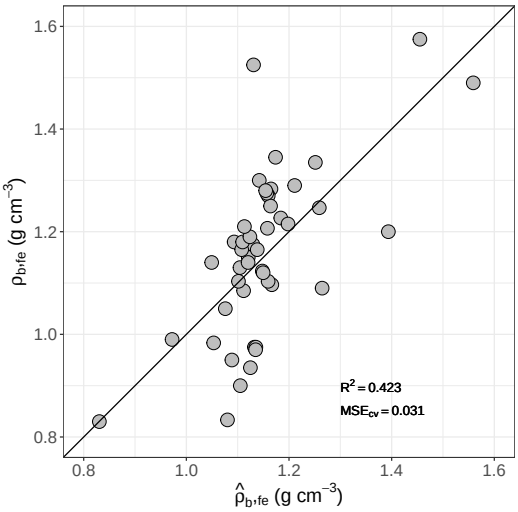

Figure 2.5: Plot showing observed fine-earth bulk density against the fine-earth bulk density predicted using the PTF model developed in this study. The solid black line represents the 1:1 line, where the predicted values are equal to actual values.

density in the WMs. The model was cross-validated using the LOOCV method (Hastie et al., 2009) which resulted in a mean squared error for the cross-validation (MSE_{cv}) of 0.031 g cm^{-3} (Fig. 2.5). Figure 2.5 shows the linear relationship between observed and predicted fine-earth bulk density. The intercept and slope were not significantly different than 0 and 1, respectively ($P = 0.02$), indicating that model was unbaised over the range of fine-earth bulk densities observed in the WMs and that differences between observed and predicted values is only due to unexplained variance (Piñeiro et al., 2008).

Figure 2.6 plots GMD as a function of depth for individual horizons across the study. A clear separation in the geometric mean size of fine-earth particles is evident between quartzite and granodiorite. The majority of granodiorite samples (66.84%) showed average particle diameters between 100 and 300 μm while most of the quartzite samples (65.81%) were less than 100 μm. Quartzite samples showed slightly coarser textures in

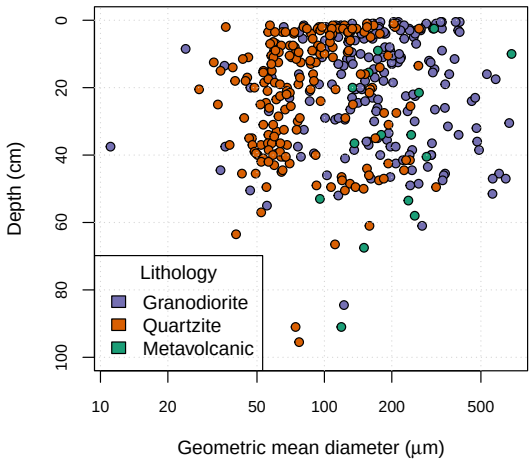

Figure 2.6: Depth trends in the geometric mean particle diameter (GMD) showing results of each horizon measured in this study excluding two samples that were sampled below 100 cm.

the upper 5-10 cm of the profiles on average compared to below that depth. In contrast, granodiorite samples showed no obvious trend with depth in the GMD data. Metavolcanic samples from the WMS site showed a similar distribution to the granodiorite sites of lower elevations.

Dust stocks varied from 3.1–60.8 kg m^{-2} across the transect (Fig. 2.7). Granodiorite pedons had more dust in the 50 cm depth (20.04 kg m^{-2}) compared to quartzite (8.22 kg m^{-2}). Interspace pedons had higher amounts of dust (20.02 kg m^{-2}) than shrub pedons (11.15 kg m^{-2}). Granodiorite pedons had more SOC (2.45 kg m^{-2}) and SIC (0.85 kg m^{-2}) in the 50 cm depth compared to quartzite (1.90 kg m^{-2} SOC; 0.02 kg m^{-2} SIC). Soil organic carbon stocks increased with elevation until 3,100 m likely due to the decrease in vegetation above that elevation (Fig. 2.8a). That is, there is only one shrub site

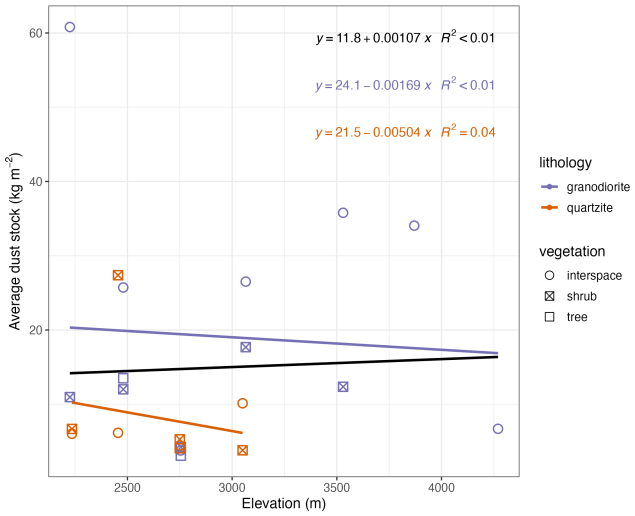

Figure 2.7: This plot illustrates the relationship between elevation (m) and average dust stock (kg m^{-2}) in the upper 50 cm of soil across different lithologies (Granodiorite and Quartzite). The black linear trend line is for the general data, which shows that dust stock remains relatively same across all the elevations. Dust stock for granodiorite is higher than quartzite at every elevation.

at 3,700 m and above that elevation, only interspace sites. Soil inorganic carbon decreases with elevation probably due to the increase in MAP above that elevation translocating SIC deeper into the profile (Fig. 2.8b).

Soil pH was highest at the lowest elevations and decreased up the transect (Fig. 2.9a), likely reflecting the increase in MAP at higher elevations. Electrical conductivity ranged between 0 and 0.4 dS m^{-1} and followed a similar inverse pattern with elevation (Fig. 2.9b). We observed slightly higher EC values under shrub compared to interspace areas. The highest values of NaF pH (>9)—which indicate the presence of amorphous material (e.g., volcanic ash)—were observed only at the lowest elevation (2,200 m) although a clear decreasing trend up the transect similar to the 1:1 pH and EC data is evident in Fig. 2.9c.

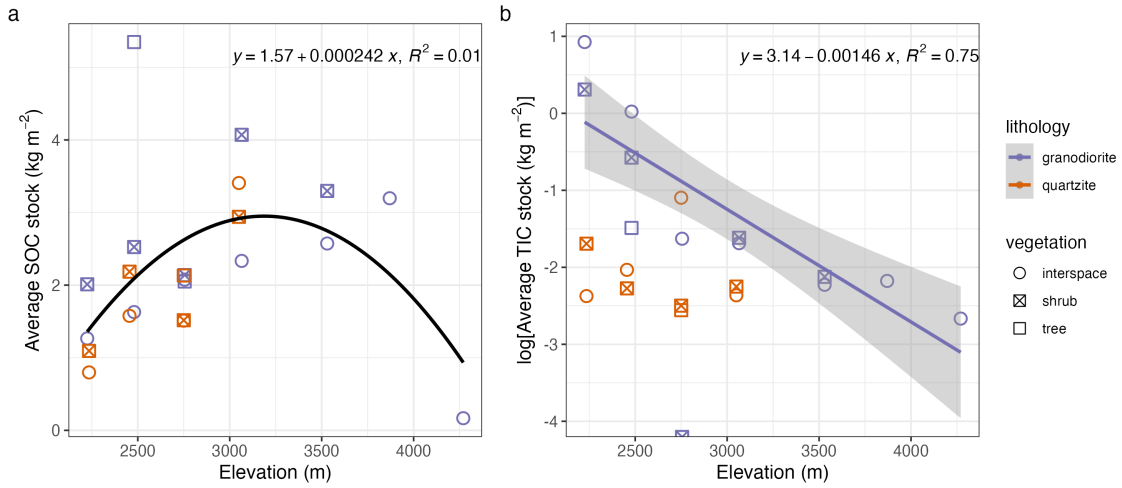

Figure 2.8: Elevational trends in average (a) SOC and (b) SIC stocks in the upper 50 cm of soils in this study. The line shown in (a) is a second order polynomial fit to all the data; the line shown in (b) is a linear model fit to just the granodiorite data (purple).

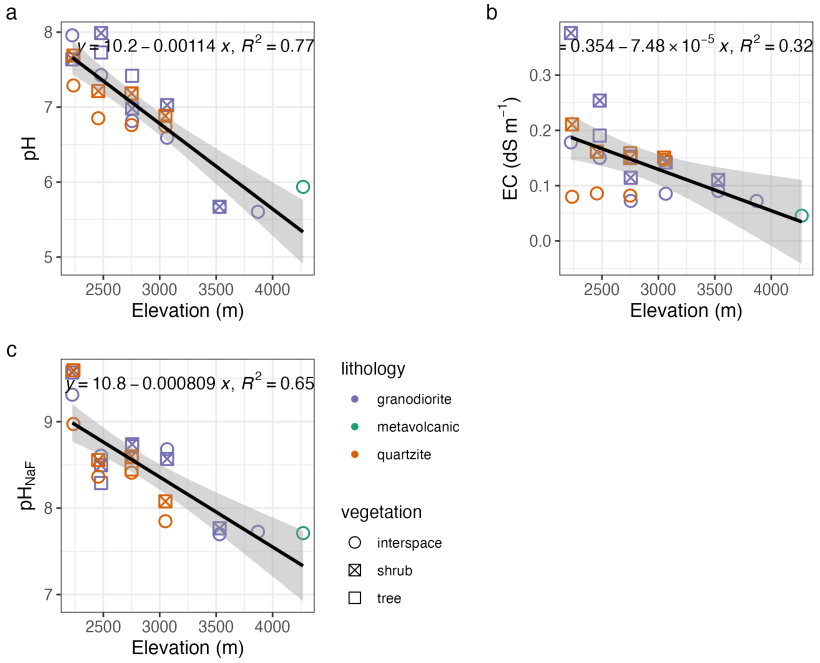

Figure 2.9: Elevational trends in (a) 1:1 pH, (b) EC, and (c) NaF pH

2.4 Discussion

2.4.1 Vesicular horizon formation

Lithologically-controlled surface roughness influences the dust influx into fractures of rocks or in gaps between rocks at the land surface. In the WMs, granodiorite separates into fine gravels and grus via physical weathering (Wright & Mooney, 1965) whereas quartzite outcrops are broken down into large, sharp, angular rock fragments. This difference in physical weathering patterns between the granodiorite and quartzite results in a larger volume fraction of sands and gravels that occur between the larger clasts in soils developed in granodiorite compared to quartzite. Soils developed in quartzite, in contrast, contain minimally weathered angular fragments that create large interstitial pores

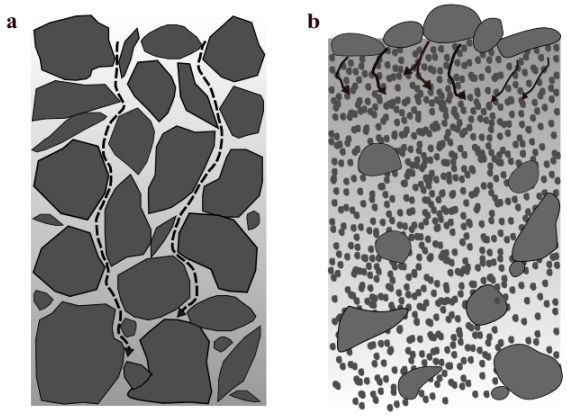

Figure 2.10: Proposed model for the effects of quartzite and granodiorite on the development of V horizons in the WMs. (a) Quartzite increases the water flow to deeper depths; more dust gets translocated deeper restricting embedding and V horizon formation. (b) Smaller grus under granodiorite favors the accumulation of eolian fines near the surface which retards the flow of water through the creation of smaller and more tortuous flow paths preventing deep translocation of water and dust and encourages the surface embedding of rocks and V horizon formation.

between quartzite clasts. These pores are not filled with the finer weathering products of the quartzite as in the case of granodiorite and thus remain relatively open for the movement of water and dust. The small grus and fine-earth material derived from weathering in the granodiorite lithology provides a matrix between the surface clasts within which dust can be incorporated and concentrated near the surface as illustrated in Fig. 2.10. That is, the larger volume fraction of weathered material between rock fragments creates conditions by which the dust has less pore space to fill in compared to quartzite. In addition, the residuum-derived material infilling the spaces between rocks in granodiorite creates greater pore tortuosity compared to quartzite that retards the movement of water and further encourages the concentration of eolian sediment near the surface. The increased concentra-

tion of dust near the surface means that the surface rocks at granodiorite sites have greater potential for embedding.

This is important because V horizon formation is positively correlated to the embedding of surface rocks—a condition necessary to maintain a continuous surface seal and prevent the escape of trapped air during infiltration thus allowing the formation of vesicular pores (Valentin, 1994). The larger interstitial pores due to the angular and largely unweathered quartzite increases the macroporosity of these sites allowing for greater infiltration of water and deeper penetration of dust into these soils. The increased movement of dust deeper into the profile further lowers the potential for concentrating dust at the surface of quartzite pedons which also lowers the potential for embedding of surface clasts. The differences between granodiorite and quartzite to create sealed surfaces via likely explains the higher occurrence of V horizons under granodiorite.

Vesicular horizons are less likely to form under vegetation in arid environments due to the potential disruption caused by roots or burrowing animals, which can destroy the surface embedding (D. S. Shafer et al., 2007). Consequently, V horizons are more prone to develop in interspace (i.e., non-canopy) areas (Evenari et al., 1974). In the case of granodiorite, however, V horizons were present not only in interspace sites, where expected, but also under vegetation including shrubs and trees. There are at least two possible explanations for this finding in the WMs. The first is that the development of V horizons and establishment of vegetation in the WMs is coeval. For example, the vegetation likely promotes the deposition of eolian material (Langford, 2000) in these areas which may encourage surface rock embedding and V horizon formation under granodiorite. The second possibility is that

the development of V horizons precedes the establishment of the vegetation and that the V horizons under the vegetative canopy represent a largely relict feature. Lower infiltration rates common under desert pavement and V horizons (Graham et al., 2008), may allow runoff to be concentrated toward slightly lower lying local areas within these larger sloping landforms. In general, vesicular horizons encourage runoff because of the air-filled vesicular porosity and the development of platy structure in well-developed vesicular horizons which increases tortuosity and restricts infiltration (Blackburn, 1975; M. H. Young et al., 2004). These adjacent lower lying areas may be preferential sites for the growth of vegetation that encroaches into already formed V horizons (Brown & Dunkerley, 1996). It is currently unclear which of these mechanisms are responsible for the occurrence of V horizons under vegetation formed in granodiorite pedons or if both contribute to this phenomenon.

2.4.2 Climatic, lithologic, and vegetation controls on soil water flux

The climate and lithology in the WMs appears to have a dominant control on the flux of soil water. Differences in the rock fragments and their weathering products between the two contrasting lithologies create differences in the effective amount of moisture and depth to which infiltrating meteoric water reaches in these soils. As discussed above, granodiorite and quartzite weathers differently resulting in larger interstitial macropores under the quartzite compared to smaller macropores in the grus weathered from granodiorite. Infiltrating water reaches deeper in quartzite soils because of these larger interstitial macropores. Granodiorite soils tend to form V horizons at higher frequencies due to the concentration of dust near the surface of these pedons. These V horizons reduce the infiltration rate of the soil and promote surface runoff. As a result, less of the rainfall reaching

the surface infiltrates into granodiorite soils. Indeed, this was confirmed by observations from a separate infiltration study at the 2,500 m elevation granodiorite (GR3) and quartzite (WP5) sites where a hand-pump sprayer was used to apply 6 cm of water at a rate of approximately 1.12 cm hr^{-1} in the interspace at both sites. We observed that the granodiorite site began to generate runoff at 13 min into the start of the experiment compared to 52 min for quartzite. This difference is noteworthy especially considering that the granodiorite site was more gently sloping (29%) than the quartzite site (40%). Across the WM transect, elevations above 3,100 m receive on average over 80% of their precipitation in the form of snow compared to 15-25% at lower elevation sites (Powell & Klieforth, 1991). The consequence of having the majority of the precipitation falling in the form of snow at these higher elevations is a temporal lag in the infiltration of meteoric water (Bayard et al., 2005). That is, the snow acts as a type of capacitor that stores the majority of the snow water above the soil surface and keeps it from infiltrating until the air temperature rises above freezing with the rate at which water moves into the soil dependent, in part, on the rate of snowmelt. Depending on the temperature and amount of snowfall in a given year at these higher elevations, surface soil layers can become frozen. When this happens, water within macropores of the soil will freeze before water in the smaller matrix pores restricting water flow to shallow layers and increasing the potential for runoff (Iwata, 2011). This restriction in soil water penetration, may explain the shallow depths of soil profiles observed at the higher elevations.

In contrast, at lower elevations, the majority of the precipitation is in the form of rainfall which encourages the preferential movement of water and translocation of soil

material deep into the profile. This results in deeper water flux into these soils leading to deeper soil profiles and is evident in the decreasing elevational trend in PDI up the transect where soil profile development appears to be governed by the greater amount of snow received at these sites (Table 2.1). At higher elevations, the predominance of snow significantly impacts soil water movement, directing infiltration toward matrix pores that result in the development of shallower soils. In addition, the decrease in soil temperature up the transect results in more frequent occurrences of frozen soil at higher elevations and several studies have shown that soil frost impedes the water movement (Li et al., 2024; Nagare et al., 2012). Since the water does not travel as fast in frozen soil, the translocation of material is restricted to shallower depths, resulting in lower PDI for higher elevation soils. Given that the PDI largely reflects the effects of translocation of soil materials (Koop et al., 2020), it appears that translocation is governed by SWE and soil temperature.

The EC and 1:1 pH elevational gradient results (Fig. 2.9) add further evidence of the effects of increased snowfall on the genesis of soils in the WMs. Despite the narrow range of values, EC was negatively associated with elevation indicating that salts were less concentrated and, thus, flushed deeper through the matrix into the profiles at the higher elevations. Similarly, 1:1 pH was negatively associated with elevation and likely reflects the effect of water movement through the matrix removing carbonate from the otherwise calcareous dust incorporated into the soils. This is also shown in the NaF pH data (Fig. 2.9c) where less amorphous material is left in the fine-earth fraction of the soil at higher elevations. Assuming similar inputs of volcanic ash at all the sites (i.e., the sites are relatively closely situated, have similar aspects and slopes, and are positioned on the same windward side of

the range), the negative association of NaF pH with elevation indicates a greater amount of chemical weathering within the matrix. Thus, in comparison to the PDI data, which indicated greater soil development at lower elevations, the soil chemical data suggest greater weathering at higher elevations. This seeming contradiction may indicate that the increase in the proportion of MAP falling as snow at higher elevations drives a greater proportion of soil moisture into the matrix and with longer residence times compared to lower elevations where convective rainfall dominates the movement of water into macropores bypassing the matrix. This would result in soils with greater chemical weathering signatures at higher elevations (e.g., pH and EC data) and soils with greater evidence of translocation at lower elevations (e.g., Bt horizon thickness and PDI data) as was found in this study.

Quartzite PDIs showed a steeper elevational gradient compared to granodiorite (Fig. 2.3b) indicating that soil development in quartzite in the WMs may be more sensitive to the partitioning of precipitation into rainfall vs snowfall. That is, as more of the precipitation falls as snow under quartzite, the resulting decrease in penetration depth of infiltrating water especially above 2,800 m may explain the rapid decline in soil development. The coarse angular rock fragments in quartzite soils results in larger interstitial macropores between rock fragments which increase the saturated hydraulic conductivity of the soil and the amount of water transported to deeper horizons. For example, a study conducted by Hlaváčiková et al. (2019) in stony soils of mountain catchments showed a positive relation between macropore flow and stoniness of the soil; macropores with diameters greater than 0.75 mm increased with increasing stoniness. Macropores, in general, are well known to have a large effect on soil water flux. For example, Watson & Luxmoore (1986) reported that soil

macropores constituted ∼1% of total soil volume in their study but contributed to 70% of the water flow. When soils under quartzite and granodiorite lithology are exposed to similar rainfall conditions, soils derived from quartzitic lithology are likely to have a greater potential for preferential flow (PF) compared to soils under granodiorite because of the presence of these macropores. In addition, the larger interstitial macropores of the quartzite soils may be more sensitive to freezing conditions compared to granodiorite since (for the reasons explained above) water in macropores tends to freeze before water in smaller matrix pores restricting PF, the percolation depth of water, and the potential for translocation of soil material. The greater frequency of V horizons in granodiorite soils, which tends to restrict macropore flow, likely exacerbates the difference in water flow between graniodiorite and quartzite pedons where matrix-dominated flow is favored in the former and PF through macropores in the latter.

Vegetation appeared to have a relatively minor impact on soil water flux in our study. Even the presence of roots under shrubs and trees (where present) did not significantly impact PDI, pH, or EC. Instead, the impact of vegetation was outweighed by the influence of climate and lithology which appear to be the dominant drivers of water flux in these soils. This may be because the roots are exploiting existing macropores within these rocky soils instead of forming new root channels that would otherwise impact soil water movement.

2.4.3 Soil formation in the WMs

Climate is the primary factor controlling soil formation in the White Mountains. Across the elevational gradient, the amount of snowfall compared to rainfall an elevation

receives appears to determine the type of flow—matrix vs macropore—which ultimately influences soil development. At lower elevations, precipitation occurs mainly as rainfall. This allows preferential movement of water through soil macropores and facilitates the translocation of soil material to deeper depths. In contrast, higher elevations receive a major proportion of precipitation as snow. The higher viscosity of water at low temperatures slows its movement through soil pores (Sharma & Kumar, 2023). The amount of water infiltrating is determined from the rate at which the snow melts allowing water to move into the matrix instead of more conductive macropores. This matrix flux slows water movement and restricts the translocation of soil material resulting in shallower soil development (as determined from the largely translocational index—PDI) at higher elevations.

At a given elevation, soil development in the WMs is controlled by varying degrees of dust deposition which is determined by lithology-controlled land surface characteristics. Surface roughness is high in quartzite soils because quartzite weathering forms large, angular rock fragments encouraging the accumulation of more dust. Dust travels through the large interstitial pores between the quartzite fragments and gets deposited in the deeper layers whereas for granodiorite, dust accumulates within the surface and embeds the surface rocks. As described above, this leads to the formation of vesicular horizons under the granodiorite and restricts the translocation of clays and carbonates to deeper horizons. The presence of large interstitial pores between quartzite fragments allows the water to flow preferentially through these large-sized macropores in quartzite allowing translocation of soil carbon, clay and carbonates to be stored deeper in soils developed in quartzite compared to soils developed in granodiorite. The large interstitial pores in the soils derived from quartzite

tend to restrict the embedding of surface rocks and thus the formation of vesicular horizons. This promotes deeper infiltration of soil water and helps explain why soils developed on quartzite in the WMs showed greater evidence of translocation of clays and carbonates in the profile (i.e., Bt and Bk horizons) than under granodiorite. Indeed, soils with vesicular horizons have been observed to be thin with low SOC content (Goossens & Buck, 2009) and experience limited leaching, leading to the accumulation of carbonate at shallow depths (McFadden et al., 1992). The likely greater occurence of matrix flow in granodiorite soils favors the formation of argillic and calcic horizons giving rise to the more abundant Typic Haplargids, Typic Calciargids, and Typic Calcids observed in the granodiorite pedons of this study. Thus, translocation of clays and carbonates are restricted in granodiorite soils that form V horizons compared to quartzite that allows deeper translocation of these materials through the interstitial macropores.

Figure 2.6 shows a difference in source materials between the granodiorite and the quartzite pedons. The granodiorite contributes some residuum to the eolian sediment through weathering, which leads to coarser particle sizes in the soil. Specifically, weathering of granodiorite releases mineral particles that mix with the incoming dust, creating a heterogeneous mixture with a broader range of particle sizes. In contrast, the quartzite pedons do not weather significantly and contribute little to the fine-earth fraction. Consequently, the soil particles in quartzite pedons are finer and closely resemble the particle size distribution of the dust alone. The minimal weathering of quartzite means that the dust particles remain relatively unaffected by coarser residuum in these pedons and thus maintain a finer particle-size distribution. Any dust that does undergo weathering in the quartzite pedons

only becomes finer, further differentiating the particle size distribution from that of granodiorite pedons. This indicates that in quartzite pedons, the soil particles in the fine-earth fraction are derived almost entirely from dust deposition, with no significant input from in-situ weathering. In contrast, granodiorite pedons have a dual source of particles: dust deposition and residuum that contribute to the soil composition.

Dust stocks in the upper 50 cm of the soil were higher in granodiorite compared to quartzite reflecting the potential for granodiorite soils to concentrate dust near the surface. This finding corresponds with the greater occurrence of V horizons in these pedons and supports the hypothesis that diffusive flow through the matrix is more prevalent in granodiorite soils compared to quartzite.

2.5 Conclusions

Soil genesis in the arid White Mountains is primarily governed by climatic conditions, with temperature and precipitation gradients across the elevational transect playing a crucial role in determining soil water movement. At lower elevations, increased rainfall facilitates rapid water percolation through soil macropores, leading to the formation of soils driven by relatively deep translocation. Conversely, at higher elevations, the predominance of snowfall significantly impacts soil water movement, directing infiltration toward matrix pores that result in the development of shallower soils. In addition to climatic influences, lithology exerts a substantial control over soil formation processes. Granodiorite, due to its higher susceptibility to weathering compared to quartzite, breaks down into grus. In contrast, quartzite, being more resistant to weathering, results in the accumulation of

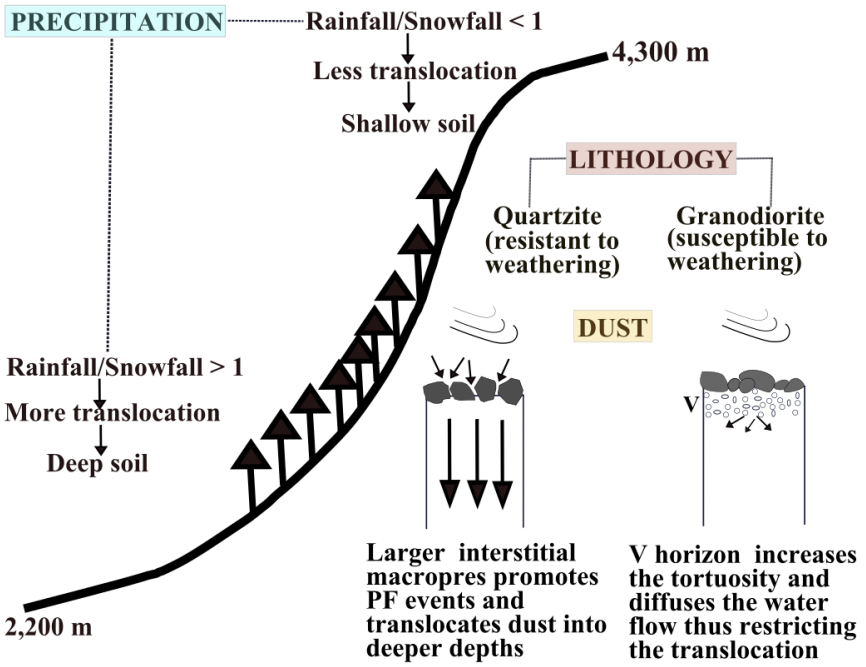

Figure 2.11: This figure illustrates the key factors influencing soil formation along the elevational transect of the White Mountains. Climate, particularly precipitation and temperature, is the primary factor affecting soil development. At lower elevations, higher rainfall moves soil materials to deeper layers, while at higher elevations, more snowfall slows soil water movement, resulting in shallower soils. Additionally, the different types of lithologies at each elevation weather differently. Granodiorite weathers more easily than quartzite. Dust interacts differently with these rocks: on granodiorite, it forms a V horizon by combining with finer, weathered material, which restricts water movement and leads to shallower soils. In contrast, on quartzite, dust moves to deeper layers through larger pores, promoting deeper soil development.

larger rock fragments within the soil matrix. The addition of eolian dust further modifies soil properties in these lithologically distinct environments. Within granodiorite-dominated sites, the deposition of dust leads to the development of V horizons, which restricts the deep infiltration of meteoric water. This results in limited translocation and relatively shallow soil development. On the other hand, quartzite-dominated sites, exposed to similar dust influx, exhibit deeper soil development due to deep translocation of dust via interstitial macropores. These findings contribute to a more comprehensive understanding of soil genesis in arid mountain environments, providing valuable insights for future studies on soil hydrology and landscape evolution in similar settings.

References

Allen, C. D. (2007). Interactions across spatial scales among forest dieback, fire, and erosion in northern New Mexico landscapes. *Ecosystems*, *10*(5), 797–808.

Archer, S. R., & Predick, K. I. (2008). Climate change and ecosystems of the Southwestern United States. *Rangelands*, *30*(3), 23–28.

Bayard, D., Stähli, M., Parriaux, A., & Flühler, H. (2005). The influence of seasonally frozen soil on the snowmelt runoff at two alpine sites in southern switzerland. *Journal of Hydrology*, *309*(1), 66-84. doi: https://doi.org/10.1016/j.jhydrol.2004.11.012

Bilzi, A. F., & Ciolkosz, E. J. (1977). Time as a factor in the genesis of four soils developed in recent alluvium in Pennsylvania. *Soil Science Society of America Journal*, *41*, 122–127. doi: 10.2136/sssaj1977.03615995004100010033x

Blackburn, W. H. (1975). Factors influencing infiltration and sediment production of semiarid rangelands in Nevada. *Water Resources Research*, *11*(6), 929–937.

Blair, T. C. (1999). Sedimentology of the debris-flow-dominated Warm Spring Canyon alluvial fan, Death Valley, California. *Sedimentology*, *46*(5), 941–965.

Brown, K., & Dunkerley, D. (1996). The influence of hillslope gradient, regolith texture, stone size and stone position on the presence of a vesicular layer and related aspects of hillslope hydrologic processes: a case study from the australian arid zone. *CATENA*, *26*(1), 71-84. doi: https://doi.org/10.1016/0341-8162(95)00034-8

Burnham, K. P., & Anderson, D. R. (2004). Multimodel inference: Understanding AIC and BIC in model selection. *Sociological Methods Research*, *33*, 261-304.

Clements, T., Merriam, R., Stone, R., Eymann, J., & Reade, H. (1957). *A study of desert surface conditions* (Tech. Rep.). Natick, MA: Quartermaster Research and Development Center, Environmental Protection Research Division.

Cooke, R. U. (1970). Stone Pavements in Deserts. *Annals of the Association of American Geographers*, *60*(3), 560–577.

Dale, V. H., Joyce, L. A., McNulty, S., Neilson, R. P., Ayres, M. P., Flannigan, M. D., ... Wotton, B. M. (2001). Climate change and forest disturbances. *BioScience*, *51*(9), 723–734.

Dixon, J. C. (1994). Geomorphology of desert environments. In *Geomorphology of desert environments* (pp. 61–78). Chapman and Hall, London.

Durner, W., Iden, S. C., & von Unold, G. (2017). The integral suspension pressure method (isp) for precise particle-size analysis by gravitational sedimentation. *Water Resources Research*, *53*, 33-48.

Edwards, A. L. (1976). *An introduction to linear regression and correlation.* San Francisco, CA: W.H. Freeman and Company.

Engleman, E. E., Jackson, L. L., & Norton, D. R. (1985). Determination of carbonate carbon in geological materials by coulometric titration. *Chemical Geology*, *53*, 125-128.

Evenari, M., Noy-Meir, I., & Goodall, D. (1985). *Hot Deserts and Arid Shrublands*. New York, NY: Elsevier.

Evenari, M., Yaalon, D. H., & Gutterman, Y. (1974, 06). Note on soils with vesicular structure in deserts. *Zeitschrift für Geomorphologie*, *18*(2), 162-172. doi: 10.1127/zfg/18/1974/162

Frisbie, J. A., Graham, R. C., & Lee, B. D. (2014). A plaster cast method for determining soil bulk density. *Soil Science*, *179*(2), 103–106.

Gaire, N. P., Koirala, M., Bhuju, D. R., & Borgaonkar, H. P. (2014). Treeline dynamics with climate change at the central Nepal Himalaya. *Climate of the Past*, *10*(4), 1277–1290.

Gee, G. W., & Or, D. (2002). Particle-size analysis. In J. H. Dane & G. C. Topp (Eds.), (p. 255-293). Soil Science Society of America. doi: 10.2136/sssabookser5.4.c12

Goossens, D., & Buck, B. (2009). Dust emission by off-road driving: Experiments on 17 arid soil types, Nevada, USA. *Geomorphology*, *107*(3-4), 118–138.

Graham, R. C., Hirmas, D. R., Wood, Y. A., & Amrhein, C. (2008). Large near-surface nitrate pools in soils capped by desert pavement in the Mojave Desert, California. *Geology*, *36*(3), 259–262.

Grossman, R. B., & Reinsch, T. G. (2002). Bulk density and linear extensibility. In J. H. Dane & G. C. Topp (Eds.), (p. 201-228). Soil Science Society of America. doi: https://doi.org/10.2136/sssabookser5.4.c9

Hall, C. A. J. (1991). Natural History of the White-Inyo Range Eastern California. In *Natural history of the white-inyo range eastern california.* University of California Press.

Harden, J. W. (1982). A quantitative index of soil development from field descriptions: Examples from a chronosequence in central california. *Geoderma*, *28*(1), 1-28. doi: https://doi.org/10.1016/0016-7061(82)90037-4

Harrison, E., & Dorn, R. (2014). Introducing a terrestrial carbon pool in warm desert bedrock mountains, southwestern USA. *Global Biogeochemical Cycles*, *28*, 253–268.

Hastie, T., Tibshirani, R., & Friedman, J. (2009). Model assessment and selection. In *The elements of statistical learning* (2nd ed., p. 219-257). Springer New York, NY. doi: https://doi.org/10.1007/978-0-387-84858-7

Hillel, D. (1998). *Environmental Soil Physics.* Academic Press, San Diego, CA.

Hirmas, D. R., & Graham, R. C. (2011). Pedogenesis and soil-geomorphic relationships in an arid mountain range, Mojave Desert, California. *Soil Science Society of America Journal*, *75*, 192–206.

Hirmas, D. R., Graham, R. C., & Kendrick, K. J. (2011). Soil-geomorphic significance of land surface characteristics in an arid mountain range, Mojave Desert, USA. *Catena*, *87*(3), 408–420. doi: 10.1016/j.catena.2011.07.011

Hlaváčiková, H., Holko, L., Danko, M., & Novák, V. (2019, July). Estimation of macropore flow characteristics in stony soils of a small mountain catchment. *Journal of Hydrology*, *574*, 1176-1187. doi: 10.1016/j.jhydrol.2019.05.009

Huenneke, L. F. (2001). Deserts. In F. Chapin, O. Sala, & E. Huber-Sannwald (Eds.), *Global biodiversity in a changing environment. ecological studies (analysis and synthesis)* (pp. 201–222). New York, NY: Springer, New York, NY.

Iwata, Y. (2011). Snowmelt infiltration. In J. Gliński, J. Horabik, & J. Lipiec (Eds.), *Encyclopedia of agrophysics* (pp. 736–736). Dordrecht: Springer Netherlands. doi: 10 .1007/978-90-481-3585-1_140

Koop, A. N., Hirmas, D. R., Sullivan, P. L., & Mohammed, A. K. (2020). A generalizable index of soil development. *Geoderma*, *360*(February 2019), 113898.

Lal, R., Monger, C., Nave, L., & Smith, P. (2021). The role of soil in regulation of climate. *Philosophical Transactions of the Royal Society B*, *376*.

LaMarche, V. C. (1973). Holocene climatic variations inferred from treeline fluctuations in the White Mountains, California. *Quaternary Research*, *3*(4), 632–660.

Langford, R. (2000). Nabkha (coppice dune) fields of south-central new mexico, u.s.a. *Journal of Arid Environments*, *46*(1), 25-41. doi: https://doi.org/10.1006/jare.2000.0650

Li, H., Li, M., Che, R., & Zhou, J. (2024, 07). Impact of freeze–thaw process on soil temperature and water after long-term grassland and bare land in northeast china. *Journal of Soils and Sediments*, *24*, 1-13. doi: 10.1007/s11368-024-03860-4

Lybrand, R. A., & Rasmussen, C. (2018). Climate, topography, and dust influences on the mineral and geochemical evolution of granitic soils in southern arizona. *Geoderma*, *314*, 245-261. doi: https://doi.org/10.1016/j.geoderma.2017.10.042

Marchand, D. E. (1970). Soil contamination in the White Mountains, Eastern California. *Geological Society Of America Bulletin*, *81*(8), 2497–2506. doi: 10.1130/0016-7606(1970)81

Marchand, D. E. (1973). Edaphic control of plant distribution in the White Mountains , Eastern California. *Ecology*, *54*(2), 233–250.

Margulis, S. A., Cortés, G., Girotto, M., & Durand, M. (2016). A landsat-era sierra nevada snow reanalysis (1985–2015). *Journal of Hydrometeorology*, *17*(4), 1203 - 1221. doi: 10.1175/JHM-D-15-0177.1

McFadden, L. D., McDonald, E. V., Wells, S. G., Anderson, K., Quade, J., & Forman, S. L. (1998). The vesicular layer and carbonate collars of desert soils and pavements: formation, age and relation to climate change. *Geomorphology*, *24*(2-3), 101–145.

McFadden, L. D., & Tinsley, J. C. (1985). Rate and depth of pedogenic -carbonate accumulation in soils : Formulation and testing of a compartment model. *Geological Society of America*.

McFadden, L. D., Wells, S. G., Brown, W. J., & Enzel, Y. (1992). Soil genesis on beach ridges of pluvial lake Mojave implications for holocene lacustrine and eolian events in the Mojave Desert, Southern California. *Catena*, *19*, 77–97.

McFadden, L. D., Wells, S. G., & Jercinovich, M. J. (1987). Influences of eolian and pedogenic processes on the origin and evolution of desert pavements. *Geology*, *15*, 504 – 508.

Meadows, D. G., Young, M. H., & McDonald, E. V. (2008). Influence of relative surface age on hydraulic properties and infiltration on soils associated with desert pavements. *Catena*, *72*(1), 169–178.

Mooney, H. (1973). Plant communities and vegetation. In R. M. I. Lloyd & R. S. E. Mitchell (Eds.), *A flora of the white mountains, california and nevada* (p. 7-17). University of California Press. doi: 10.1525/9780520340305

Munson, S., Belnap, J., Schelz, C., Moran, M., & Carolin, T. (2011, 06). On the brink of change: plant responses to climate on the colorado plateau. *Ecosphere*, *2*, art68. doi: 10.1890/ES11-00059.1

Nagare, R. M., Schincariol, R. A., Quinton, W. L., & Hayashi, M. (2012). Effects of freezing on soil temperature, freezing front propagation and moisture redistribution in peat: laboratory investigations. *Hydrology and Earth System Sciences*, *16*(2), 501–515. doi: 10.5194/hess-16-501-2012

Neter, J., & Wasserman, W. (1974). *Applied linear statistical models: Regression, analysis of variance, and experimental designs*. R. D. Irwin, Homewood, Illinois.

North, M., Water, K., Stephens, S., & Collins, B. (2009, 12). Climate, rain shadow, and human-use influences on fire regimes in the eastern sierra nevada, california, usa. *Fire Ecology*, *5*. doi: 10.4996/fireecology.0503020

Parsons, A. J., & Abrahams, A. (2009). *Geomorphology of desert environments*. Springer.

Piñeiro, G., Perelman, S., Guerschman, J. P., & Paruelo, J. M. (2008). How to evaluate models: Observed vs. predicted or predicted vs. observed? *Ecological Modelling*, *216*(3-4), 795–809. doi: 10.1016/j.ecolmodel.2008.05.006

Powell, D. R., & Klieforth, H. E. (1991). Weather and climate. In *Natural history of the white-inyo range eastern california.* University of California Press Ltd.

PRISM Climate Group, O. S. U. (2014). https://prism.oregonstate.edu. (Accessed: June, 2021.)

R Core Team. (2024). R: A language and environment for statistical computing [Computer software manual]. Vienna, Austria. Retrieved from `https://www.R-project.org/`

Rasmussen, C., McGuire, L., Dhakal, P., & Pelletier, J. D. (2017). Coevolution of soil and topography across a semiarid cinder cone chronosequence. *Catena*, *156*(January), 338–352. doi: 10.1016/j.catena.2017.04.025

Reheis, M. C. (1997). Dust deposition downwind of Owens (dry) Lake, 1991-1994: Preliminary findings. *Journal of Geophysical Research Atmospheres*, *102*(22). doi: 10.1029/97jd01967

Reheis, M. C., & Kihl, R. (1995). Dust deposition in southern Nevada and California,1984-1989: Relations to climate, source area, and source lithology. *Journal of Geophysical Research Atmospheres*, *100*, 8893–8918.

Rundel, P. W. (2008). The alpine flora of the White Mountains, California. *Madrono*, *55*(3), 202–215.

Schoeneberger, P., Wysocki, D., Benham, E., & Staff, S. S. (2012). *Field book for describing and sampling soils, version 3.0.* Natural Resources Conservation Service, National Soil Survey Center, Lincoln, NE.

Schulman, E. (1958). Bristlecone pine, oldest known living thing. *The National Geographic Magazine*, *113*(3), 355–372.

Shafer, D. S., Young, M. H., Zitzer, S. F., Caldwell, T. G., & McDonald, E. V. (2007). Impacts of interrelated biotic and abiotic processes during the past 125 000 years of landscape evolution in the Northern Mojave Desert, Nevada, USA. *Journal of Arid Environments*, *69*(4), 633–657. doi: 10.1016/j.jaridenv.2006.11.011

Shafer, S. L., Bartlein, P. J., & Thompson, R. S. (2001). Potential changes in the distributions of western north america tree and shrub taxa under future climate scenarios. *Ecosystems*, *4*(3), 200–215. doi: 10.1007/s10021-001-0004-5

Sharma, P. K., & Kumar, S. (2023). Soil temperature and plant growth. In *Soil physical environment and plant growth: Evaluation and management* (pp. 175–204). Cham: Springer International Publishing.

Soil Survey Laboratory Staff. (2022). *Kellog Soil Survey Laboratory methods manual* (Tech. Rep. Nos. Soil Survey Investigations Report No. 42, Version 6.0). U.S. Department of Agriculture, Natural Resources Conservation Service.

Soil Survey Staff. (2022). *Keys to soil taxonomy* (13th ed.; Tech. Rep.). Washington, DC: U.S. Gov. Print. Office.

Turk, J. K., & Graham, R. C. (2011). Distribution and properties of vesicular Horizons in the western United States. *Soil Science Society of America Journal*, *75*(4), 1449–1461.

USGS. (2021). https://www.usgs.gov/. (Accessed: June, 2021.)

Valentin, C. (1994). Surface sealing as affected by various rock fragment covers in West Africa. *Catena*, *23*(1-2), 87–97.

Venables, W. N., & Ripley, B. D. (2002). *Modern applied statistics with s* (Fourth ed.). New York: Springer. Retrieved from `http://www.stats.ox.ac.uk/pub/MASS4`

Watson, K., & Luxmoore, R. (1986). Estimating macroposity in a forest watershed by use of a tension infiltrometer. *Soil Science Society of America Journal*, *50*(3), 578–582.

Wright, R., & Mooney, H. (1965). Distribution of Bristlecone Pine in the White Mountains of California. *The American Midland Naturalist*, *73*(2), 257–284.

Young, J. A., & Evans, R. A. (1986). Erosion and deposition of fine sediments from playas. *Journal of Arid Environments*, *10*(2), 103–115.

Young, M. H., McDonald, E. V., Caldwell, T. G., Benner, S. G., & Meadows, D. G. (2004). Hydraulic properties of a desert soil chronosequence in the mojave desert, usa. *Vadose Zone Journal*, *3*(3), 956-963. doi: https://doi.org/10.2136/vzj2004.0956

Ziyaee, A., Karimi, A., Hirmas, D. R., Kehl, M., Lakzian, A., Khademi, H., & Mechem, D. B. (2018). Spatial and temporal variations of airborne dust fallout in Khorasan Razavi Province, Northeastern Iran. *Geoderma*, *326*(November 2017), 42–55.

Chapter 3

SOIL HYDROLOGY OF THE WHITE MOUNTAINS, CA

Abstract

The soil hydrology of arid and semi-arid mountains is not well understood despite the potential for these areas to contribute significantly to water resources in the lower lying desert areas. The White Mountains (WMs), located in the rain shadow of the Sierra Nevada, provide a unique opportunity to study the soil hydrology of these systems, particularly in understanding the effects of lithology, vegetation, and eolian dust on soil water movement. This study focuses on the distinct hydrological characteristics of the soils developed on two primary lithologies in the WMs: granodiorite and quartzite. Climate data were obtained from weather stations installed approximately every 300 m along the transect. Soil moisture and temperature sensors were installed at two depths within the dominant

vegetation present at each site along the transect which have been recording data since 2013. In 2022, new higher-frequency soil sensors were installed to replace the lower temporal resolution sensors. Analyses of the soil moisture data tended to support the hypotheses generated in Chapter 2 from an examination of the soil morphological and chemical data from the same sites. Granodiorite—prone to weathering more than quartzite—decomposes into grus, leading to a soil matrix that supports slower, diffusive water movement. In contrast, quartzite, being inert, forms angular rock fragments that facilitate rapid preferential flow (PF) through interstitial macropores. The diffusive movement of water results in consistent sensor detection and uniform distribution. In contrast, quartzite promotes water flow through macropores, resulting in deeper but more spatially variable movement, with some water bypassing sensors.

3.1 Introduction

Arid and semi-arid lands cover about one third of the Earth's land surface (Huenneke, 2001). Within these regions, arid and semi-arid mountains play a critical role in hydrology, contributing to 50-90% of discharge (Messerli et al., 2004). Understanding the hydrology of arid mountain ecosystems is crucial for managing water resources sustainably, especially in light of increasing water scarcity as these ecosystems are vulnerable to long-term shifts in precipitation and increases in temperature due to climate change (Arenson et al., 2022). These shifts will significantly impact the demand, availability, and quality of water with potentially significant impacts to the ecosystems within these arid environments (Beniston, 2003).

Arid ecosystems have unique flora and fauna that are adapted to these water scarce environments. Understanding the hydrology of these mountains helps in understanding and conserving these ecosystems and the biodiversity they support. Arid ecosystems of the southwestern US are sensitive to climate change because most of the plant species live near the edge of their physiological water needs. Therefore, only slight changes in precipitation and temperature may change species cover, composition, and geographic distribution (Archer & Predick, 2008). Climate change will affect the plant zones asscociated with arid lands, with treelines moving up in elevation in response to warmer and drier conditions (LaMarche, 1973; Gaire et al., 2014). As a response to future climate change, species distributions are expected to shift, such as big sagebrush (*Artemisia tridentata*) moving northward and the creosote bush (*Larrea tridentata*) spread in areas currently occupied by big sagebrush (Shafer et al., 2001). Due to climate-induced increases in temperatures, plant mortality rates are higher than regeneration rates, which has significant negative ecological impacts such as reduced carbon sequestration, changes in species composition and diversity, nutrient cycling, and altered ecohydrological patterns of runoff and erosion (Dale et al., 2001; Allen, 2007).

The White Mountains (WMs), lying immediately to the east of the Sierra Nevada range, presents a unique opportunity to study the soil hydrology of arid ecosystems. These mountains lie in the rain shadow of the Sierra Nevadas and receive only approximately one-third of the precipitation received by the western (windward) side of the Sierra Nevadas at the same elevation (Wright & Mooney, 1965). In addition to the extremely dry climate, these mountains are characterized by a steep temperature and precipitation gradient,

with contrasting lithologies over a range of elevations providing an opportunity to study the hydrology of soils formed on different lithologies across an elevational transect. These mountains also receive a large amount of eolian dust from Owens lake playa with an average rate of approximately 5-10 g m^{-2} yr^{-1} (Reheis, 1997). The two primary lithologies at the WMs—granodiorite and quartzite—weather very differently and the way eolian dust interacts with each of these parent materials affects soil development and hydrology. Granodiorite is more prone to weathering than quartzite and decomposes into grus, whereas quartzite, being largely inert in this dry environment, presents as angular, coarse rock fragments (Chapter 2). The accumulation of large amounts of dust within both of these parent materials, but especially quartzite, results in a clast-supported matrix with very low fine-earth (< 2 mm) bulk density (Chapter 2). Morphological and chemical evidence from soils developed in these two lithologies suggest that quartzite has a greater propensity for rapid interstitial macropore preferential flow while granodiorite favors slower diffusive flux of water through the soil matrix (Chapter 2).

The overall objective of this study was to test these hypotheses presented in Chapter 2. Specifically, we sought to: 1) understand how granodiorite and quartzite, with their distinct weathering products, impact the movement of soil water; 2) examine the impact of vegetation on soil hydraulic properties; and 3) explore the role of vesicular horizon formation on soil hydrology. This study aims to shed light on the hydrology of arid mountain environments and, ultimately, improve predictions of climate change impacts on these fragile ecosystems.

3.2 Methods

To study the soil hydrology of the WMs, four elevations—2,200, 2,500, 2,800, and 3,100 m—were chosen. At each elevation, sites were chosen within mapped granodiorite and quartzite geologic units (USGS, 2021). Thus, 8 sites in total were studied: 4 on granodiorite and 4 on quartzite. In increasing order of elevation, the names of the granodiorite sites were GR2, GR3, GR4, and GR5, and the name of the quartzite sites were WP4b, WP5, WP6b, and WP7. Beginning in 2013, moisture (S-SMD-M005, Onset, Bourne, MA) and temperature (HOBO U-23, Onset, Bourne, MA) sensors were installed at the 2,200 m elevation sites at two depths—10 and 50 cm—within the two dominant vegetative covers (shrub and interspace) present at GR2 and WP4b. Sensors were installed at other sites in later years following the installation schedule shown in Table 3.1 and data were collected at a 12-hour frequency. In June 2022, the sensors installed between 2013 and 2020 were replaced by new moisture and temperature sensors (CS655, Campbell Scientific, Logan, UT) at 10 and 50 cm under interspace, shrub, and tree (if present) at all sites with the exception of the interspace pedon at GR3 which was a new installation (Table 3.1). These sensors were coupled to a datalogger connected to a cellular modem (CR300-CELL, Campbell Scientific, Logan, UT) that allowed real-time monitoring and retrieval of soil data; sensor data were recorded every 10 min after installation.

Seven weather stations installed by the Scripps Institute of Oceanography along the transect have been recording atmospheric data since 2006 every minute (Table 3.2). Although the weather stations were collecting data since 2006, retrieving these data required

Table 3.1: Soil sensor data within the study area of the White Mountains from 2013-2023. The GR2-5 sites are on granodiorite; WP4b-7 sites are on quartzite. In 2022, sensors were replaced at all locations at the lower four elevations (i.e., 2,200, 2,500, 2,800, 3,100 m) with a cellular datalogger to allow real-time monitoring and collection of soil moisture and temperature data.

Site	**Vegetation**	**Depth(cm)**	**'13**	**'14**	**'15**	**'16**	**'17**	**'18**	**'19**	**'20**	**'21**	**'22**	**'23**
GR2	Interspace	10	B	B	B	M	B	B	B	B	B	B	B
(2,200 m)		50	B	B	B	M	B	B	B	B	B	B	B
	Shrub	10	B	B	B	B	B	B	B	B	B	B	B
		50	B	B	B	B	B	B	B	B	B	B	B
WP4b	Interspace	10	B	B	B	B	B	B	B	B	B	B	B
(2,200 m)		50	B	B	B	B	B	B	B	B	B	B	B
	Shrub	10	B	B	B	B	B	B	B	B	B	B	B
		50	B	B	B	B	B	B	B	B	B	B	B
GR3	Interspace	10										B	B
(2,500 m)		50										B	B
	Shrub	10	T	T	T	T	T	T	T	T	T	B	B
		50	T	T	T	T	T	T	T	T	T	B	B
	Tree	10	T	T	T	T	T	T	T	T	T	B	B
		50	T	T	T	T	T	T	T	T	T	B	B
WP5	Interspace	10	T	T	T	T	T	T	T	T	T	B	B
(2,500 m)		50	T	T	T		T	T	T	T	T	B	B
	Shrub	10	T	T	T	T	T	T	T	T	T	B	B
		50	T	T	T	T	T	T	T	T	T	B	B
GR4	Interspace	10				T	T	B	B	T	T	B	B
(2,800 m)		50				T	T	B	B	T	T	B	B
	Shrub	10				T	T	B	B	T	T	B	B
		50				T	T	B	B	T	T	B	B
	Tree	10				T	T	T	T	T	T	B	B
		50				T	T	B	B	T	T	B	B
WP6b	Interspace	10	T	T	T	T	T	B	B	B	B	B	B
(2,800 m)		50	T	T	T	T	T	B	B	B	B	B	B
	Shrub	10	T	T	T	T	T	B	B	B	B	B	B
		50	T	T	T	T	T	B	B	B	M	B	B
	Tree	10	T	T	T	T	T	T	T	T	T	B	B
		50	T	T	T	T	T	B	B	B	B	B	B
GR5	Interspace	10						B	B	B	B	B	B
(3,100 m)		50						B	B	B	B	B	B
	Shrub	10						B	B	B	B	B	B
		50						B	B	B	B	B	B
WP7	Interspace	10						B	B	T	T	B	B
(3,100 m)		50	T	T	T	T	T	B	B	T	T	B	B
	Shrub	10						B	B	T	T	B	B
		50	T	T	T	T	T	B	B	T	T	B	B

B, Both temperature and moisture sensors; T, Temperature sensors only; M, Moisture sensors only

Table 3.2: Weather stations at the White Mountains measuring soil temperature, soil moisture, barometric pressure, air temperature, relative humidity, cumulative precipitation, solar radiation, wind speed, and maximum gust.

Weather station	**Elevation (m)**	**Latitude (°)**	**Longitude (°)**
Fish Slough	1289	37.4792	-118.4030
Sore Thumb	1578	37.5108	-118.3248
Over the Hill	1855	37.5156	-118.3167
Piute Creek Overlook	2133	37.5107	-118.3304
Glider Port	2476	37.5211	-118.2950
Beer Can	2768	37.5290	-118.2843
Valley View	3125	37.5292	-118.2628

physical access to the dataloggers. Because, at the time of analysis of this dissertation, these data were last collected on 30 Nov 2022 before the start of the winter months that receive most of the precipitation, the high-frequency soil moisture time series recorded from the sensors installed in 2022 were analyzed independently of the weather station data. To study the movement of water in soils under different lithologies and vegetation types, a controlled irrigation experiment was conducted in July 2023. At 2,500 m elevation, both shrub and interspace areas at the granodiorite (GR3) and quartzite (WP5) sites that had installed moisture and temperature sensors were irrigated using a hand-pump sprayer with an adjustable wand (N-80 2-Gallon Garden Sprayer, Tarbor Tools, Kibbutz Beit Rimon, Israel). A total of 76 L of water was applied evenly over a plot measuring 2.1 x 0.6 m for each vegetation type. The rate of water application for GR3 and WP5 was 0.41 L min^{-1} and 0.53 L min^{-1}, respectively. During irrigation, water was applied a few centimeters above the sensors to ensure that even if there was lateral flow, it would be captured by the sensors. Soil moisture sensor data generated from this experiment were used to understand soil water movement under different lithologies and vegetation types.

Weather station data at a frequency of 1 minute were analyzed to extract information about the average duration and intensity of precipitation events within the interval between Jan 2007 and Dec 2021. Individual events within each year were identified as observed increases in cumulative precipitation being separated by at least 24 hours. The duration and total quantity of water for each event was averaged for each year and the mean annual data computed.

To compare the movement of water under granodiorite and quartzite for each site, pore water velocity between the 10 cm and 50 cm sensors was calculated as follows. Plotted soil moisture data were inspected and peaks were visually identified in the record. Peaks that were identified in the 10-cm record were associated with peaks in the 50-cm record if they occurred within 48 hours of the 10-cm peak. Pore water velocity was calculated as the distance between the sensors (40 cm) divided by the lag time between associated peaks. To ensure comparability between the two lithologies, these data were then filtered to include only calculated velocity values where both the granodiorite and quartzite sites at a given elevation were associated with the same precipitation event (i.e., the two lithologies needed to contain 10-cm peaks separated by less than 1 day). The velocity data were then square root-transformed, and the average was calculated for each site.

Fine-earth saturated hydraulic conductivity ($K_{\mathrm{sat_{fe}}}$) was predicted from ROSETTA (Zhang & Schaap, 2017) using sand, silt, clay, and fine-earth bulk density as predictors. The $K_{\mathrm{sat_{fe}}}$ was converted to saturated hydraulic conductivity on whole soil basis ($K_{\mathrm{sat_{ws}}}$) as follows:

$$K_{\mathrm{sat_{ws}}} = K_{\mathrm{sat_{fe}}} \cdot \frac{\phi_{\mathrm{ws}}}{\phi_{\mathrm{fe}}} \tag{3.1}$$

where ϕ_{ws} is whole soil porosity and ϕ_{fe} is fine-earth porosity. The effective saturated hydraulic conductivity K_{eff} was calculated for each pedon for the upper 50 cm using the following equation:

$$K_{\text{eff}} = \frac{\sum_{j=1}^{N} L_j}{\sum_{j=1}^{N} \frac{L_j}{K_j}} \tag{3.2}$$

where L is the thickness of each horizon and N the number of horizons in each pedon.

Using the procedure to identify peaks described above for the pore water velocity calculation, the number of soil moisture peaks observed for 10 cm and 50 cm from 2013–2020 was recorded. In addition, monthly comparisons were made between specific combinations of the two lithologies and two vegetation types (i.e., interspace and shrub) at each depth using the sensors installed in 2022 as follows. For each month between June 2022 and December 2023, the number of days with a peak in the soil moisture time series was recorded for each depth within each lithology and vegetation type separately. The number of days with identified peaks was divided by the number of days in that month to calculate the probability for a day in that month to contain a peak soil moisture event. The difference between these monthly probabilities were computed for each comparison (e.g., 10-cm granodiorite interspace vs 10-cm quartzite interspace). The number of positive and negative monthly probability differences were counted, recorded, and subtracted to obtain a value that represented the number of months that favored one side of the comparison. For example, if the 10-cm soil moisture records at the 2,200 m interspace areas were compared between granodiorite and quartzite and a value of -2 was computed, this would be

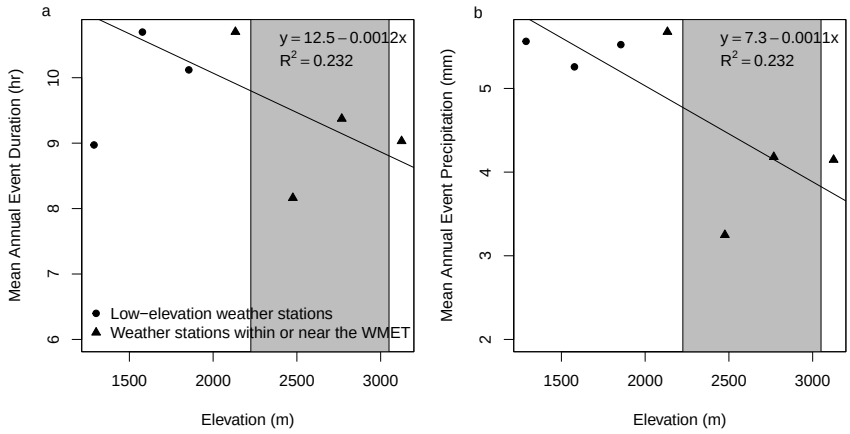

Figure 3.1: Mean annual data summarized from the weather stations in Table 3.2 showing (a) the average length of time of individual precipitation events and (b) the average precipitation magnitude per event. Only data between Jan 2007 and Dec 2021 were used for this analysis. The shaded region shows the range in elevations of the sites along the White Mountain elevational transect (WMET) used in this study. The four stations within or near the WMET were used to fit the linear trends shown in (a) and (b).

interpreted to mean that there were 2 months where the monthly probability for quartzite was higher than for granodiorite.

3.3 Results and Discussion

The relationship between elevation and precipitation is evident in the general decrease in both mean annual event duration and precipitation magnitude with increasing elevation (Fig. 3.1). Although there was an increase in the number of events, the weather station data showed a greater propensity for shorter and lower magnitude events up the transect. However, this trend was not significant ($P > 0.5$ for both linear models shown in Fig. 3.1) owing to the anomalously low values observed at the Glider Port station.

The two dominant rock types and the soils they produce have a critical role in controlling how precipitation is stored and transported. For example, lithology controls land surface roughness in the WMs where quartzite weathers to coarse rock fragments and granodiorite weathers to finer gravels and coarse sand (i.e., grus). As a result, interstitial macropores are larger between quartzite fragments. It has been shown that the presence of coarse fragments can increase resistance to soil compaction and can lower the fine-earth bulk density while increasing macroporosity (Ravina & Magier, 1984). The macropores in quartzite soils can potentially act as preferential flow paths that transport water to deeper horizons. A study conducted by Hlaváčiková et al. (2019) in stony soils of mountain catchments showed a positive relation between macropore flow and stoniness of the soil; macropores with diameters greater than 0.75 mm increased with increasing stoniness. Macropores are well known to have an effect on soil water flux. For example, Watson & Luxmoore (1986) reported that soil macropores constituted ∼1% of the total soil volume in their study but contributed to 70% of the water flow.

When the granodiorite and quartzite at 2,500 m were irrigated in 2023 with the same amount of water, there was minimal to no runoff under quartzite interspace (WP5) during the irrigation experiment in contrast to granodiorite interspace (GR3) where greater runoff, in the form of a larger wetted area, was observed (Fig. 3.2). Additionally, despite the granodiorite interspace site being irrigated at a slower rate (0.41 L min^{-1} compared to 0.53 L min^{-1}) and on a gentler slope (29% compared to 40%) than quartzite, surface runoff was initiated more quickly (13 min) after the start of the irrigation for granodiorite compared to quartzite interspace (53 min). The runoff at granodiorite under shrub started

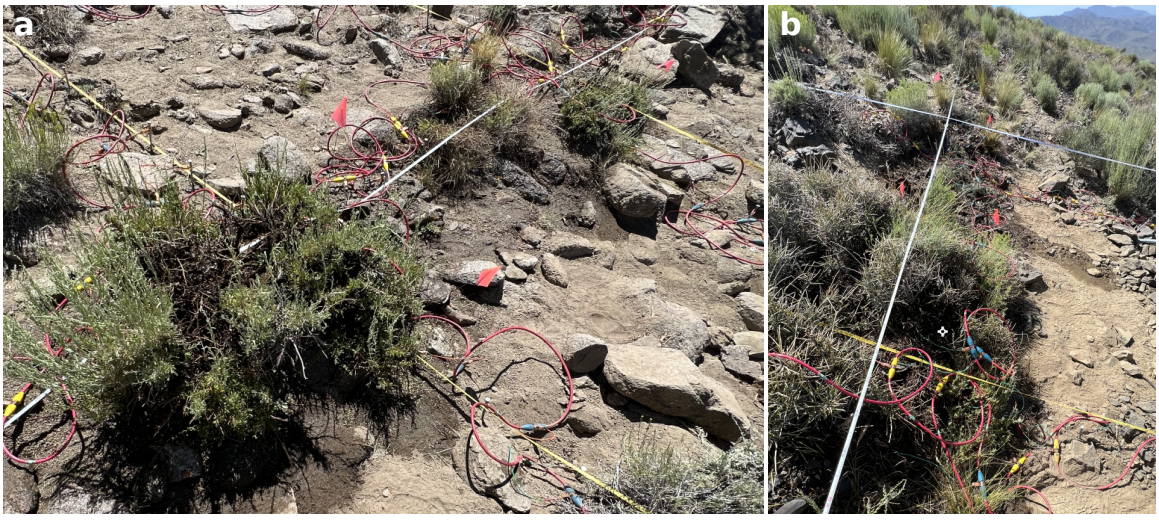

Figure 3.2: Photos showing the irrigation plots at the (a) granodiorite (GR3) and (b) quartzite (WP5) sites at ∼2,500 m. Both sites received the same irrigation rate, but runoff began in the granodiorite interspace after 13 minutes, whereas it took 52 minutes for runoff to occur in the quartzite interspace. No runoff was observed under the quartzite shrub, while a small amount was seen under the granodiorite shrub (wetted area below the shrub in panel a).

after 43 min whereas no runoff was noticed under shrub at WP5. The delayed onset of surface runoff under quartzite, which was four times slower than under granodiorite, is likely due to the propensity of quartzite soils in the WMs to generate preferential flow that would allow for a greater infiltration capacity.

A potential consequence of preferential flow at WP5 during the infiltration experiment is an increase in the spatial variability of the wetting front as water is channeled into distinct pathways occupying a minor portion of the soil volume especially at depth. In that case, the probability that the water intersects the measuring volume of the soil moisture sensor and that it does it for long enough to be detected even with the high-frequency (i.e., 10 min) setting, is relatively low. Indeed, the phenomenon of source-responsive flow where deeper soil sensors detect a rise in soil moisture before shallower sensors (if the shallower

sensors detect it at all) has been proposed as a positive diagnostic for preferential flow (Nimmo & Mitchell, 2013).

Figure 3.3 shows that for both shrub and interspace areas at WP5, soil moisture was detected at 10 cm after the addition of water but not at 50 cm. This may indicate a source-responsive behaviour where preferential flow occurs near or below 10 cm and, thus, either spatially and/or temporally bypasses the sensor measurements at 50 cm. However, neither 50-cm sensor in the interspace or shrub areas of GR3 showed an associated peak with the irrigation event (Figure 3.3c,d). In the case, of GR3 shrub (Figure 3.3c), this is likely because of vegetation-induced source-responsive flow that bypasses even the 10-cm sensor. The reason this did not happen for the WP5 shrub site may be due to the greater number of shrubs at that site compared to GR3. That is, the irrigated plot at WP5 had shrubs that were spread more evenly compared to the plot at GR3 despite the shrub canopy covering approximately the same percentage of the plot at both sites. The fewer shrubs responsible for covering the plot surface at GR3 may have induced stem flow during irrigation, spatially isolating the flow away from the 10-cm sensor. We note that the steep peak and rapid decline in the moisture response at 10 cm under the WP5 shrub plot (Figure 3.3a) also indicates an effect of vegetation at this site although apparently not sufficient to avoid the 10-cm sensor in that case. For the GR3 interspace plot (Figure 3.3d), the non-response at 50 cm could indicate source-responsive flow similar to quartzite. However, a more likely interpretation is that the presence of a thick, well-develop V horizon at this site may have absorbed and retained the irrigation water near the surface instead of allowing it to mover deeper into the profile. In addition, this site more quickly induced greater amounts of runoff compared

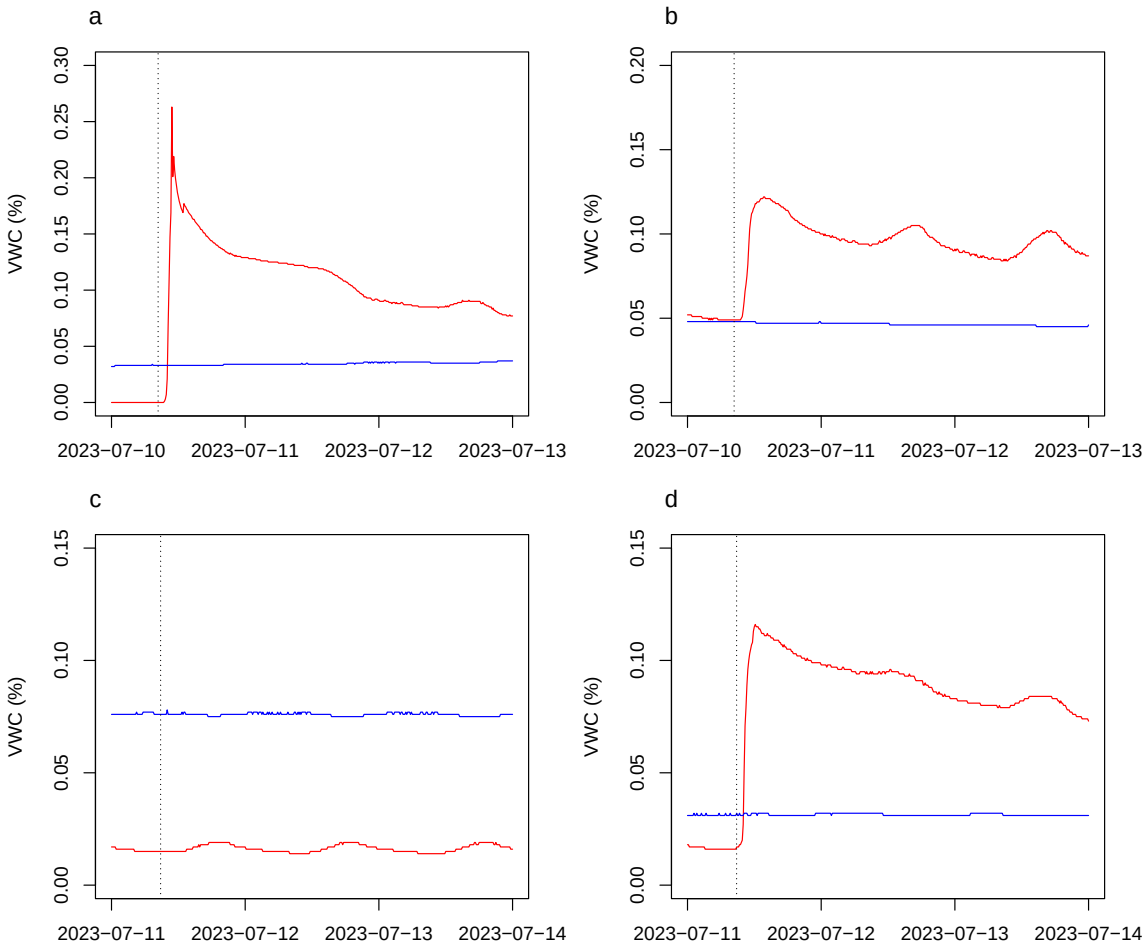

Figure 3.3: Soil moisture sensor data for two sites: WP5 (quartzite) and GR3 (granodiorite). For both sites, the red line represents moisture at a 10-cm depth and the blue line represents moisture at 50 cm. Panels (a) and (b) show data for WP5 in the shrub and interspace areas, respectively. Panels (c) and (d) show data for GR3 in the shrub and interspace areas, respectively. The dotted line inside the plot indicates when irrigation water was added to the plots.

to WP5 which also likely contributed to a lack of sufficient infiltrating water to reach the 50-cm sensor.

In general, the presence of V horizons decrease infiltration rate and encourages surface runoff. As described above, the presence of these horizons may partly explain why the deeper soil moisture sensor did not record any signal under grandiorite interspace (Fig. 3.3). Vesicular horizons are a unique feature in arid and semi-arid ecosystems and form under rough surfaces that can trap eolian dust (Meadows et al., 2008; Turk & Graham, 2011). These horizons are characterized by the presence of non-interconnected spherical and subspherical pores known as vesicles. In the case of well-developed V horizons, these vesicles merge laterally to form platy structure (Anderson et al., 2002). As a result, V horizons negatively affect soil infiltration rate because air-filled vesicular porosity and the development of platy structure (especially in well-developed vesicular horizons) increase tortuosity, slowing the flux of water (Blackburn, 1975; Graham et al., 2008).

The difference in the number of months that contain a higher soil moisture peak event probability for each sensor depth comparing granodiorite and quartzite for the same vegetation type and shrub and interspace for the same lithology is shown in Table 3.3. As discussed earlier, the diffusive movement of water under granodiorite helps to form even wetting front that is more easily captured by the top soil moisture sensors. In quartzite soils, water appears to travel through interstitial macropores that are spatially heterogenous making it more likely that water movement is not captured by the 10-cm soil moisture sensors. Rock fragments control the spatiotemporal patterns of soil water (Huang et al., 2023). Thus, the presence of non-porous quartzite rocks throughout the soil increases the

Comparison	Sensor depth (cm)	2,200 m	2,500 m	2,800 m	3,100 m
gr (I) - qz (I)	10	-2	+3	+4	+4
gr (S) - qz (S)	10	+2	-2	0	+4
gr (I) - gr (S)	10	-1	+6	+11	+4
qz (I) - qz (S)	10	+5	0	+6	+7
gr (I) - qz (I)	50	-1	-2	+1	-1
gr (S) - qz (S)	50	+1	-2	+2	0
gr (I) - gr (S)	50	+1	+1	+3	+1
qz (I) - qz (S)	50	+2	-2	+6	+1

Table 3.3: Differences in the number of months containing a higher probability for a soil moisture peak event for a given comparison. These values were calculated by subtracting the monthly probability for each lithology and vegetation type, sensor depth, and elevation, counting the occurrences of the positive and negative values from data collected between Jun 2022 and Dec 2023, and taking the difference between those counts. Positive values in this table represent the number of months with peak event probabilities that were greater for the left vs right side of the comparison; negative values, in contrast, favor the right side of the comparison. Zero values indicate that there were no differences between the number of months that favored the left or right side of the comparison. The gr and qz abbreviations indicate granodiorite and quartzite, respectively; I and S represent interspace and shrub, respectively.

spatial variability of macropores and, therefore, potential preferential flow paths. However, quartzite seems to capture more precipitation events at 50 cm than granodiorite at the two lowest elevations as seen by the greater number of negative values in Table 3.3 for those sites. This supports the idea that soil water movement in quartzite is determined by the spatial distribution of rock fragments that sometimes creates the water flow paths at the rock-soil interface near the bottom sensor especially when the precipitation is dominated by rainfall as opposed to snowfall. This is also shown by Liu et al. (2022) where preferential flow paths can develop deeply via the soil-rock interface. In granodiorite soils, it may be relatively harder for the diffused wetting front to develop a sufficient head to commonly reach the 50-cm sensor. When comparing the water movement under vegetation types for each lithology (Table 3.3), more events were recorded under interspace than shrub for

both granodiorite and quartzite by both top and bottom sensors. Big mountain sagebrush (*Artemisia tridentata*) is the most common shrub in these mountains (de Ven et al., 2007) with extensively developed lateral root systems along with a taproot system to help them scavenge for water in this dry environment (Richards & Caldwell, 1987). The maximum lateral spread of 100 cm was recorded at 40 cm depth for Big sagebrush with the taproot extending to about 225 cm (Reynolds & Fraley, 1989). The weight of small roots in the upper 30 cm of soil has been reported to comprise 50-60% of total weight, while another 25-30% of the small roots were located in the soil between 30 cm and 61 cm (Sturges, 1977). It is likely that the lateral root system of the shrubs is scavenging this water as soon as there is any precipitation in this dry environment and not letting it pass to the bottom sensors. The vegetation may also be inducing preferential flow through interception and stem flow, thus, bypassing the 50 cm sensor if not uptaken by plants. The combination of these processes results in a lower probability of detecting peak soil moisture events at 50 cm under shrubs.

These observations are supported by long-term soil moisture data recorded at 2,200, 2,800, and 3,100 m (Table. 3.4), where moisture sensors under granodiorite recorded greater numbers of soil moisture peaks at both top and bottom sensors than quartzite with the exception of the 10-cm water content in granodiorite and quartzite shrub sites at 2,800 m. There are more peaks under granodiorite than quartzite despite the greater volume of macropores under quartzite than granodiorite. As discussed above, the clast-supported matrix in quartzite soils form interstitial macropores that can act as preferential flow pathways. These water channels conduct a large amount of water to deeper horizons

Site	Elevation (m)	Lithology	Vegetation	10 cm	50 cm
GR2	2,200	Granodiorite	Interspace	57	17
WP4b	2,200	Quartzite	Interspace	40	17
GR4	2,800	Granodiorite	Interspace	16	9
WP6b	2,800	Quartzite	Interspace	13	4
GR4	2,800	Granodiorite	Shrub	13	7
WP6b	2,800	Quartzite	Shrub	13	4
GR5	3,100	Granodiorite	Interspace	12	6
WP7	3,100	Quartzite	Interspace	10	3
GR5	3,100	Granodiorite	Shrub	12	11
WP7	3,100	Quartzite	Shrub	6	5

Table 3.4: Number of peaks observed in the soil moisture records at 10 and 50 cm at sites with installed soil water content sensors over the duration shown in Table 3.1.

but form a very small volume of the whole soil. Because of this water movement through these macropores may remain undetected by soil moisture probes (Nimmo & Mitchell, 2013). Assuming that contrasting lithologies at the same elevation receive approximately the same amount of precipitation across the elevational transect from 2,200 to 3,100 m, it appears that water is bypassing the soil moisture sensors and not being recorded. The comparison of vegetation types, shows that fewer number of peaks were observed under shrubs compared to interspaces. The presence of root systems under shrubs increases the volume of soil macropores (van Noordwijk et al., 1993) and improves hydrological connectivity between macropores (Cannavo & Michel, 2013). These macropores formed by complex root networks act as a water channels that likely diverts the water away from the sensors.

Pore water velocities between 10 and 50 cm are consistently higher under granodiorite compared to quartzite across all elevations (Fig. 3.4). Since water likely flows faster and often preferentially under quartzite, bypassing the soil moisture sensors, it must flow slowly enough to be diffused in the soil matrix and, thus, captured by the bottom sensor for

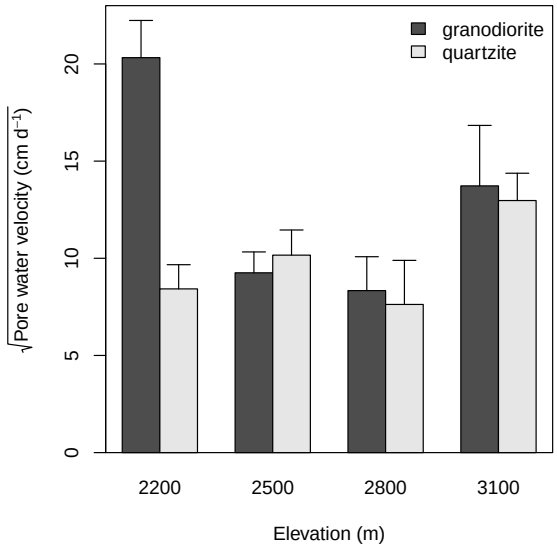

Figure 3.4: Plot of pore water velocity at each approximate elevation for granodiorite and quartzite pedons. Pore water velocity is calculated from the peaks in soil moisture at 10 and 50 cm. The whiskers represent 1 standard deviation calculated from the installed soil moisture sensor profiles at each site (interspace, shrub, and tree—if present).

the soil moisture to be recorded. Therefore, this analysis indicates that water moved slowly under quartzite compared to granodiorite. The aggregated K_{eff} for quartzite is also lower than granodiorite because of the finer soil material under quartzite (Fig. 3.5). The presence of rock fragments influence the soil physical properties such as porosity and bulk density thereby also controlling soil water movement (Huang et al., 2023; Parajuli et al., 2017; Smets et al., 2011). The presence of rock fragments decreases pore connectivity because of an increase in pore tortuosity (Hlaváčiková et al., 2019). The result of low pore connectivity may be responsible for the decrease in saturated hydraulic conductivity for quartzite compared to granodiorite (Fig. 3.5). Studies have shown that non-porous rocks reduce the hydraulic conductivity of soils by reducing the cross-sectional flow area within the fine soil fraction that is available for the movement of soil water (Poesen, 1986; Novák & Kňava,

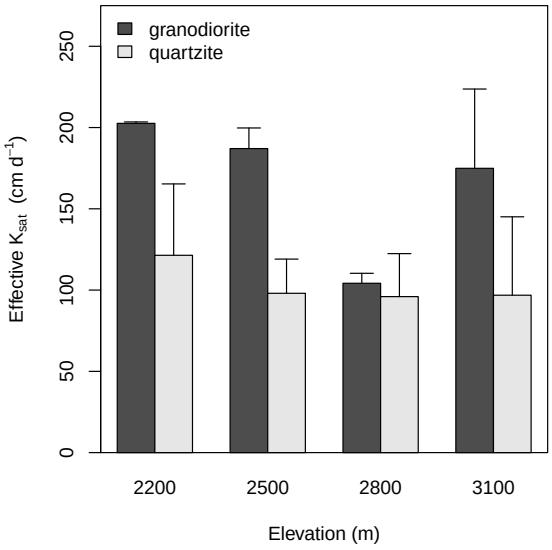

Figure 3.5: Aggregated effective K_{sat} for pedons under granodiorite and quartzite at each elevation. Error bars represent 1 standard deviation above the mean value.

2011; Hlaváčiková et al., 2015). Additionally, finer soil texture is associated with lower saturated hydraulic conductivity (Hillel, 1998). The soil under quartzite is primarily composed of eolian inputs, whereas the soil under granodiorite consists of dust and coarser in situ weathered material. Consequently, the finer texture of the soil under quartzite contributes to its lower saturated hydraulic conductivity compared to the soil under granodiorite.

The positive relationship observed between pore water velocity and K_{eff} highlights the controlling role of permeability in facilitating water movement (Fig. 3.6). As saturated hydraulic conductivity increases water flows more rapidly through the pore spaces. In rocky soils, the positive relationship between pore water velocity and saturated hydraulic conductivity reflects the unique hydrological behavior of these environments. Rocky soils, often characterized by large fractures, coarse textures, and macropores, exhibit high K_{sat} values, which allow water to move quickly through the subsurface (Shen et al., 2019; Yang

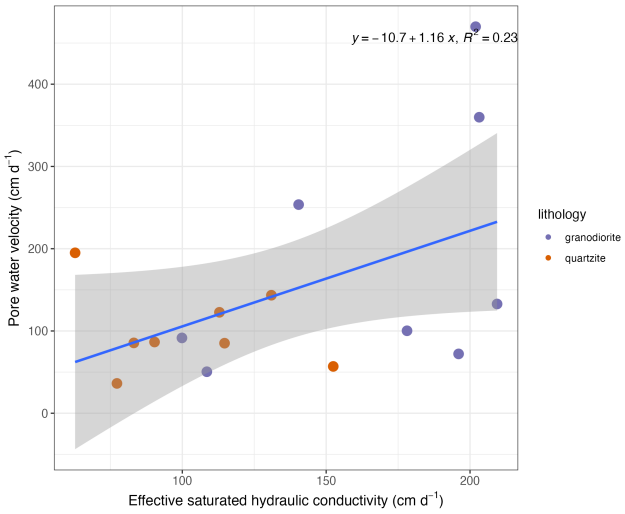

Figure 3.6: Pore water velocity vs effective saturated hydraulic conductivity, aggregated for each lithology and site across the elevational transect.

et al., 2023). This positive relationship between pore water velocity and K_{sat} in rocky soils also highlights the challenges of accurately measuring soil moisture in such environments. Due to the preferential flow paths created by fractures, water may bypass traditional soil moisture sensors, resulting in underestimation of water content since the presence of rocks increases the soil water heterogeneity (Li et al., 2014; Zhao et al., 2020).

The spatial variability in water distribution, especially in rocky terrain, complicates the assessment of water retention and movement in such landscapes (Wiekenkamp et al., 2016). When taken together, the different lines of evidence used in this study reveal distinct water movement patterns between soils under quartzite and granodiorite in response to varying precipitation intensities. Under low-intensity rainfall, soils derived from quartzite show gradual water infiltration, ensuring moisture is moved into the fine-earth matrix and recorded at both shallow and deeper sensor levels. This matrix has a lower K_{sat} than the granodiorite soils and results in a relatively low pore water velocity (Fig. 3.7a). In contrast,

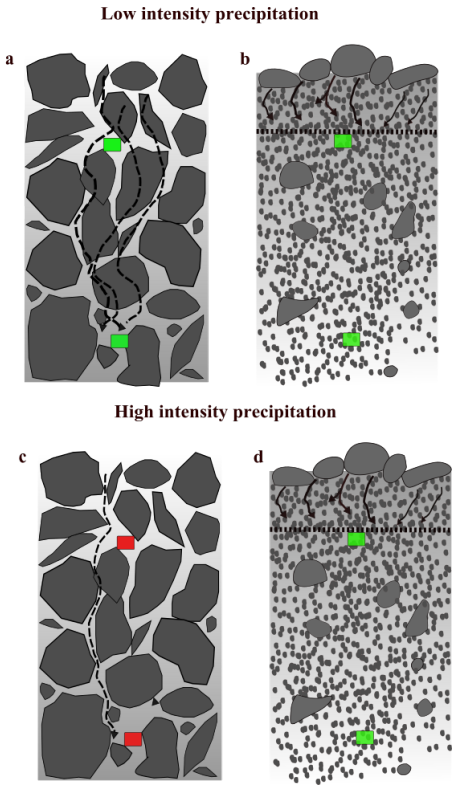

Figure 3.7: Conceptual diagram illustrating water movement in soil under granodiorite and quartzite during periods of high and low precipitation. The sensors are placed at two depths: 10 cm (top) and 50 cm (bottom). Green boxes indicate when the soil moisture sensor recorded water content, while red boxes show when water moved through the soil but was not detected by the sensor. (a) Under quartzite, the fine-earth soil particles are finer than the fine-earth fraction of the granodiorite, with a low fine-earth bulk density. During low-intensity precipitation, water is absorbed into the soil fine-earth matrix and moves slowly through the profile. This gradual movement allows the water to be recorded by both the top and bottom moisture sensors. (b) & (d) In soils under granodiorite, the presence of grus within the fine-earth eolian matrix increases the K_{sat} and allows water to move through the soil matrix even under high-intensity precipitation. This creates a wetting front that is consistently detected by both the top and bottom moisture sensors. (c) Under high-intensity precipitation, water flows more quickly through larger interstitial macropores in the soil under quartzite as the lower K_{sat} of the grus-free fine-earth matrix prevents infiltration and channels the water to preferential flow pathways in the form of interstitial macropores. This rapid movement bypasses both the top and bottom sensors, leading to undetected water flow at those depths.

granodiorite soils have a fine-earth K_{sat}, allowing water to be more consistently transmitted through the soil matrix, whether under low precipitation, resulting in moisture being detected throughout the soil column (Fig. 3.7b). During periods of high-intensity rainfall, however, quartzite soils experience rapid water movement through macropores, bypassing the lower or even the upper sensor due to preferential flow that dominates under these conditions and prevents detection by conventional sensors (Fig. 3.7c). Thus, granodiorite soils, even under high rainfall, maintain their ability to transmit and detect water flux through the profile. This suggests that the higher saturated hydraulic conductivity enables the wetting front to consistently reach both moisture sensors, demonstrating a more stable infiltration pattern compared to quartzite (Fig. 3.7d) and explains the apparent slower movement of water in quartzite soils; that is, the detection of water flux is biased toward slower pore water velocities in the case of quartzite.

3.4 Conclusions

This study highlights the importance of lithology in controlling soil water movement, with granodiorite and quartzite exhibiting distinct soil hydrological characteristics. The hydrology of the WMs is controlled by a combination of factors such as lithology, vegetation, eolian dust modifiying the soil morphological properties (e.g., formation of V horizons, which is unique to arid and semi-arid environments). Efforts to use soil moisture data to understand the soil hydrology of the WMs were limited in capturing the spatial variability of water flux. Even though quartzite has an apparent high volume of macroporosity and the soil morphology shows that the translocation of dust and formation of Bt

horizons via deeper preferential flow paths are greater in quartzite soils, sensors were not able to capture it because preferential flow paths are spatially variable (Wiekenkamp et al., 2016). The presence of rocks increases soil water heterogeneity and a large quantity of water is channeled underground at these rock-soil interface. A dye tracer experiment conducted in a semi-arid environment of West Bank Mountains showed that preferential flow paths along the rock-soil interface have a greater potential for groundwater recharge than water percolating through the soil matrix (Sohrt et al., 2014). The preferential flow paths under quartzite have a greater potential for groundwater recharge. In future, geophysical methods can be used or more sensors installed to better capture the spatial and temporal variability of soil water movement within these arid mountain soils.

References

Allen, C. D. (2007). Interactions across spatial scales among forest dieback, fire, and erosion in northern New Mexico landscapes. *Ecosystems*, *10*(5), 797–808.

Anderson, K., Wells, S., & Graham, R. (2002). Pedogenesis of vesicular horizons, Cima Volcanic Field, Mojave Desert, California. *Soil Science Society of America Journal*, *66*(3), 878–887.

Archer, S. R., & Predick, K. I. (2008). Climate change and ecosystems of the Southwestern United States. *Rangelands*, *30*(3), 23–28.

Arenson, L. U., Harrington, J. S., Koenig, C. E. M., & Wainstein, P. A. (2022, FEB). Mountain permafrost hydrology-a practical review following studies from the andes. *Geosciences*, *12*(2). doi: 10.3390/geosciences12020048

Beniston, M. (2003). Climatic change in mountain regions: A review of possible impacts. In H. F. Diaz (Ed.), *Climate variability and change in high elevation regions: Past, present & future* (pp. 5–31). Dordrecht: Springer Netherlands. doi: 10.1007/978-94-015-1252-7_2

Blackburn, W. H. (1975). Factors influencing infiltration and sediment production of semiarid rangelands in Nevada. *Water Resources Research*, *11*(6), 929–937.

Cannavo, P., & Michel, J.-C. (2013). Peat particle size effects on spatial root distribution, and changes on hydraulic and aeration properties. *Scientia Horticulturae*, *151*, 11-21. doi: https://doi.org/10.1016/j.scienta.2012.12.021

Dale, V. H., Joyce, L. A., McNulty, S., Neilson, R. P., Ayres, M. P., Flannigan, M. D., ... Wotton, B. M. (2001). Climate change and forest disturbances. *BioScience*, *51*(9), 723–734.

de Ven, C. M. V., Weiss, S. B., & Ernst, W. G. (2007). Plant species distributions under present conditions and forecasted for warmer climates in an arid mountain range. *Earth Interactions*, *11*(9), 1 - 33. doi: 10.1175/EI205.1

Gaire, N. P., Koirala, M., Bhuju, D. R., & Borgaonkar, H. P. (2014). Treeline dynamics with climate change at the central Nepal Himalaya. *Climate of the Past*, *10*(4), 1277–1290.

Graham, R. C., Hirmas, D. R., Wood, Y. A., & Amrhein, C. (2008). Large near-surface nitrate pools in soils capped by desert pavement in the Mojave Desert, California. *Geology*, *36*(3), 259–262.

Hillel, D. (1998). *Environmental Soil Physics*. Academic Press, San Diego, CA.

Hlaváčiková, H., Novák, V., & Holko, L. (2015). On the role of rock fragments and initial soil water content in the potential subsurface runoff formation. *Journal of Hydrology and Hydromechanics*, *63*(1), 71–81.

Hlaváčiková, H., Holko, L., Danko, M., & Novák, V. (2019, July). Estimation of macropore flow characteristics in stony soils of a small mountain catchment. *Journal of Hydrology*, *574*, 1176-1187. doi: 10.1016/j.jhydrol.2019.05.009

Huang, L., Bao, W., Hu, H., Traselin Nkrumah, D., & Li, F. (2023). Rock fragment content alters spatiotemporal patterns of soil water content and temperature: Evidence from a

field experiment. *Geoderma*, *438*, 116613. doi: https://doi.org/10.1016/j.geoderma.2023.116613

Huenneke, L. F. (2001). Deserts. In F. Chapin, O. Sala, & E. Huber-Sannwald (Eds.), *Global biodiversity in a changing environment. ecological studies (analysis and synthesis)* (pp. 201–222). New York, NY: Springer, New York, NY.

LaMarche, V. C. (1973). Holocene climatic variations inferred from treeline fluctuations in the White Mountains, California. *Quaternary Research*, *3*(4), 632–660.

Li, S., Ren, H., Xue, L., Chang, J., & Yao, X. (2014). Influence of bare rocks on surrounding soil moisture in the karst rocky desertification regions under drought conditions. *Catena*, *116*, 157-162. doi: https://doi.org/10.1016/j.catena.2013.12.013

Liu, T., Peng, X., Dai, Q., & Xu, S. (2022, 09). Role of the preferential flow at rock–soil interface in the water leaking process in near-surface fissures filled with soils in the karst rock desertification area. *Applied Water Science*, *12*. doi: 10.1007/s13201-022-01730-3

Meadows, D. G., Young, M. H., & McDonald, E. V. (2008). Influence of relative surface age on hydraulic properties and infiltration on soils associated with desert pavements. *Catena*, *72*(1), 169–178.

Messerli, B., Viviroli, D., & Weingartner, R. (2004). Mountains of the World: Vulnerable Water Towers for the 21st Century. *AMBIO: A Journal of the Human Environment*, *33*(sp13), 29 – 34. doi: 10.1007/0044-7447-33.sp13.29

Nimmo, J. R., & Mitchell, L. (2013). Predicting vertically nonsequential wetting patterns with a source-responsive model. *Vadose zone journal : VZJ.*, *12*(4).

Novák, V., & Kňava, K. (2011, 11). The influence of stoniness and canopy properties on soil water content distribution: Simulation of water movement in forest stony soil. *European Journal of Forest Research*, *131*. doi: 10.1007/s10342-011-0589-y

Parajuli, K., Sadeghi, M., & Jones, S. B. (2017). A binary mixing model for characterizing stony-soil water retention. *Agricultural and Forest Meteorology*, *244-245*, 1-8. doi: https://doi.org/10.1016/j.agrformet.2017.05.013

Poesen, J. (1986). Surface sealing as influenced by slope angle and position of simulated stones in the top layer of loose sediments. *Earth surface processes and landforms*, *11*(1), 1–10.

Ravina, I., & Magier, J. (1984). Hydraulic conductivity and water retention of clay soils containing coarse fragments. *Soil Science Society of America Journal*, *48*, 736-740. doi: 10.2136/sssaj1984.03615995004800040008x

Reheis, M. C. (1997). Dust deposition downwind of Owens (dry) Lake, 1991-1994: Preliminary findings. *Journal of Geophysical Research Atmospheres*, *102*(22). doi: 10.1029/97jd01967

Reynolds, T. D., & Fraley, L. (1989). Root profiles of some native and exotic plant species in southeastern idaho. *Environmental and Experimental Botany*, *29*(2), 241-248. doi: https://doi.org/10.1016/0098-8472(89)90056-7

Richards, J., & Caldwell, M. (1987, 10). Hydraulic lift: Substantial nocturnal water transport between soil layers by artemisia tridentata roots. *Oecologia*, *73*, 486-489. doi: 10.1007/BF00379405

Shafer, S. L., Bartlein, P. J., & Thompson, R. S. (2001). Potential changes in the distributions of western north america tree and shrub taxa under future climate scenarios. *Ecosystems*, *4*(3), 200–215. doi: 10.1007/s10021-001-0004-5

Shen, Y., Wang, D., Chen, Q., Tang, Y., & Chen, F. (2019). Large heterogeneity of water and nutrient supply derived from runoff of nearby rock outcrops in karst ecosystems in sw china. *Catena*, *172*, 125-131. doi: https://doi.org/10.1016/j.catena.2018.08.020

Smets, T., López-Vicente, M., & Poesen, J. (2011). Impact of subsurface rock fragments on runoff and interrill soil loss from cultivated soils. *Earth Surface Processes and Landforms*, *36*(14), 1929–1937.

Sohrt, J., Ries, F., Sauter, M., & Lange, J. (2014). Significance of preferential flow at the rock soil interface in a semi-arid karst environment. *Catena*, *123*, 1-10. doi: https://doi.org/10.1016/j.catena.2014.07.003

Sturges, D. L. (1977). Soil water withdrawal and root characteristics of big sagebrush. *The American Midland Naturalist*, *98*(2), 257–274.

Turk, J. K., & Graham, R. C. (2011). Distribution and properties of vesicular Horizons in the western United States. *Soil Science Society of America Journal*, *75*(4), 1449–1461.

USGS. (2021). https://www.usgs.gov/. (Accessed: June, 2021.)

van Noordwijk, M., Schoonderbeek, D., & Kooistra, M. (1993). Root—soil contact of field-grown winter wheatααcommunication no. 45 of the dutch programme on soil ecology of arable farming systems. In L. Brussaard & M. Kooistra (Eds.), *Soil structure/soil biota*

interrelationships (p. 277-286). Amsterdam: Elsevier. doi: https://doi.org/10.1016/B978-0-444-81490-6.50027-3

Watson, K., & Luxmoore, R. (1986). Estimating macroposity in a forest watershed by use of a tension infiltrometer. *Soil Science Society of America Journal*, *50*(3), 578–582.

Wiekenkamp, I., Huisman, J., Bogena, H., Lin, H., & Vereecken, H. (2016). Spatial and temporal occurrence of preferential flow in a forested headwater catchment. *Journal of Hydrology*, *534*, 139-149. doi: https://doi.org/10.1016/j.jhydrol.2015.12.050

Wright, R., & Mooney, H. (1965). Distribution of Bristlecone Pine in the White Mountains of California. *The American Midland Naturalist*, *73*(2), 257–284.

Yang, W., Peng, X., Dai, Q., Li, C., Xu, S., & Liu, T. (2023). Storage infiltration of rock-soil interface soil on rock surface flow in the rocky desertification area. *Geoderma*, *435*, 116512. doi: https://doi.org/10.1016/j.geoderma.2023.116512

Zhang, Y., & Schaap, M. G. (2017). Weighted recalibration of the Rosetta pedotransfer model with improved estimates of hydraulic parameter distributions and summary statistics (Rosetta3). *Journal of Hydrology*, *547*(November 2017), 39–53.

Zhao, Z., Shen, Y., Jiang, R., & Wang, Q. (2020). Rock outcrops change infiltrability and water flow behavior in a karst soil. *Vadose Zone Journal*, *19*(1), 1–15.

Chapter 4

SOIL WEATHERING AND GEOCHEMISTRY OF THE WHITE MOUNTAINS, CALIFORNIA

Abstract

This study investigates the role of dust in soil formation and geochemistry in the White Mountains (WMs). Soil development in this range is influenced by both in situ weathering and continuous dust input resulting in unique properties for two of the dominant parent materials in the WMs: granodiorite and quartzite. Granodiorite weathers into finer particles (i.e., grus) compared to quartzite, leading to increased chemical weathering with

increasing precipitation at higher elevations in the range. Conversely, coarser fragments of quartzite undergo comparatively little weathering and breakdown. Soils in these areas form primarily within deposits of eolian sediment and show minimal changes in weathering of the fine-earth matrix along the elevational transect. We examined the chemical index of alteration which indicated that granodiorite soils exhibit consistently increasing weathering throughout up the transect from 2,200 to 3,100 m, whereas quartzite soils show minimal weathering changes along that same transect. Additionally, observed differences in the translocation of Ca and K in these soils is likely explained by the greater solubility of Ca in the calcareous dust and differences in water flow between the two lithologies. Granodiorite pedons tend to form V horizons which diffuse infiltrating water and restrict deep percolation by concentrating water through the grus-infused fine-earth matrix. In contrast, water flow in quartzite is likely directed toward interstitial macropores that act as preferential pathways for the transmission of water, dust, and solutes deeper in the profile. The increased proportion of MAP as snowfall received at the highest elevations resulted in carbonate accumulation at shallower depths likely due to slower moving water controlled by snow melt in comparison to lower elevations. Strain calculations using zirconium and titanium indicate the accumulation of eolian inputs and soil dilation. The consistently positive strain values suggest significant dust incorporation into the soil, with deeper translocation shown in quartzite profiles supporting the hypothesized mechanism of greater preferential flow in quartzite due to the angular unweathered clasts. This research enhances our understanding of the complex mechanisms of soil formation in arid mountain environments, which is crucial for predicting how these landscapes will respond to climate change and human activities.

4.1 Introduction

Arid ecosystems, characterized by their unique climatic conditions and ecological significance, play a pivotal role in global biodiversity, hydrological cycles, and climate regulation (Laity, 2009). Arid environments often have high diurnal temperature variations, leading to rapid heating and cooling of rocks (Routson et al., 1977). This thermal stress can promote physical and chemical weathering, releasing nutrients into the soil (McFadden et al., 2005). The interactions between geological substrates and climatic factors shape the landscape of arid regions by influencing geochemical weathering, erosion, and sediment transport and, thus, affecting landform evolution and soil formation (Muhs et al., 2001). Studying these biogeochemical processes in arid ecosystems is crucial for understanding their resilience to environmental changes and for developing strategies for sustainable land management and conservation in these fragile environments (Ramond et al., 2022). The geochemical signatures in arid ecosystems serve as indicators of past and present climatic conditions (Maslov et al., 2003). For example, they can help in reconstructing historical climate patterns (Muhs et al., 2001), informing predictions about future climate scenarios (Zhao et al., 2021), and assessing the resilience and adaptability of arid landscapes to environmental stressors (Turner & Gardner, 2015).

Among these arid landscapes, arid mountain regions offer a particularly complex setting for studying these processes. The unique combination of elevation, temperature fluctuations, and geological substrates in mountain environments creates distinctive geochemical signatures that can provide deeper insights into past climatic variations. The arid White Mountains (WMs) in eastern California provides an ideal environment, where the

interplay of extreme aridity and high elevation creates a distinctive ecological setting. This research focuses on the WMs not only for their inherent scientific interest but also for their broader implications in understanding arid mountain systems hydrology worldwide. The WMs are uniquely important for several reasons. First, these mountains receive a considerable amount of dust from Owens lake playa at an average rate of 5-10 g m^{-2} yr^{-1} (Reheis, 1997), which can profoundly affect soil geochemistry and, consequently, the local flora and fauna (Marchand, 1973). This dust deposition plays a crucial role in delivering nutrients to these otherwise nutrient-poor landscapes, yet its impacts on soil geochemical processes are not fully understood (Muhs et al., 2001). Secondly, the WMs provide lithological diversity to study the effects of different parent materials on soil formation and weathering. Additionally, it offers a unique opportunity to examine the interaction between dust and different lithologies, exploring their effects on soil weathering and properties (Marchand, 1970). Despite their importance, there remain significant gaps in our understanding of the WMs. The current literature lacks comprehensive studies on the interaction between the lithological diversity, dust deposition, and the resulting geochemical characteristics of the soils in this range. Moreover, there is a lack of understanding regarding how the input of dust on different lithologies influence their weathering processes and soil formation in arid mountain ecosystems. These gaps limit our ability to predict how such environments will respond to environmental changes, including climate change, and constrain our understanding of their role in the broader Earth system.

This study aims to bridge these gaps by providing a detailed examination of the soil geochemistry and chemical weathering in the WMs. We use chemical weathering indices

to characterize the weathering profiles of the soils and summarize the major element oxide chemistry of each sample into a single value (Price & Velbel, 2003). This chapter constructs a detailed geochemical framework that reflects the soil-environmental interactions within this mountain range. Understanding the geochemistry of soil is crucial for exploring the stories of past climatic conditions, biogeochemical cycles, and landscape evolution (Gall, 1994; Lybrand & Rasmussen, 2018). Weathering indices, in particular, offer a quantifiable measure of the extent and nature of weathering processes, providing insights into the rates of soil formation, mineral transformation, and the subsequent implications for nutrient cycling and ecosystem health (Nesbitt & Young, 1982; Maynard, 1992; Bäumler & Zech, 2000). This chapter will shed light on the underexplored aspects of the geochemical dynamics in the WMs and also offer broader implications for the study of arid mountain ecosystems worldwide, thereby advancing our understanding of their role in Earth's interconnected environmental systems.

4.2 Methods

The WMs are located in eastern California, near the border with Nevada. They are known for their unique geological features, steep elevational range, and physiographic position in the rain shadow of the Sierra Nevadas. Soils were sampled across the elevational transect ranging from 2,200 m to 3,100 m representing a range of mean annual precipitation (MAP) between 232 mm at the lowest elevations and 397 mm at the highest elevation sites (Chapter 2). Eight sites were selected on contrasting lithologies (i.e., granodiorite and quartzite) at an elevational increment of 300 m. Sites GR2 and WP4b were at ∼2,200 m,

Elements	Detection limits (ppm)
Mg	< 3000
K, Ca, Ti	< 25
Mn, Fe, Zr	< 5
Al, Si	< 400
P	< 50

Table 4.1: Detection limits of the elements analyzed using pXRF.

GR3 and WP5 at ∼2,500 m, GR4 and WP6b at ∼2,800 m, and GR5 and WP7 at ∼3,100 m. At each site, soil samples were collected from two vegetation types: shrub and interspace. Within each vegetation type, four pits (30 cm wide × 40 cm long × 50 cm deep) were excavated in both the north-south and east-west directions, positioned 10 and 15 m away from the center point, respectively. A representative pit was chosen, and sampled up to a depth of 1 m. Soils were described and horizon depths determined following Schoeneberger et al. (2012). Fine-earth samples were collected, ball-milled, and subsequently scanned with a portable X-ray fluorescence (pXRF) spectrometer (Vanta, Olympus, Waltham, MA, USA) containing a large area silicon drift detector and 8-50 kV rhodium X-ray tube. The pXRF was used to scan samples to determine the concentrations of Mg, Al, K, Ca, Ti, Si, Mn, Fe, P, and Zr. Detection limits of these elements are presented in Table 4.1.

The GeoChem mode was selected during scanning following Weindorf & Chakraborty (2020); this mode has two beams of different energies (10 and 40 kV) for quantitative identification of elements covering a large part of the periodic table that maximizes the signal to noise ratio. Scans were run for 120 seconds on each beam. Polyethylene pXRF cups and 4 μm polypropylene film were used to contain the sample during scanning. For each batch of samples, the pXRF was calibrated using an alloy coin provided by the manufacturer (316,

Olympus, Waltham, MA, USA). After scanning every 20 samples, two National Institutes of Standards and Technology (NIST) certified standards were also scanned. These standards were 2710a (Montana I soil) and 2711a (Montana II soil). Certified values of the elements of these two standards were compared with pXRF values and used to calculate correction factors (CFs) as the ratio of the certified value of the element present in the standard to the pXRF value of the same element:

$$CF = \frac{C_{i_{\mathrm{CV}}}}{C_{i_{\mathrm{XRF}}}} \tag{4.1}$$

where $C_{i_{\mathrm{CV}}}$ is the certified value of Fe (e.g., 2711a) and $C_{i_{\mathrm{XRF}}}$ is the pXRF value of Fe determined on the same standard sample. The average CFs from the two standards were multiplied by their respective pXRF elemental values determined from each sample to obtain the final corrected pXRF values (Chakraborty et al., 2019).

These elements were then converted into their oxide equivalents and used to calculate the eluvial-illuvial coefficient (EIC) using the equation of Muir & Logan (1982):

$$\mathrm{EIC}_h = \left(\frac{\frac{S_h}{X_h}}{\frac{S_p}{X_p}} - 1 \right) \cdot 100 \tag{4.2}$$

where S represents the element oxide of interest, X is the stable element oxide, h refers to the horizon of interest, and p refers to the parent material within which the soil formed. Individual ratios were taken for K_2O, and CaO with TiO_2 for each pedon. The EICs for the parent material (i.e., C horizons) were assigned values of zero. Chemical index of alteration (CIA) (Nesbitt & Young, 1982) was modified to exclude Na_2O because Na was too light to

be analyzed by pXRF; CIA was calculated as follows.

$$\text{CIA} = \frac{\text{Al}_2\text{O}_3}{\text{Al}_2\text{O}_3 + \text{CaO} + \text{K}_2\text{O}} \cdot 100 \tag{4.3}$$

where the oxides of each element are given in percent.

Strain of each weathered horizon ($\epsilon_{i,w}$) was calculated following Brimhall et al. (1992):

$$\epsilon_{i,w} = \frac{\rho_p C_{i,p}}{\rho_w C_{i,w}} - 1 \tag{4.4}$$

where ρ_p is the fine-earth bulk density for the C horizon assumed to represent the parent material within which the soil formed, $C_{i,p}$ is the concentration of a selected immobile element (i.e., Zr, and Si) in the parent material given in percent, ρ_w is the fine-earth bulk density of the weathered horizon of interest, and $C_{i,w}$ is the concentration of a selected immobile element (i.e., Zr, and Si) in the weathered horizon. The ρ_p for each site was calculated by taking the mean of the fine-earth bulk densities of all C horizons at each respective site. For the GR4 site, there were no C horizons described; thus, the mean of ρ_p for GR3 and GR5 (i.e., one elevation above and below the GR4 site, respectively) was used instead. The strains for C horizons were assigned zero values since the numerator and denominator in the Eq. 4.4 would be equivalent, yielding zeros for parent material. The EIC, CIA, and ϵ values were calculated for each pedon and then aggregated for each site and vegetation type. To facilitate comparison between sites, the final EIC, CIA, and ϵ values for the aggregated pedons were recalculated on a regular 5 cm interval using a weighted

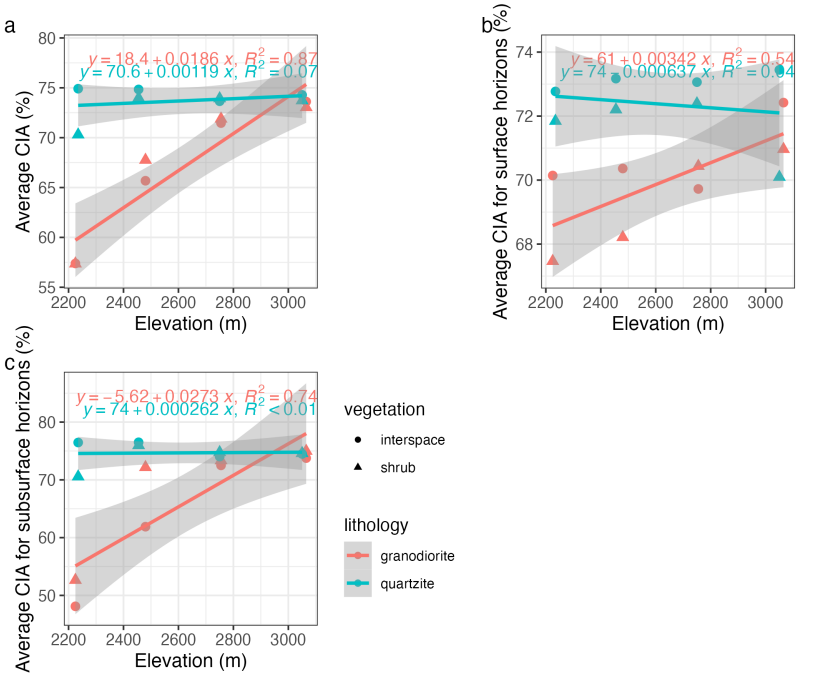

Figure 4.1: Average chemical index of alteration (CIA) for granodiorite and quartzite across the elevational transect calculated using (a) all A, V, and B horizons, (b) just surface (A and V) horizons, and (c) just subsurface (B) horizons.

average. Data analyses and visualizations were conducted in R version 4.4.0 (R Core Team, 2024).

4.3 Results

Figure 4.1a shows the weathering of granodiorite and quartzite across the elevational transect. Greater CIA values indicate a greater extent of chemical weathering with values at or below 50% indicating fresh, unweathered material. The fine-earth material of granodiorite was increasingly weathered along the transect with increasing precipitation whereas quartzite remained relatively constant across transect. No difference was

observed in the elevational trends in surface (Fig. 4.1b) and subsurface (Fig. 4.1c) horizons for quartzite as seen from slopes not significantly different from zero in Fig. 4.1. However, under granodiorite, surface and subsurface horizons both show increased weathering with increasing precipitation up the transect ($P < 0.01$).

The strain calculations for Zr (Fig. 4.2) and Si (Fig. 4.3) follow similar trends for each site. All strain values are positive for both granodiorite and quartzite indicating a dilation likely from the addition of dust into these profiles. The strain depth trend generally decreases in granodiorite indicating lower amounts of eolian material are translocated to deeper depths (e.g., below 30 cm at 2,200 and 2,500 m). In contrast, quartzite trends were constant or even increasing with depth for the lowest two elevations and decrease with depth only after 60 cm at the highest elevations. The deeper relatively high strain values under quartzite compared to granodiorite may indicate greater quantities of translocated dust under quartzite than granodiorite.

The positive EIC values show gains while negative values indicate loss of the element oxide relative to the parent material. The EIC calculated for CaO_2 shows a roughly increasing trend for both interspace and shrub granodiorite pedons at 2,200 m and interspace pedons in granodiorite at 2,500 m (Fig. 4.4). Pedons in granodiorite at 2,800 m and quartzite at 2,200–2,800 m show negative or near zero Ca EIC values without obvious depth trends with the exception of shrub pedons in quartzite at 2,200 m which increased to positive values below 40 cm. Both interspace and shrub pedons of granodiorite and quartzite at 3,100 m showed similar depth trends in Ca EIC where values were positive near the surface and decreased toward zero with depth. In contrast, the EIC calculated for K_2O showed

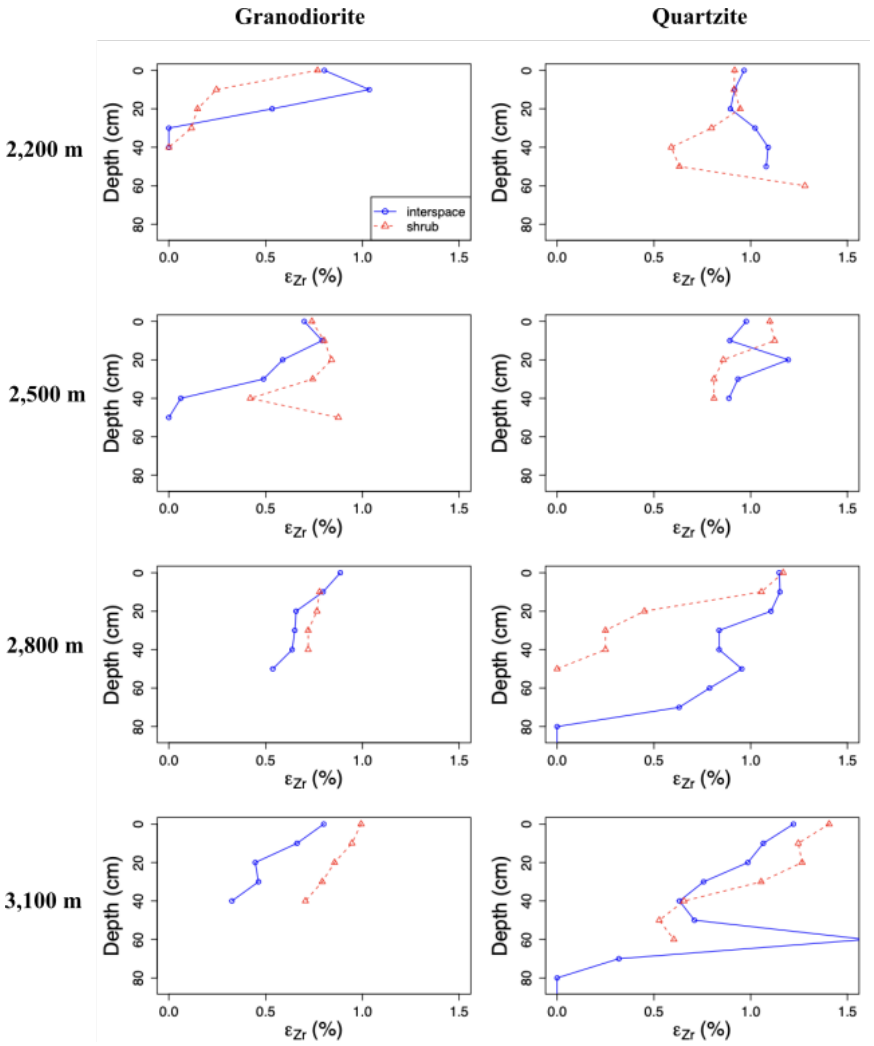

Figure 4.2: Strain values calculated using Zr as the immobile element plotted against depth for different lithologies and vegetation types at each elevation. Strain represents volume changes during weathering. Positive Zr strain shows dilations likely caused by the addition and incorporation of dust.

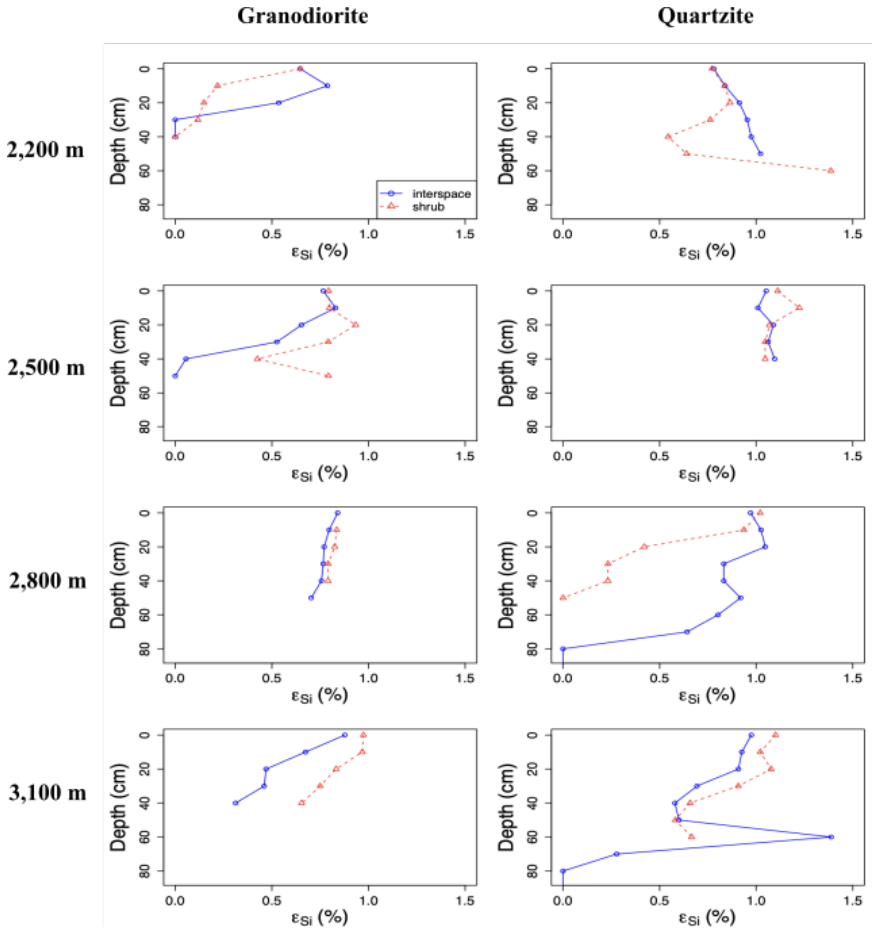

Figure 4.3: Strain values calculated using Si as the immobile element plotted against depth for different lithologies and vegetation types at each elevation. Positive Si strain show trends similar to Fig. 4.2.

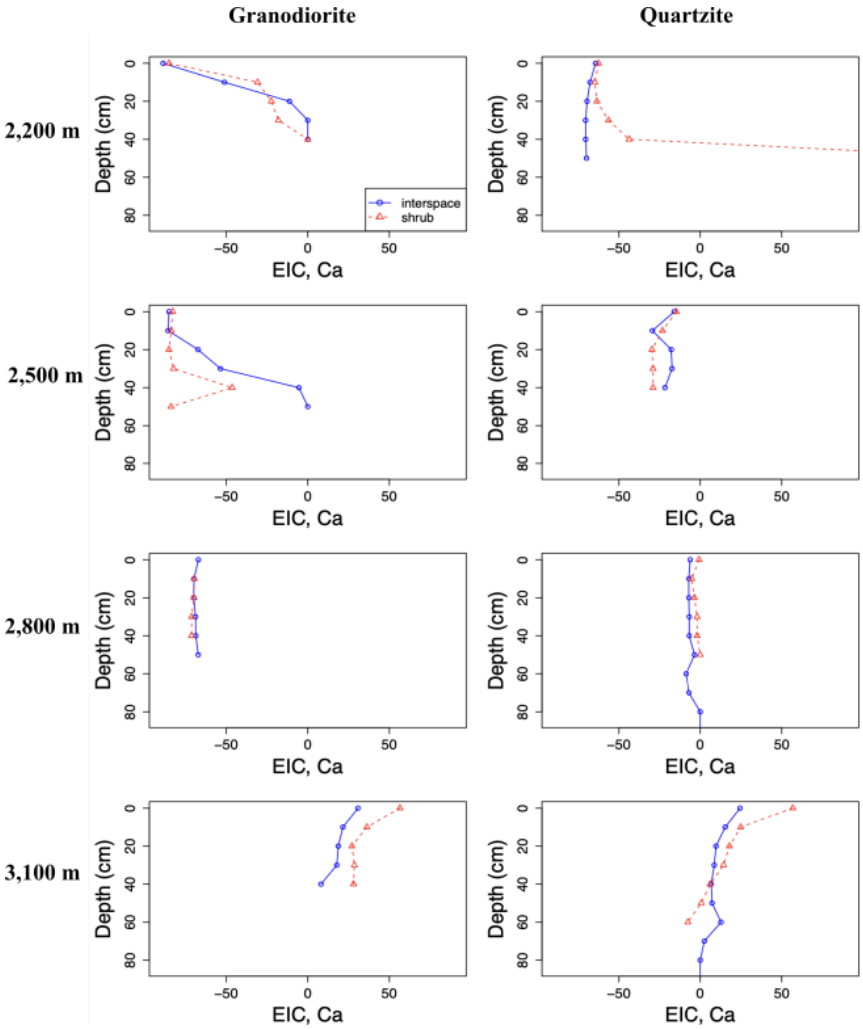

Figure 4.4: Eluvial-illuvial coefficient (EIC) calculated for CaO_2 using TiO_2 as the stable element. Positive values reflect a gain and negative values a loss relative to 100%.

similar decreasing trends at all sites where the values were positive near the surface and decreased to zero or just below for both interspace and shrub pedons (Fig. 4.5).

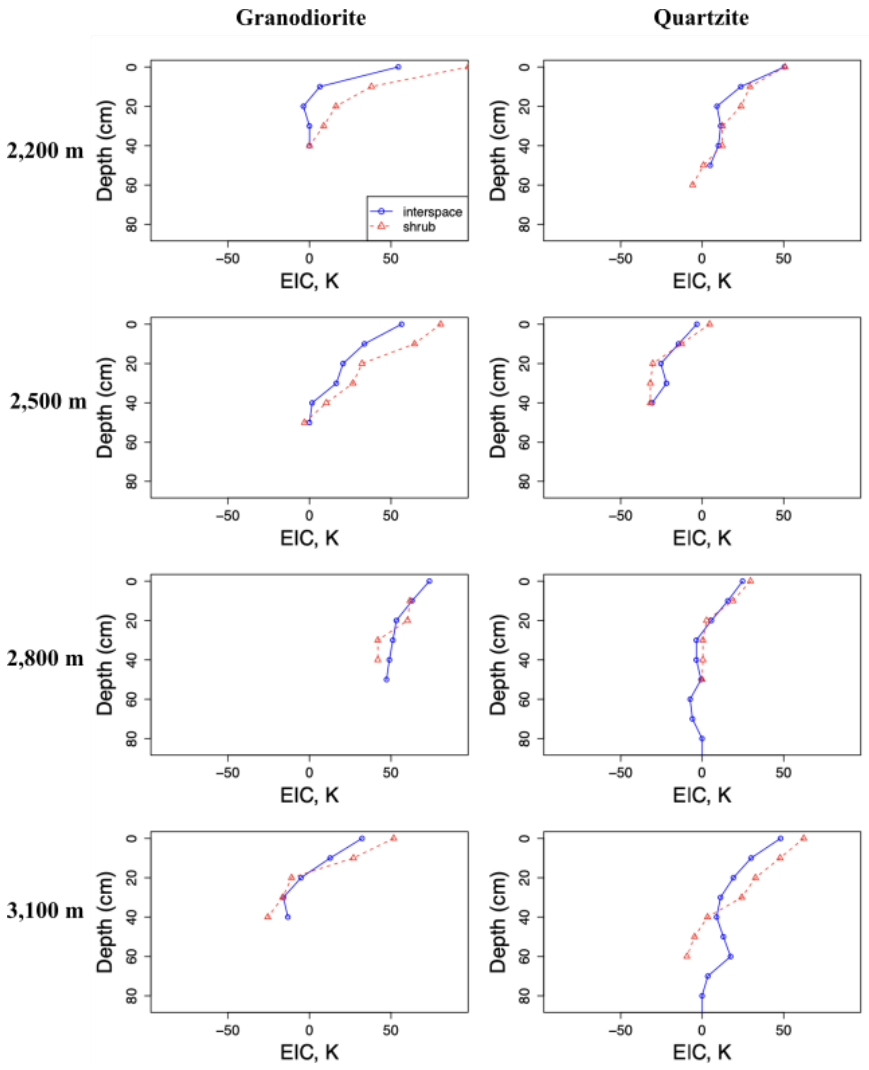

Figure 4.5: K_2O-EIC values calculated using TiO_2 as the stable element for the pedons in this study.

4.4 Discussion

Soil development in the WMs is a complex process involving the potential in situ weathering of residuum parent materials and the addition of eolian fines from the lower-lying adjacent Owens valley (Reheis, 1997; Marchand, 1973). The soil forms within these eolian fines which significantly shapes the properties of soils within these mountains (McAuliffe et al., 2018; Loba et al., 2020). Chemical weathering indices for granodiorite and quartzite in the WMs provides evidence for this dual parent material system in the case of granodiorite and loess so for quartzite pedons. The physically-weathered quartzite rock fragments remain angular and sharp within the profile and indicate little chemical weathering or contribution to the fine-earth soil matrix. However, the granodiorite weathers into grus and provides fresh, coarse (i.e., sandy) material to the fine-earth matrix. Morphological evidence (Chapter 2) suggests that dust deposition on quartzite-dominated lithologies gets translocates through the large interstitial macropores formed by the coarse angular clasts. However, in granodiorite, dust is concentrated near the surface due to smaller interstitial pores via grus infilling between clasts. Since the contribution from granodiorite residuum is fresh material and thus susceptible to chemical weathering, the CIA increases as the precipitation increases with elevation (Fig. 4.1a). With increasing elevation, a greater portion of the precipitation falls as snow, which melts and infiltrates the soil matrix relatively slowly, promoting chemical weathering of the fine-earth material over time. In contrast, at lower elevations, precipitation typically falls as rain which tends to move more quickly through the soil with a greater propensity for macropore preferential flow reducing the residence time of water and the interaction between water and fine-earth minerals resulting in limited

weathering (DeWalle & Rango, 2008; Hammond et al., 2019). This propensity for preferential flow is more pronounced in quartzite than granodiorite partly because the increased contribution of grus to the fine-earth matrix increases its conductivity allowing more of the meteoric water to move as diffusive flow through the matrix. Since a greater proportion of the fine-earth material in quartzite is sourced directly from eolian fines that have already weathered ex situ before being transported up the mountian range, the fine-earth matrix shows little change in CIA with incrasing elevation (Fig. 4.1).

Dust arising from Owens valley contains calcium carbonate with the average content ranging from 8-31% and an average flux of 0.7–6.6 g m^{-2} yr^{-1} (Reheis & Kihl, 1995). The EIC for Ca (Fig. 4.4) is mostly negative at the lower elevations because Ca is leached down the profile at the lower elevation. However, at the highest elevation, the coefficient becomes slightly positive due to the slower movement of water through the soil matrix, leading to Ca accumulation at shallower depths. At lower elevations, since most of the precipitation is in the form of rainfall, the water moves faster via the larger interstitial macropores (Hui et al., 2015). This faster movement of water in combination with the greater solubility of $CaCO_3$ in comparison to K-bearing silicates is likely to be responsible for the leaching of Ca from the upper horizons and deposition within deeper horizons in comparison to K_2O. In addition, K_2O shows gain at the surface of all the sites likely because dust has K-felspar as the second largest abundant dust component in the WMs Marchand (1970). K-felspar is known to be very resistant to weathering, so it is likely that it is accumulated by dust faster than it is weathered and leached from the soil profile (Blum, 1994; White et al., 2001).

The calculated strain values for the immobile elements Zr and Ti are all positive indicating dilation (Figs. 4.2 and 4.3). Dust is an exogenous source of fine particles that, when deposited, contribute to soil dilation by increasing the soil volume (Bern et al., 2015). In general, the strain values are higher for the upper horizons and decrease with depth. Granodiorite strain values decline more quickly with depth compared to quartzite. This difference indicates greater translocation of dust in quartzite than granodiorite. Granodiorite pedons tend to form vesicular horizons that diffuse infiltrating water and impede the translocation of dust deep in the profile. In contrast, interstitial macropores under quartzite encourage preferential flow and the comparatively deeper translocation of dust.

4.5 Conclusions

Dust contributes significantly to the pedogenesis of WM soils. This research reveals that soil development in this region is a complex interplay of in situ weathering and continuous dust input. This dual contribution shapes the unique properties of the soil formed under granodiorite and quartzite lithologies. Granodiorite weathering into finer particles leads to increased chemical weathering with elevation and precipitation. Conversely, coarse fragments of quartzite encourage the translocation of eolian fines, with minimal changes in weathering despite varying precipitation levels likely due the tendency for quartzite soils to direct infiltrating water toward preferential flow paths bypassing the matrix and because the fine-earth matrix is composed almost entirely of previously weathered eolian material. The contrasting physical and chemical weathering processes in these lithologies emphasize the critical role of dust in soil profile development in arid mountain soils. This research

enhances our understanding of the complex mechanisms of soil formation in arid mountain environments.

References

Bäumler, R., & Zech, W. (2000). Quaternary paleosols, tephra deposits and landscape history in south kamchatka, russia. *Catena*, *41*(1-3), 199–215.

Bern, C. R., Thompson, A., & Chadwick, O. A. (2015). Quantification of colloidal and aqueous element transfer in soils: The dual-phase mass balance model. *Geochimica et Cosmochimica Acta*, *151*, 1-18. doi: https://doi.org/10.1016/j.gca.2014.12.008

Blum, A. E. (1994). Feldspars in weathering. In I. Parsons (Ed.), *Feldspars and their reactions* (pp. 595–630). Dordrecht: Springer Netherlands. doi: 10.1007/978-94-011-1106-5_15

Brimhall, G. H., Chadwick, O. A., Lewis, C. J., Compston, W., Williams, I. S., Danti, K. J., ... Bratt, J. (1992). Deformational mass transport and invasive processes in soil evolution. *Science*, *255*(5045), 695–702.

Chakraborty, S., Li, B., Deb, S., Acree, A., De, P., & Panda, P. (2019, 03). Use of portable x-ray fluorescence spectrometry for classifying soils from different land use land cover systems in india. *Geoderma*, *338*, 5-13. doi: 10.1016/j.geoderma.2018.11.043

DeWalle, D. R., & Rango, A. (2008). Snowmelt-runoff processes. In *Principles of snow hydrology* (p. 235–265). Cambridge University Press.

Gall, Q. (1994). The proterozoic thelon paleosol, northwest territories, canada. *Precambrian Research*, *68*(1-2), 115–137.

Hammond, J. C., Harpold, A. A., Weiss, S., & Kampf, S. K. (2019). Partitioning snowmelt and rainfall in the critical zone: effects of climate type and soil properties. *Hydrology and Earth System Sciences*, *23*(9), 3553–3570. doi: 10.5194/hess-23-3553-2019

Hui, Y., Jianhong, L., Jiarui, C., & Jianhua, C. (2015). Soil calcium speciation at different geomorphological positions in the yaji karst experimental site in guilin, china. *Journal of Resources and Ecology*, *6*(4), 224–229.

Laity, J. J. (2009). *Deserts and desert environments* (Vol. 3). John Wiley & Sons.

Loba, A., Sykuła, M., Kierczak, J., Łabaz, B., Bogacz, A., & Waroszewski, J. (2020, 01). In situ weathering of rocks or aeolian silt deposition: key parameters for verifying parent material and pedogenesis in the opawskie mountains-a case study from sw poland. *Journal of Soils and Sediments*. doi: 10.1007/s11368-019-02377-5

Lybrand, R. A., & Rasmussen, C. (2018). Climate, topography, and dust influences on the mineral and geochemical evolution of granitic soils in southern arizona. *Geoderma*, *314*, 245-261. doi: https://doi.org/10.1016/j.geoderma.2017.10.042

Marchand, D. E. (1970). Soil contamination in the White Mountains, Eastern California. *Geological Society Of America Bulletin*, *81*(8), 2497–2506. doi: 10.1130/0016-7606(1970)81

Marchand, D. E. (1973). Edaphic control of plant distribution in the White Mountains , Eastern California. *Ecology*, *54*(2), 233–250.

Maslov, A., Krupenin, M., & Gareev, E. (2003, 09). Lithological, lithochemical, and geochemical indicators of paleoclimate: Evidence from riphean of the southern urals. *Lithology and Mineral Resources*, *38*, 427-446. doi: 10.1023/A:1025575120343

Maynard, J. (1992). Chemistry of modern soils as a guide to interpreting precambrian paleosols. *The Journal of Geology*, *100*(3), 279–289.

McAuliffe, J. R., McFadden, L. D., & Hoffman, M. T. (2018). Role of aeolian dust in shaping landscapes and soils of arid and semi-arid south africa. *Geosciences*, *8*(5). doi: 10.3390/geosciences8050171

McFadden, L., Eppes, M., Gillespie, A., & Hallet, B. (2005, 01). Physical weathering in arid landscape due to diurnal variation in the direction of solar heating. *Geological Society of America Bulletin - GEOL SOC AMER BULL*, *117*. doi: 10.1130/B25508.1

Muhs, D., Bettis, A., Been, J., & McGeehin, J. (2001, 11). Impact of climate and parent material on chemical weathering in loess-derived soils of the mississippi river valley. *Soil Science Society of America Journal - SSSAJ*, *65*, 1761-1777. doi: 10.2136/sssaj2001.1761

Muir, J. W., & Logan, J. (1982). Eluvial/illuvial coefficients of major elements and the corresponding losses and gains in three soil profiles. *The Journal of soil science.*, *33*(2).

Nesbitt, H., & Young, G. (1982, 10). Early proterozoic climates and plate motions inferred from major element chemistry of lutites. *Nature*, *299*. doi: 10.1038/299715a0

Price, J. R., & Velbel, M. A. (2003). Chemical weathering indices applied to weathering profiles developed on heterogeneous felsic metamorphic parent rocks. *Chemical Geology*,

202(3), 397-416. (Controls on Chemical Weathering) doi: https://doi.org/10.1016/j.chemgeo.2002.11.001

R Core Team. (2024). R: A language and environment for statistical computing [Computer software manual]. Vienna, Austria. Retrieved from `https://www.R-project.org/`

Ramond, J.-B., Jordaan, K., Díez, B., Heinzelmann, S. M., & Cowan, D. A. (2022). Microbial biogeochemical cycling of nitrogen in arid ecosystems. *Microbiology and Molecular Biology Reviews*, *86*(2), e00109-21. doi: 10.1128/mmbr.00109-21

Reheis, M. C. (1997). Dust deposition downwind of Owens (dry) Lake, 1991-1994: Preliminary findings. *Journal of Geophysical Research Atmospheres*, *102*(22). doi: 10.1029/97jd01967

Reheis, M. C., & Kihl, R. (1995). Dust deposition in southern Nevada and California,1984-1989: Relations to climate, source area, and source lithology. *Journal of Geophysical Research Atmospheres*, *100*, 8893–8918.

Routson, R. C., Wildung, R. E., & Garland, T. R. (1977). Mineral weathering in an arid watershed containing soil developed from mixed basaltic-felsic parent materials. *Soil Science*, *124*(5), 303–308.

Schoeneberger, P., Wysocki, D., Benham, E., & Staff, S. S. (2012). *Field book for describing and sampling soils, version 3.0.* Natural Resources Conservation Service, National Soil Survey Center, Lincoln, NE.

Turner, M., & Gardner, R. (2015). *Landscape ecology in theory and practice: Pattern and process, second edition.* doi: 10.1007/978-1-4939-2794-4

Weindorf, D. C., & Chakraborty, S. (2020). Portable x-ray fluorescence spectrometry analysis of soils. *Soil Science Society of America journal.*, *84*, 1384–1392.

White, A. F., Bullen, T. D., Schulz, M. S., Blum, A. E., Huntington, T. G., & Peters, N. E. (2001). Differential rates of feldspar weathering in granitic regoliths. *Geochimica et Cosmochimica Acta*, *65*(6), 847-869. doi: https://doi.org/10.1016/S0016-7037(00)00577-9

Zhao, Y. F., Wang, X., Jiang, S. L., Zhou, X. H., Liu, H. Y., Xiao, J. J., ... Wang, K. C. (2021). Climate and geochemistry interactions at different altitudes influence soil organic carbon turnover times in alpine grasslands. *Agriculture, Ecosystems & Environment*, *320*, 107591. doi: https://doi.org/10.1016/j.agee.2021.107591

Chapter 5

CONCLUSIONS

This dissertation provides a detailed exploration of soil genesis, hydrology, and geochemistry in arid mountain ecosystems, focusing on the White Mountains (WMs) of eastern California. Set within the context of an elevational transect, this work offers new insights into how climate, parent material, and dust deposition interact to shape soils of arid mountains. The key findings of this research contribute to a growing understanding of soil development in regions where water is a critical limiting factor, especially as these regions face increasing pressure from climate change.

Results from Chapter 2 demonstrate that both climate and lithology play vital roles in soil development. At lower elevations, more frequent rainfall promotes deeper translocation of water and, thus, deeper soil profiles. In contrast, snowfall dominates at higher elevations, directing water flow into matrix pores and resulting in the development of shallower soils. The contrasting weathering characteristics of granodiorite and quartzite also contributed to differential soil formation. The higher susceptibility to weathering of

granodiorite resulted in the formation of grus and encouraged development of vesicular (V) horizons, whereas the resistance to weathering of coarser quartzite rock fragments maintained large interstitial macropores promoting the translocation of dust and development of comparatively deeper soils. These findings highlight the importance of understanding how dominant residuum parent materials interact with eolian sedimentation and precipitation characteristics to influence soil profile development. In particular, the ubiquitous deposition of dust modifies the physical and chemical properties of soils across lithological types, especially through the formation of V horizons.

The hydrological study of the WMs in Chapter 3 revealed significant differences in water infiltration and retention between the two contrasting lithologies. Granodiorite soils, with their propensity to form V horizons, restricts deep infiltration and promotes surface runoff, particularly in areas with limited vegetation cover. This suggests that V horizons create a positive feedback loop, limiting the amount of water that percolates into deeper soil layers and thereby increasing the challenges of water scarcity in these fragile ecosystems. On the other hand, coarser quartzite fragments facilitate deeper water movement, resulting in more efficient translocation of dust and water into the soil profile. The findings of Chapter 3 have broader implications for understanding water-limited ecosystems, as they suggest that lithology-induced differences in water infiltration could play a significant role in determining the distribution and survival of plant species. The bristlecone pines (*Pinus longaeva*), the oldest living tree species, which rely on scarce water resources, are especially vulnerable to shifts in soil hydrology driven by climate change. Future research should investigate how

lithological variations might buffer or exacerbate these vulnerabilities, particularly in the context of increasing aridity.

Results from Chapter 4 confirms the role of dust in shaping the chemical composition of soils, with significant differences observed between soils formed under granodiorite and quartzite. Granodiorite soils exhibited increased chemical weathering with elevation and precipitation, likely due to the finer particles produced by weathering processes and the influence of dust inputs. Quartzite soils, however, showed minimal changes in weathering patterns, likely due to preferential water flow paths that bypass the soil matrix. The accumulation of eolian dust in both lithologies emphasizes the importance of external material inputs to the pedogenesis of arid mountain soils. These findings enhance our understanding of the complex mechanisms that drive soil formation in arid regions. The research suggests that dust influx, combined with lithological and climatic controls, plays an important role in the long-term evolution of these landscapes.

The work presented in this dissertation contributes to our understanding of how arid mountain soils develop over time, particularly, in response to lithological and climatic variability. These findings have several broader implications. The results of this study provide valuable insights into the hydrological and geochemical processes that control soil formation in arid regions. Understanding these processes is crucial for developing effective soil conservation strategies in dryland ecosystems, especially as climate change threatens to increase desertification and alter precipitation patterns. By linking soil hydrology to the survival of keystone species like the bristlecone pine, this research emphasizes the critical role that soils play in sustaining ecosystems under extreme environmental conditions. Moreover,

the study suggests that eolian dust inputs could influence carbon storage capacity in arid soils, which has important implications for global carbon dynamics in the face of increasing atmospheric CO_2.

Further work is needed to investigate the long-term effects of climate change on soil-water interactions, especially in these high-elevation ecosystems where snowpack dynamics are crucial. Additionally, the role of dust in altering both physical and chemical weathering processes in different lithologies deserves further exploration, particularly as dust deposition rates could increase in response to land use changes.

Appendix A

Weather Station Locations and Soil Sensor Information

Table A.1: Weather stations at the White Mountains measures soil temperature, soil moisture, barometric pressure, air temperature, relative humidity, cumulative precipitation, solar radiation, wind speed, and maximum gust. In addition to the other parameters, the Barcroft station measures snow depth, rainfall, and photosynthetically active radiation.

Weather station	**Elevation (m)**	**Latitude (°)**	**Longitude (°)**
Fish Slough	1289	37.4792	-118.4030
Sore Thumb	1578	37.5108	-118.3248
Over the Hill	1855	37.5156	-118.3167
Piute Creek Overlook	2133	37.5107	-118.3304
Glider Port	2476	37.5211	-118.2950
Beer Can	2768	37.5290	-118.2843
Valley View	3125	37.5292	-118.2628
Barcroft	3783	37.5830	-118.2372
WM Summit Station	4342	37.6341	-118.25583

Table A.2: Soil sensor data within the study area of the White Mountains from 2013-2023. The GR2-5 sites are on granodiorite; WP4b-7, WP8, and BAR sites are on quartzite. In 2022, sensors were replaced at all locations at the lower four elevations (i.e., 2,200, 2,500, 2,800, 3,100 m) with a cellular datalogger to allow real-time monitoring and collection of soil moisture and temperature data.

Site	**Vegetation**	**Depth(cm)**	**'13**	**'14**	**'15**	**'16**	**'17**	**'18**	**'19**	**'20**	**'21**	**'22**	**'23**
GR2	Interspace	10	B	B	B	M	B	B	B	B	B	B	B
(2,200 m)		50	B	B	B	M	B	B	B	B	B	B	B
	Shrub	10	B	B	B	B	B	B	B	B	B	B	B
		50	B	B	B	B	B	B	B	B	B	B	B
WP4b	Interspace	10	B	B	B	B	B	B	B	B	B	B	B
(2,200 m)		50	B	B	B	B	B	B	B	B	B	B	B
	Shrub	10	B	B	B	B	B	B	B	B	B	B	B
		50	B	B	B	B	B	B	B	B	B	B	B
GR3	Interspace	10										B	B
(2,500 m)		50										B	B
	Shrub	10	T	T	T	T	T	T	T	T	T	B	B
		50	T	T	T	T	T	T	T	T	T	B	B
	Tree	10	T	T	T	T	T	T	T	T	T	B	B
		50	T	T	T	T	T	T	T	T	T	B	B
WP5	Interspace	10	T	T	T	T	T	T	T	T	T	B	B
(2,500 m)		50	T	T	T		T	T	T	T	T	B	B
	Shrub	10	T	T	T	T	T	T	T	T	T	B	B
		50	T	T	T	T	T	T	T	T	T	B	B
GR4	Interspace	10				T	T	B	B	T	T	B	B
(2,800 m)		50				T	T	B	B	T	T	B	B
	Shrub	10				T	T	B	B	T	T	B	B
		50				T	T	B	B	T	T	B	B
	Tree	10				T	T	T	T	T	T	B	B
		50				T	T	B	B	T	T	B	B
WP6b	Interspace	10	T	T	T	T	T	B	B	B	B	B	B
(2,800 m)		50	T	T	T	T	T	B	B	B	B	B	B
	Shrub	10	T	T	T	T	T	B	B	B	B	B	B
		50	T	T	T	T	T	B	B	B	M	B	B
	Tree	10	T	T	T	T	T	T	T	T	T	B	B
		50	T	T	T	T	T	B	B	B	B	B	B
GR5	Interspace	10						B	B	B	B	B	B
(3,100 m)		50						B	B	B	B	B	B
	Shrub	10						B	B	B	B	B	B
		50						B	B	B	B	B	B
WP7	Interspace	10						B	B	T	T	B	B
(3,100 m)		50	T	T	T	T	T	B	B	T	T	B	B
	Shrub	10						B	B	T	T	B	B
		50	T	T	T	T	T	B	B	T	T	B	B
WP8	Interspace	10											
(3,700 m)		50	T	T	T	T	T	T	T	T	T		
	Shrub	10											
		50	T	T	T	T	T	T	T	T	T		
BAR	Interspace	10	T	B	B	B	B	B	B	B	B		
(4,000 m)		30	M	M	M	M	M	M	M	M	M		
		50	B	B	B	B	B	B	B	B	B		
		75	M	M	M	M	M	M	M	M	M		
WMS	Interspace	10	T	T	T	T	T	T	T				
(4,300 m)		50	T	T	T	T	T	T	T				

B, Both temperature and moisture sensors; T, Temperature sensors only; M, Moisture sensors only

Appendix B

Calculated Strain and EIC

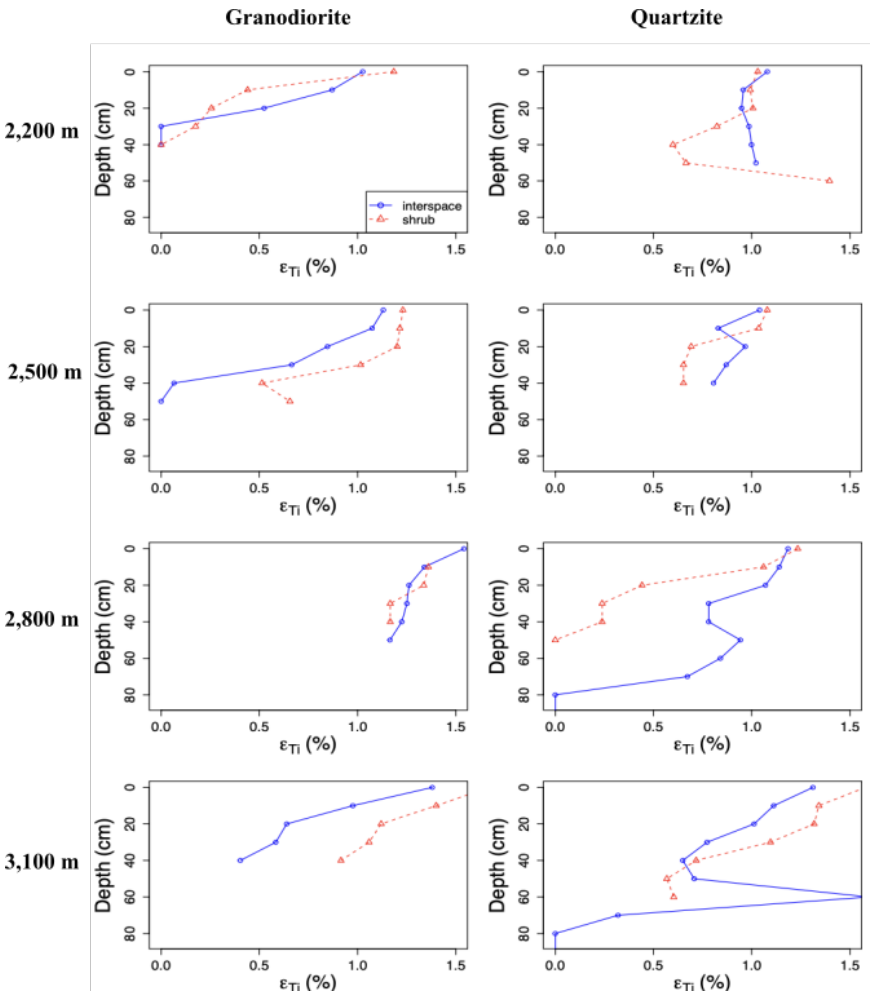

Figure B.1: Strain values calculated using Ti as the immobile element plotted against depth for different lithologies and vegetation types at each elevation.

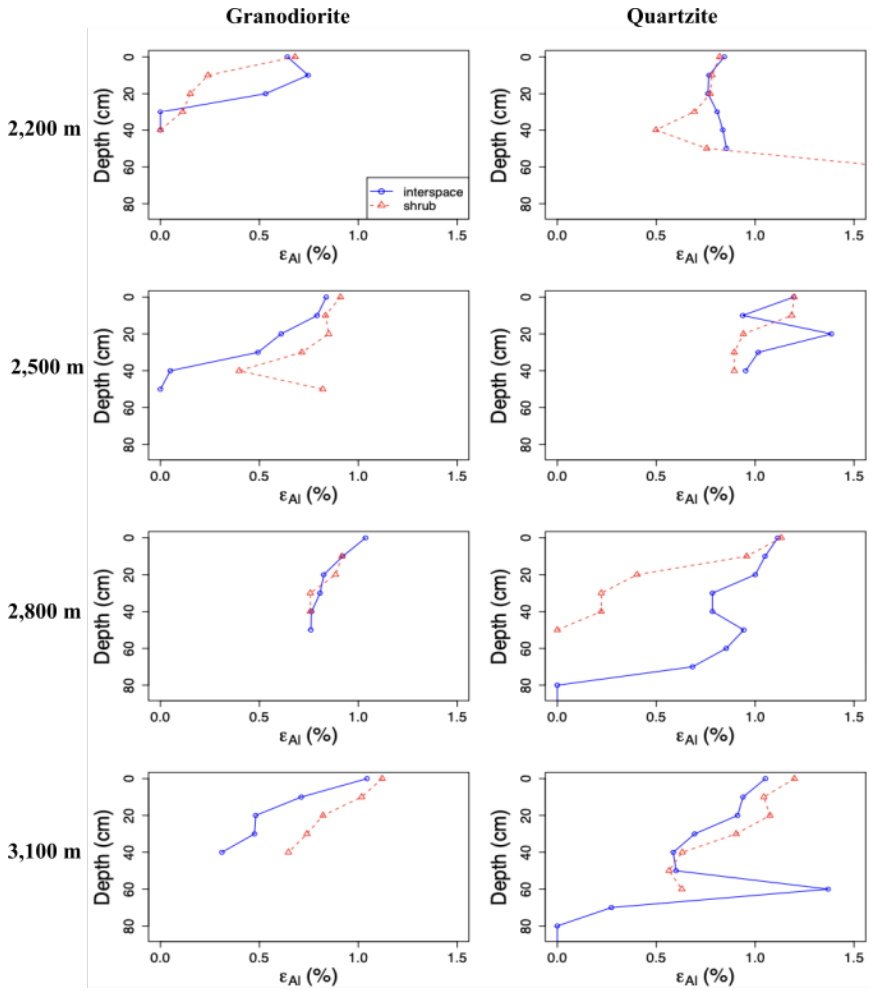

Figure B.2: Strain values calculated using Al as the immobile element plotted against depth for different lithologies and vegetation types at each elevation.

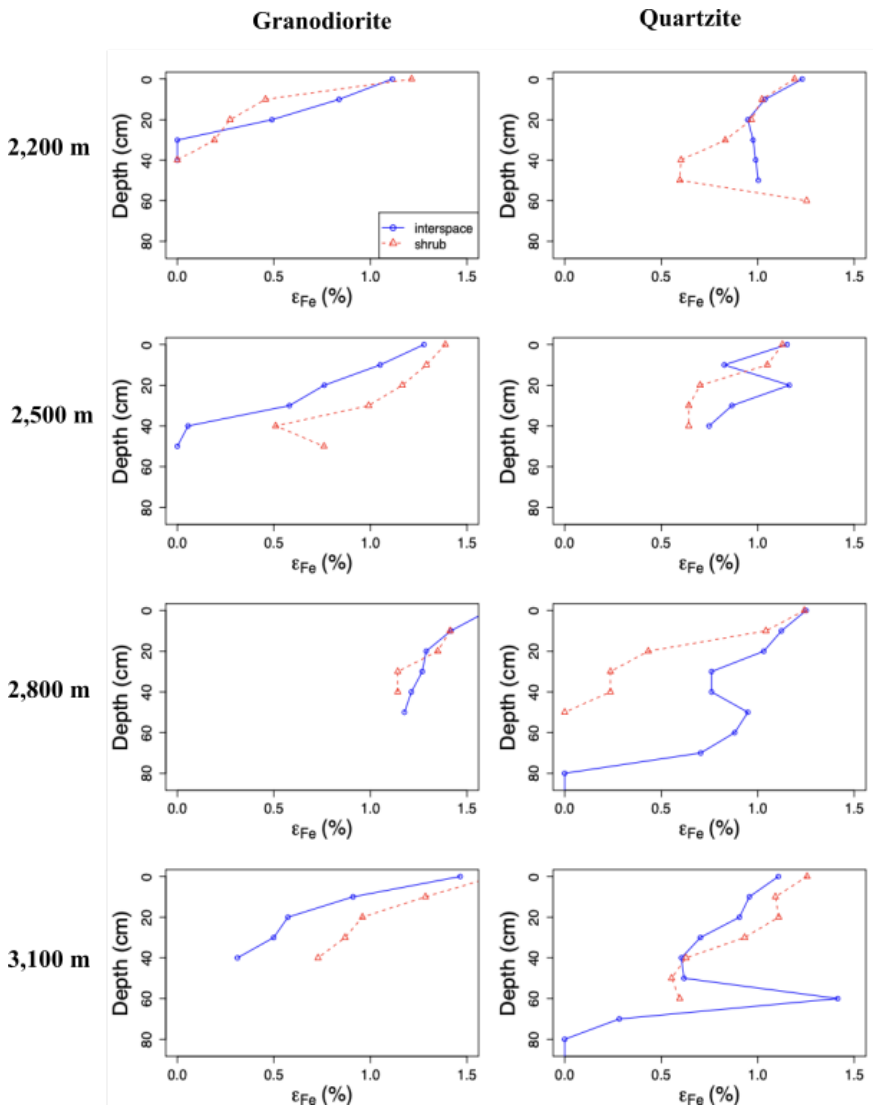

Figure B.3: Strain values calculated using Fe as the immobile element plotted against depth for different lithologies and vegetation types at each elevation.

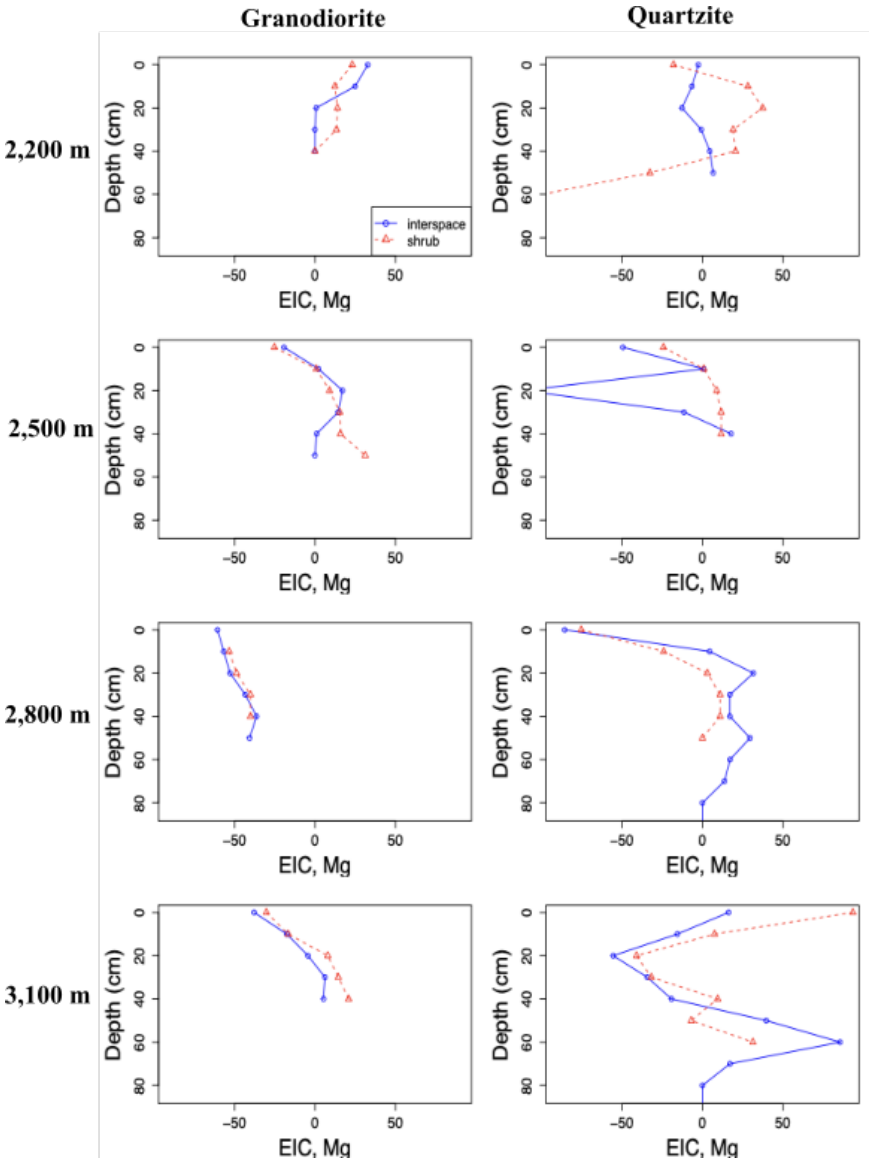

Figure B.4: Eluvial-illuvial coefficient (EIC) calculated for MgO using TiO_2 as the stable element. Positive values reflect a gain and negative values a loss relative to 100%.

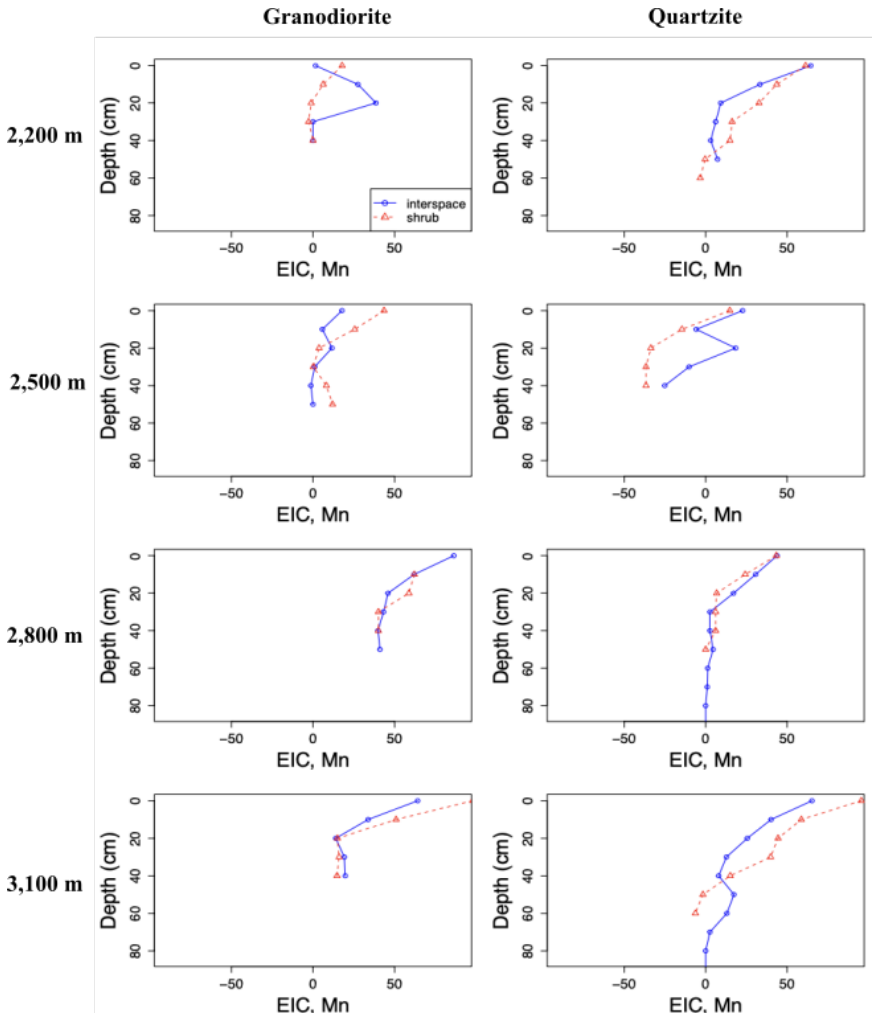

Figure B.5: Eluvial-illuvial coefficient (EIC) calculated for MnO_2 using TiO_2 as the stable element. Positive values reflect a gain and negative values a loss relative to 100%.

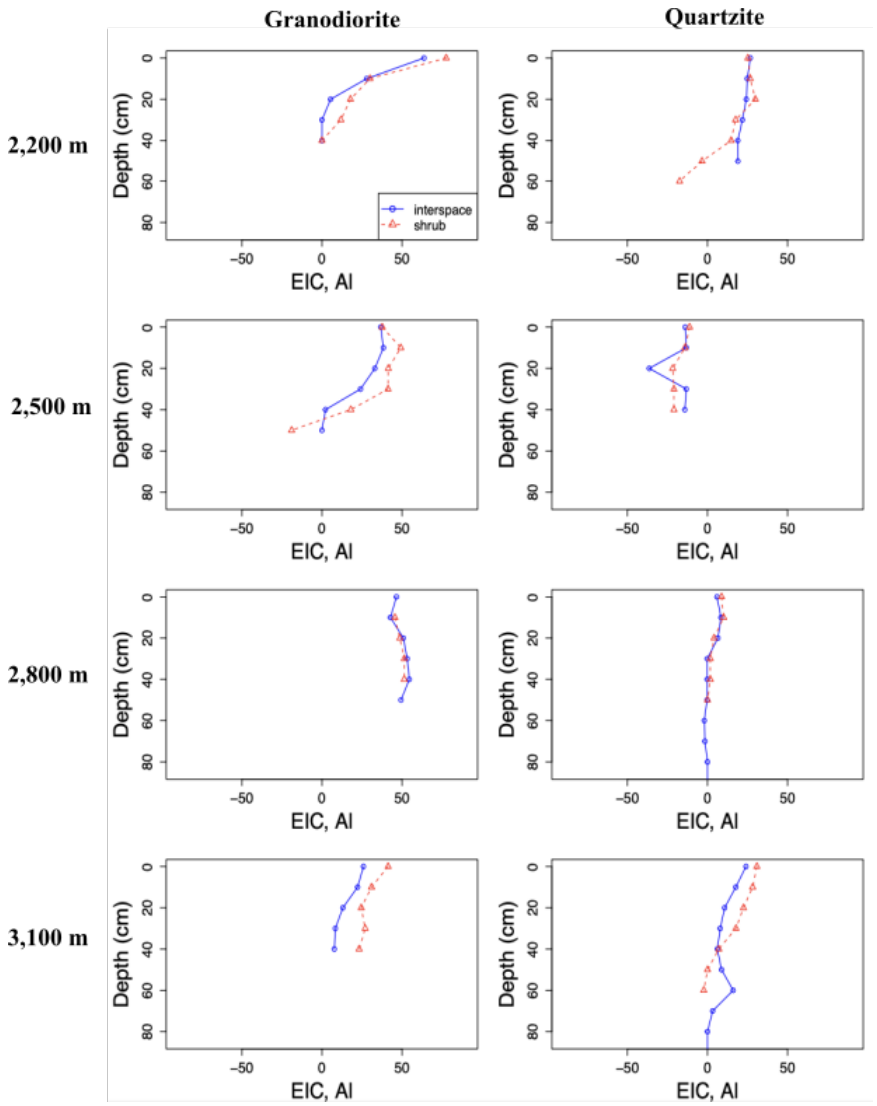

Figure B.6: Eluvial-illuvial coefficient (EIC) calculated for Al_2O_3 using TiO_2 as the stable element. Positive values reflect a gain and negative values a loss relative to 100%.

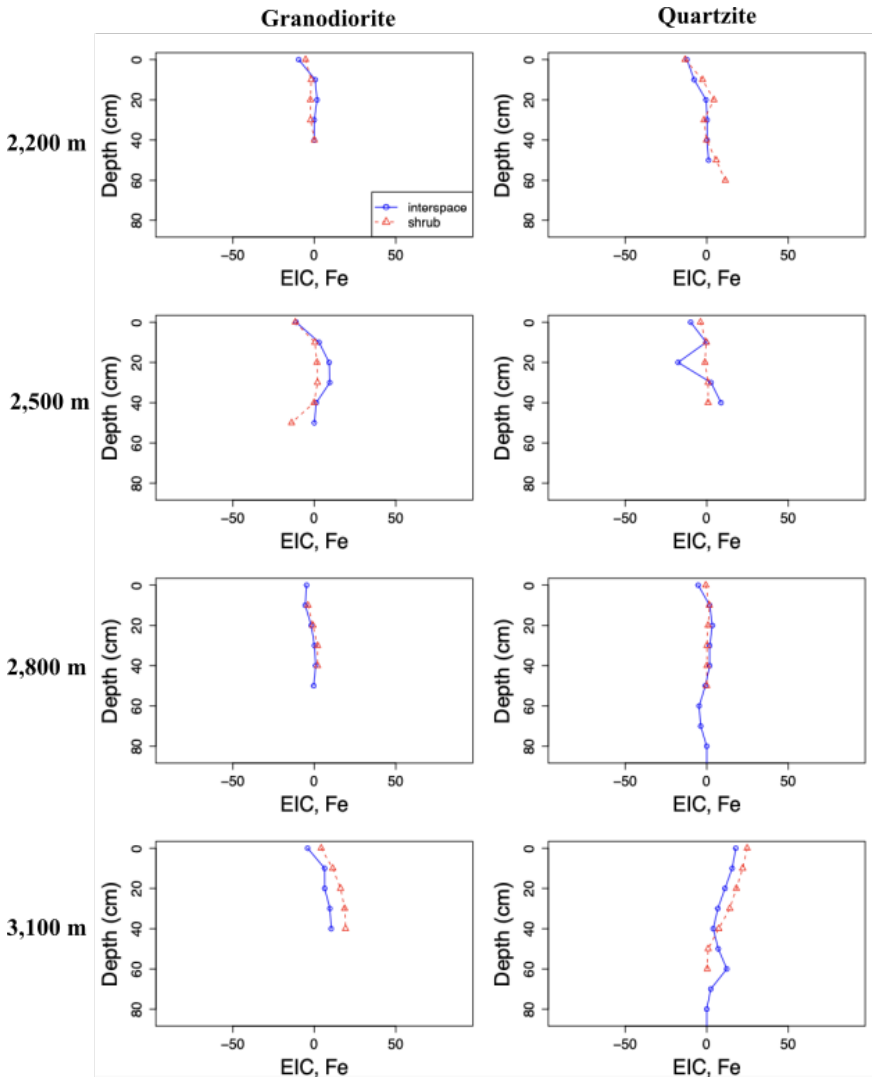

Figure B.7: Eluvial-illuvial coefficient (EIC) calculated for Fe_2O_3 using TiO_2 as the stable element. Positive values reflect a gain and negative values a loss relative to 100%.